JPTM

Journal of Pathology and Translational Medicine

March 2020
Vol. 54 / No.2
jpatholtm.org
pISSN: 2383-7837
eISSN: 2383-7845

Introduction to Digital Pathology and Computer-Aided Pathology

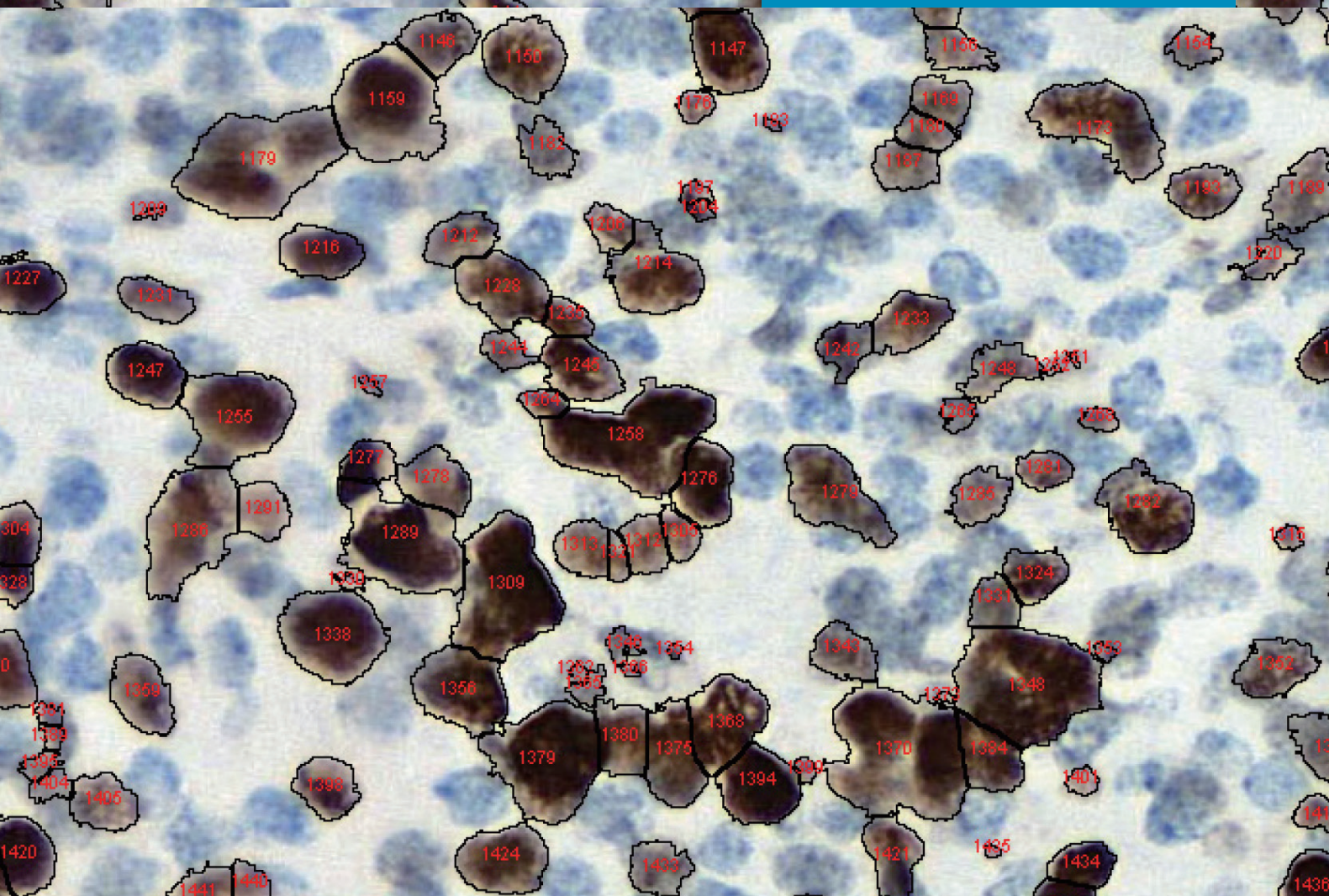

Journal of Pathology and Translational Medicine

Volume 54 • Number 2 • March 2020 (bimonthly)
Published since 1967
Printed on 11 March 2020 Published on 15 March 2020

J Pathol Transl Med
pISSN: 2383-7837
eISSN: 2383-7845

Aims & Scope

The Journal of Pathology and Translational Medicine is an open venue for the rapid publication of major achievements in various fields of pathology, cytopathology, and biomedical and translational research. The Journal aims to share new insights into the molecular and cellular mechanisms of human diseases and to report major advances in both experimental and clinical medicine, with a particular emphasis on translational research. The investigations of human cells and tissues using high-dimensional biology techniques such as genomics and proteomics will be given a high priority. Articles on stem cell biology are also welcome. The categories of manuscript include original articles, review and perspective articles, case studies, brief case reports, and letters to the editor.

Subscription Information

To subscribe to this journal, please contact the Korean Society of Pathologists/the Korean Society for Cytopathology. Full text PDF files are also available at the official website (http://jpatholtm.org). *Journal of Pathology and Translational Medicine* is indexed by Emerging Sources Citation Index (ESCI), PubMed, PubMed Central, Scopus, KoreaMed, KoMCI, WPRIM, Directory of Open Access Journals (DOAJ), and CrossRef. Circulation number per issue is 700.

Contact the Korean Society of Pathologists/the Korean Society for Cytopathology

Publishers: Choi, Chan, MD, Hong, Soon Won, MD
Editors-in-Chief: Jung, Chan Kwon, MD, Park, So Yeon, MD
Published by the Korean Society of Pathologists/the Korean Society for Cytopathology

Editorial Office
Room 1209 Gwanghwamun Officia, 92 Saemunan-ro, Jongno-gu, Seoul 03186, Korea
Tel: +82-2-795-3094 Fax: +82-2-790-6635 E-mail: office@jpatholtm.org

#1508 Renaissancetower, 14 Mallijae-ro, Mapo-gu, Seoul 04195, Korea
Tel: +82-2-593-6943 Fax: +82-2-593-6944 E-mail: office@jpatholtm.org

Printed by iMiS Company Co., Ltd. (JMC)
Jungang Bldg. 18-8 Wonhyo-ro 89-gil, Yongsan-gu, Seoul 04314, Korea
Tel: +82-2-717-5511 Fax: +82-2-717-5515 E-mail: ml@smileml.com

Manuscript Editing by InfoLumi Co.
210-202, 421 Pangyo-ro, Bundang-gu, Seongnam 13522, Korea
Tel: +82-70-8839-8800 E-mail: infolumi.chang@gmail.com

Front cover image: Under- and over-nuclear segmentation results of Ki-67 immunostaining in ImageJ (Fig. 1). p128.

Journal of Pathology and Translational Medicine

J Pathol Transl Med
pISSN: 2383-7837
eISSN: 2383-7845

Volume 54, Number 2, March 2020

CONTENTS

CONTENTS CONTINUED

CORRIGENDUM

Instructions for Authors for *Journal of Pathology and Translational Medicine* are available at http://jpatholtm.org/authors/authors.php

JPTM
Journal of Pathology and Translational Medicine 2020; 54: 125-134
https://doi.org/10.4132/jptm.2019.12.31

REVIEW

Introduction to digital pathology and computer-aided pathology

Soojeong Nam[1]*, Yosep Chong[2]*, Chan Kwon Jung[2]*, Tae-Yeong Kwak[3]*, Ji Youl Lee[4], Jihwan Park[5,6], Mi Jung Rho[5], Heounjeong Go[1]

[1]Department of Pathology, Asan Medical Center, University of Ulsan College of Medicine, Seoul;
[2]Department of Hospital Pathology, College of Medicine, The Catholic University of Korea, Seoul;
[3]Deep Bio Inc., Seoul;
[4]Department of Urology, College of Medicine, The Catholic University of Korea, Seoul;
[5]Catholic Cancer Research Institute, College of Medicine, The Catholic University of Korea, Seoul;
[6]Department of Biomedicine & Health Sciences, College of Medicine, The Catholic University of Korea, Seoul, Korea

Digital pathology (DP) is no longer an unfamiliar term for pathologists, but it is still difficult for many pathologists to understand the engineering and mathematics concepts involved in DP. Computer-aided pathology (CAP) aids pathologists in diagnosis. However, some consider CAP a threat to the existence of pathologists and are skeptical of its clinical utility. Implementation of DP is very burdensome for pathologists because technical factors, impact on workflow, and information technology infrastructure must be considered. In this paper, various terms related to DP and computer-aided pathologic diagnosis are defined, current applications of DP are discussed, and various issues related to implementation of DP are outlined. The development of computer-aided pathologic diagnostic tools and their limitations are also discussed.

Key Words: Digital pathology; Computer-aided pathology; Artificial intelligence; Deep learning

Received: December 24, 2019 **Accepted:** December 31, 2019
Corresponding Author: Heounjeong Go, MD, PhD, Department of Pathology, Asan Medical Center, University of Ulsan College of Medicine, 88 Olympic-ro 43-gil, Seoul 05505, Korea
Tel: +82-2-3010-5888, Fax: +82-2-472-7898, E-mail: damul37@amc.seoul.kr

*Soojeong Nam, Yosep Chong, Chan Kwon Jung, and Tae-Yeong Kwak contributed equally to this work.

Digital pathology (DP) is now one of the biggest issues facing the field of pathology. DP is a remarkable innovation that changes the paradigm of microscope-based pathology, which has existed for over 100 years. DP alters the way diagnostic tools represent pathologic images from the microscope to the computer screen and has changed storage media from glass slides to digitalized image files. Digitalized pathologic images stored in computer servers or cloud systems can be transmitted over the Internet, thus changing the temporal and spatial domain of pathologic diagnosis. In addition, machine learning allows software assisting in diagnosis to be developed and applied more actively and effectively.

This review describes various concepts related to DP and computer-aided pathologic diagnosis (CAPD), current applications of DP, and various issues related to the implementation of DP. It also briefly introduces the development of computer-aided diagnostic tools and their limitations.

DIGITAL PATHOLOGY AND COMPUTER-AIDED PATHOLOGY

DP, which initially delineated the process of digitizing whole slide images (WSIs) using advanced slide scanning technology, is now a generic term that includes artificial intelligence (AI)–based approaches for detection, segmentation, diagnosis, and analysis of digitalized images [1]. WSI indicates digital representation of an entire histopathologic glass slide at microscopic resolution [2]. Over the last two decades, WSI technology has evolved to encompass relatively high resolution, increased scanner capacity, faster scan speed, smaller image file sizes, and commercialization. The development of appropriate image management systems (IMS) and a seamless interface connection between existing hospital systems such as electronic medical records (EMR), picture archiving communication systems (PACS), and laboratory information systems (LIS) (also referred to as the pathol-

pISSN 2383-7837
eISSN 2383-7845

ogy order communication system) has stabilized, cheaper storage systems have been established, and streaming technology for large image files has been developed [3,4]. Mukhopadhyay et al. [5] evaluated the diagnostic performance of digitalized images compared to microscopic images on specimens from 1,992 patients with different tumor types diagnosed by 16 surgical pathologists. Primary diagnostic performance with digitalized WSIs was not inferior to that achieved with light microscopy-based approaches (with a major discordance rate from the reference standard of 4.9% for WSI and 4.6% for microscopy) [5].

Computer-aided pathology (CAP, also referred to as computer-aided pathologic diagnostics, computational pathology, and computer-assisted pathology) refers to a computational diagnosis system or a set of methodologies that utilizes computers or software to interpret pathologic images [2,6]. The Digital Pathology Association does not limit the definition of computational pathology to computer-based methodologies for image analysis, but rather as a field of pathology that uses AI methods to combine pathologic images and metadata from a variety of related sources to analyze patient specimens [2]. The performance of computer-aided diagnostic tools has improved with the development of AI and computer vision technology. Digitalized WSIs facilitate the development of computer-aided diagnostic tools through AI applications of intelligent behavior modeled by machines [7].

Machine learning (ML) is a subfield within AI that develops algorithms and technologies. In 1959, Arthur Samuel defined ML as a "field of study that gives computers the ability to learn without being explicitly programmed" [8]. Artificial neural networks (ANNs) are a statistical learning algorithm inspired by biological neural networks such as the human neural architecture in ML. ANN refers to a general model of artificial neurons (nodes) that form a network by synapse binding and have the ability to solve problems by changing synapse strength through learning [9]. Deep learning (DL), a particular approach of ML, comprises multiple layers of neural networks that usually include an input layer, an output layer, and multiple hidden layers [10]. Convolutional neural networks (CNNs) are a type of deep, feed-forward ANN used to analyze visual images. CNN is classified as a DL algorithm that is most commonly applied to image analysis [11]. Successful computer-aided pathologic diagnostic tools are being actively devised using AI techniques, particularly DL models [12].

APPLICATION OF DIGITAL PATHOLOGY

DP covers all pathologic activities using digitalized pathologic images generated by digital scanners, and encompasses the primary diagnosis on the computer monitor screen, consultation by telepathology, morphometry by image analysis software, multidisciplinary conferences and student education, quality assurance activities, and enhanced diagnosis by CAP.

Recently, primary diagnosis on computer monitor screens using digitalized pathologic images has been practically approved by the Food and Drug Administrations (FDA) of the United States of America, the European Union, and Japan [13-15]. Dozens of validation studies have compared the diagnostic accuracy of DP and conventional microscopic diagnosis during the last decade [5,16]. Although most studies have demonstrated no inferiority of the diagnostic accuracy of whole slide imaging compared to conventional microscopy, study sample sizes were mostly limited, and the level of evidence was not high enough (only level III and IV). Therefore, an appropriate internal validation study for diagnostic concordance between whole slide imaging and conventional microscopic diagnosis should be performed before implementing DP into individual laboratories according to the guidelines suggested by major study groups and leading countries.

Telepathology primarily indicates a system that enables pathologic diagnosis by transmitting live pathology images through online connections using a microscopic system with a remote-controlled, motorized stage. The limited meaning of "telediagnosis" can be used in certain clinical situations in which a pathologic diagnosis is made in a remote facility without pathologists. Due to recent advances in whole slide imaging technology, faster and more accurate acquisition and sharing of high quality digital images is now possible. Telepathology has evolved so that DP data can be easily used, shared, and exchanged on various systems and devices using cloud systems. Because of this ubiquitous accessibility, network security and deidentification of personal information have never been more important [13].

Morphometric analysis and CAPD techniques will be further accelerated by implementation of DP. Ki-67 labeling index is traditionally considered one of the most important prognostic markers in breast cancer, and various image analysis software programs based on ML have been developed for accurate and reproducible morphometric analysis. However, DL is more powerful for more complex pathologic tasks such as mitosis detection for breast cancers, microtumor metastasis detection in sentinel lymph nodes, and Gleason scoring for prostate biopsies. Furthermore, DP facilitates the use of DL in pathologic image analysis by providing an enormous source of training data.

DP is also a new opportunity for life-changing advances in

 https://doi.org/10.4132/jptm.2019.12.31

education and multidisciplinary conferences. It enables easy sharing of pathologic data to simplify preparation of education and conference materials. DP mostly uses laboratory automation systems and tracking identification codes, which reduces potential human errors and contributes to patient safety. DP also simplifies pathologic review of archived slides. By adopting CAPD tools based on DL to review diagnosis, quality assurance activities can be performed quickly and with less effort. DL can be used to assess diagnostic errors and the staining quality of each histologic slide.

When combined with other medical information, such as the EMR, hospital information system (HIS), public health information and resources, medical imaging data systems like PACS, and genomic data such as next-generation sequencing, DP provides the basis for revolutionary innovation in medical technology.

IMPLEMENTATION OF DIGITAL PATHOLOGY SYSTEM FOR CLINICAL DIAGNOSIS

Recent technological advances in WSI systems have accelerated the implementation of digital pathology system (DPS) in pathology. The use of WSI for clinical purposes includes primary diagnosis, expert consultation, intraoperative frozen section consultation, off-site diagnosis, clinicopathologic conferences, education, and quality assurance. The DPS for in vitro diagnostic use comprises whole digital slide scanners, viewing and archiving management systems, and integration with HIS and LIS. Image viewing software includes image analysis systems. Pathologists interpret WSIs and render diagnoses using the DPS set up with adequate hardware, software, and hospital networks.

Most recent WSI scanners permit high-speed digitization of whole glass slides and produce high-resolution WSI. However, there are still differences in scanning time, scan error rate, image resolution, and image quality among WSI scanners. WSI scanners differ with respect to their functionality and features, and most image viewers are provided by scanner vendors [4]. When selecting a WSI scanner for clinical diagnosis, it is important to consider the following factors: (1) volume of slides, (2) type of specimen (eg, tissue section slides, cytology slides, or hematopathology smears), (3) feasibility of z-stack scanning (focus stacking), (4) laboratory needs for oil-immersion scanning, (5) laboratory needs for both bright field and fluorescence scanning, (6) type of glass slides (e.g., wet slides, unusual size), (7) slide barcode readability, (8) existing space constraints in the laboratory, (9) functionality of image viewer and management system provided by vendor, (10) bidirectional integration with existing information systems, (11) communication protocol (e.g., XML, HL7) between DPS and LIS, (12) whether image viewer software is installed on the server or on the local hard disk of each client workstation, (13) whether the viewer works on mobile devices, and (14) open or closed system.

It is crucial to fully integrate the WSI system into the existing LIS to implement DPS in the workflow of a pathology department and decrease turn-around-time [14]. Therefore, information technology (IT) support is vital for successful implementation of DPS. Pathologists should work closely with IT staff, laboratory technicians, and vendors to integrate the DPS with the LIS and HIS. The implementation team should meet regularly to discuss progress on action items and uncover issues that could slow or impede progress.

Resistance to digital transformation can come from any level in the department. Documented processes facilitate staff training and allow smooth onboarding. Regular support and training should be provided until all staff understand the value of DPS and perform their tasks on a regular basis.

DEVELOPMENT OF COMPUTER-AIDED PATHOLOGIC DIAGNOSTIC TOOLS

Basics of image analysis: cellular analysis and color normalization

The earliest attempt at DP, so-called cell segmentation, detected cells via nuclei, cytoplasm, and structure. Because the cells are the basic units of histopathology images, identification of the color, intensity, and morphology of nuclei and cytoplasm through cell segmentation is the first and most important step in image analysis. Cell segmentation has been tried in immunohistochemistry (IHC) analysis and hematoxylin and eosin (H&E) staining and is a fundamental topic for computational image analysis to achieve quantitative histopathologic representation.

A number of cell segmentation algorithms have been developed for histopathologic image analysis [17,18]. Several classical ML studies reported that cellular features of H&E staining, nuclear and cytoplasmic texture, nuclear shape (e.g., perimeter, area, tortuosity, and eccentricity) and nuclear/cytoplasmic ratio carry prognostic significance [19-22]. Cell segmentation algorithms have usually been studied in IHC, which has a relatively simple color combination and limited analysis color channel compared to H&E staining [23]. For example, IHC staining for estrogen receptor (ER), progesterone receptor (PR), human epidermal growth factor receptor 2 (HER2), and Ki-67 is routinely performed in breast cancer diagnostics to determine adjuvant

treatment strategy and predict prognosis [24,25]. Automated scoring algorithms for this IHC panel are the most developed and most commonly used, and some are FDA-approved [26-28]. Those automated algorithms are superior alternatives to manual biomarker scoring in most aspects. Many workflow steps can be automated or executed without pathologic expertise to reduce the use of a pathologist's time.

Conventional ML algorithms for cell segmentation utilize combinations of median filtering, thresholds, watershed segmentation, contour models, shape dictionaries, and categorizing [26]. It is often necessary to adjust detailed settings when using these algorithms to avoid under- and over-segmentation (Fig. 1). Nuclear staining (e.g., ER, PR, and Ki-67) and membranous staining (e.g., HER2) clearly shows the boundary between nuclei or cells, whereas cytoplasmic staining has no clear cell boundary, limiting algorithm development. However, the recent development of technology using DL has resulted in algorithms showing better performance [29,30]. Quantitative analysis has recently been included in various tumor diagnosis, grading, and staging criteria. Neuroendocrine tumor grading requires a distinct mitotic count and/or Ki-67 labeling index [31,32]. With recent clinical applications of targeted therapy and immunotherapy, quantification of various biomarkers and tumor microenvironmental immune cells has become important [33-35]. Therefore, accurate cell segmentation algorithms will play an important role in diagnosis, predicting prognosis, and determining treatment strategy.

Color normalization is a standardization or scaling procedure often used in the data processing phase in preparation for ML. The quality of H&E stained slides varies by institution and is affected by dye concentration, staining time, formalin fixation time, freezing, cutting skill, type of glass slide, and fading color after staining (Fig. 2). H&E stained slides also show diversity within the same institution (Fig. 2A, D). The color of each slide is also affected by the slide scanner and settings. If excessive staining variability is present in a dataset, application of a threshold may produce different results due to different staining or imaging protocols rather than due to unique tissue characteristics. Therefore, color normalization for such algorithms improves their overall performance. A number of color normalization approaches have been developed that utilize intensity thresholds, histogram normalization, stain separation, color deconvolution, structure-based color classification, and generative adversarial networks [36-41]. However, it is important to evaluate and prevent the image distortion that can result from these techniques.

Region of interest selection and manual versus automated image annotations

Pathologists play an important role in guiding algorithm development. Pathologists have expertise in the clinicopathologic purpose of algorithm development, technical knowledge of tissue processing, selecting data for use in an algorithm, and validating the quality of generated output to produce useful results. Region of interest (ROI) selection for algorithm development is usually

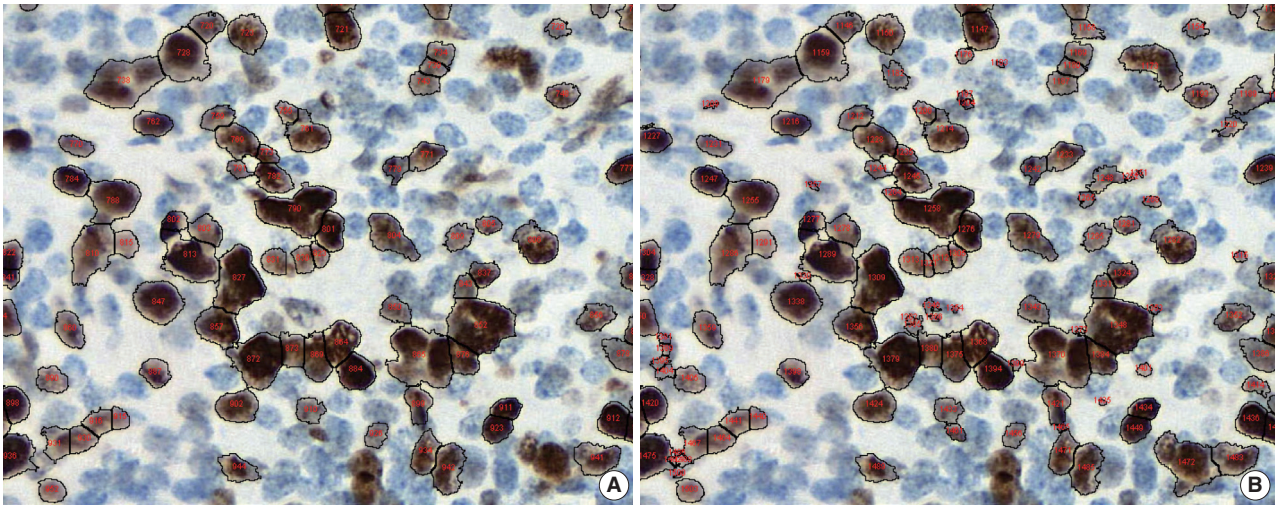

Fig. 1. Under- (A) and over-nuclear (B) nuclear segmentation. Under- and over-nuclear segmentation results in ImageJ (open-source tool). Immunohistochemical staining images for Ki-67 antibody shows nuclear presentation. As the settings for range of diameter, area eccentricity and staining intensity change, segmentation algorithm shows different results. (A) algorithm failed to detect some positive nuclei. (B) algorithm showed that too many small non-specific stains were counted in the positive nucleus, resulting in over-nuclear counting. As a result, the count of (A) algorithm was 88, and the count of (B) algorithm was 130.

https://doi.org/10.4132/jptm.2019.12.31

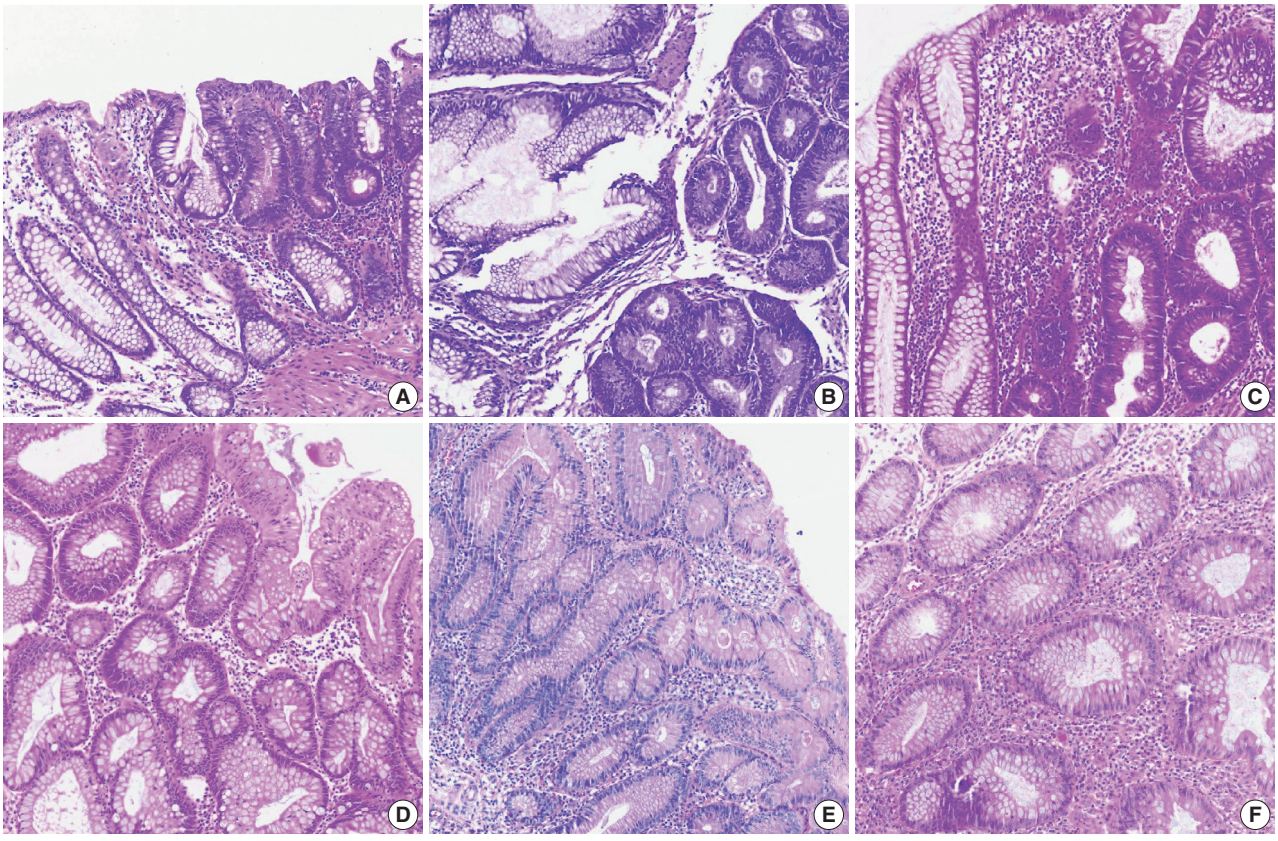

Fig. 2. Various hematoxylin and eosin (H&E) staining color attributes. (A–F) Six H&E staining images for colonic mucosa represent color properties that usually occur in various laboratory settings or image scanning methods. Panels A and D were stained in the same laboratory.

performed by a pathologist. Depending on the subject, various ROI size assignments may be required. Finely defined ROIs allow an algorithm to focus on specific areas or elements, resulting in faster and more accurate output. Annotation is the process of communicating about ROIs with an algorithm. Annotations allow the algorithm to know that a particular slide area is important and focus on it for analysis. Annotation includes manual and automatic methods. In addition to ensuring the quality of annotations, pathologists can gain valuable insight into slide data and discover specific problems or potential pitfalls to consider during algorithm development.

Manual annotation involves drawing on the slide image with digital dots, lines, or faces to indicate the ROI of the algorithm. Both inclusion and exclusion annotations may be present depending on the algorithm analysis method. Inclusion and exclusion annotations may target necrosis, contamination, and any other type of artifact. However, manual annotation is costly and time-consuming because it must be performed by skilled technicians with confirmation and approval by a pathologist. Various tools have been developed to overcome the shortcomings of manual annotations, including automated image annotation and pre-developed commercial software packages [42]. Because these tools may compromise accuracy, a pathologist must confirm the accuracy of automated annotations. Recently, several studies have tried to overcome the difficulties of the annotation step through weakly supervised learning from the label data of slides or mixing label data with detailed annotation data [43]. Crowdsourcing is also used, which involves engaging many people, including non-professionals, using web-based tools. Crowdsourcing has been used successfully for several goals [44,45]. While it is cheaper and faster than expert pathologist annotations, it is also more error-prone. Some detailed pathologic analyzes are available only to well-trained professionals.

Pathologist's role in CAPD tool development and data review

Pathologists play an important role in CAPD tool development, from the data preparation stage to review of interpretations generated by the algorithm. Pathologists should play a role in identifying and resolving problems in every process of the

algorithm during development [46]. If biomarker expression analysis via staining intensity is included in CAPD tool development, the final algorithm threshold should be reviewed and approved by a pathologist before each data generation. For example, pathologists also confirm and advise whether cells or other structures are correctly identified and enumerated, whether the target tissue can be correctly identified and analyzed separately from other structures, and whether staining intensity is properly classified. The algorithm does not have to be performed with 100% precision and accuracy, but a reasonable level of performance must be met that is relevant to the general goals of the analysis. Clinical studies that inform treatment decisions or prognosis may need to meet more stringent criteria for accurate classification, including staining methods and types of scanners. Certain samples that do not meet these predetermined criteria should be detected and excluded from the algorithm.

When the test CAPD tool meets the desired performance criteria, validation can be performed on a series of slides. Pathologists should review the resulting data derived from the algorithm to examine the CAPD tool's performance. Analysis review should inform general questions, data interrogated through image analysis, and clinical impact on patients. Only results from CAPD tools that have passed pathologist and general performance criteria should be included in the final step. Quality assurance at different stages of slide creation is important to achieve optimal value in image analysis. Thus, humans are still required for quality assurance of digital images before they are processed by image analysis algorithms. Similarly, the technical aspects of slide digitization can affect the results of digital images and final image analysis. Color normalization techniques can help to solve these problems.

To clinically use a CAPD tool, it is important to know the intended use of the algorithm and ensure that the CAPD tool is properly validated for specific tissue conditions, such as frozen tissue, formalin-fixed tissue, or certain types of organs. In the future, commercial solutions for CAP will be available in the clinical field. However, CAPD tools must be internally validated by pathologists at each institution before they are used for clinical practice.

LIMITATIONS OF CURRENT COMPUTER-AIDED PATHOLOGY

As many have already pointed out, the current AI-based CAP has several limitations. Tizhoosh and Liron have listed a number of problems that CAP should address, including vulnerability to adversarial attacks, capability limited to a certain diagnostic task, obscured diagnostic process, and lack of interpretability [47]. Specifically, lack of interpretability is unacceptable to the medical society. Other literature lists practical issues which may apply to pathologic AI: slow execution time of CAP, opacity of CAPD development process, insufficient clinical validation of CAP, and limited impact on health economics [48]. Another substantial issue mentioned was frequent workflow switching induced by limited integration of CAPD applications within the current pathology workflow. Beyond disease detection and grading, CAP should be able to provide an integrated diagnosis with a number of analyses on various data [49]. Rashidi et al. [50] emphasized the role of pathologists in developing CAPD tools, especially in dealing with CAP performance problems caused by lack of data and model limitations. These limitations can be summarized as follows: (1) lack of confidence in diagnosis results, (2) inconvenience in practical use, and (3) simplicity of function (Table 1). These limitations can be overcome by close collaboration among AI researchers, software engineers, and medical experts.

Confidence in diagnostic results can be improved by formalizing the CAP development and validation processes, expanding the size of validation data, and enhancing understanding of the CAPD.

CAPD products can only enter the market as medical devices with the approval of regulatory agencies. The approval process for medical devices requires validation of the medical device development process, including validation of CAPD algorithms if applicable [51]. It is notable that regulatory agencies are already preparing for regulation of adaptive medical devices that learn from information acquired in operation. To formalize the validation process, it is desirable to assess the performance change of the CAP based on input variation induced by several factors, such as quality of tissue samples, slide preparation process, staining

Table 1. Current limitations of AI-based computer-assisted pathological diagnosis

Limitations
Lack of confidence in diagnostic results
Opacity of the diagnostic process
Lack of interpretability of diagnostic results
Opacity in the AI development process
Insufficient validation of AI
Inconvenience in practical use
Slow execution time of AI
Lack of clinical workflow integration
Simplicity of function
Limited to certain data and specific tasks

AI, artificial intelligence.

https://doi.org/10.4132/jptm.2019.12.31

protocol, and slide scanner characteristics. This is similar to the validation process for existing in vitro diagnostic devices such as reagents. Validation data that covers diverse demographics is desirable. The use of validation data covering multiple countries and institutions increases the credibility of validation results [43]. Regulatory agencies require data from two or more medical institutions in clinical trials for medical device approval, so CAPDs introduced in the market as approved medical devices should be sufficiently validated.

The ability to explain CAP is a hot topic in current AI research. According to a recently published book on the interpretability of ML, which comprise the majority of current AI, interpretation approaches to complex ML models are largely divided into two categories: visualization of important features in the decision process and example-based interpretation of decision output [52]. Important feature visualization in ML models includes Visualizing Activation Layers [53], SHAP [54], Grad-CAM [55], and LIME [56]. These methods can be used to interpret a model's decision process by identifying parts of the input that have played a role. In applications to pathologic image analysis, an attention mechanism was used to visualize epithelial cell areas [57]. Arbitrary generated counterfactual examples can be used to describe how input change affects to model output [58]. Case-based reasoning [59,60] can be combined with the interpretation target model to demonstrate consistency between model output and reasoning output of the same input [61]. Similar image search can also be used to show that AI decisions are similar to human annotations on the same pathologic image, and systems such as SMILY can be used for this purpose [62].

Inconvenience in practical use can be solved by accelerating execution of AI and integrating it with other existing IT systems in medical institutions. In addition to hardware that provides sufficient computing power, software optimization must be achieved to accelerate AI execution. This includes removal of data processing bottlenecks and data access redundancy as well as model size reduction. Medical IT systems include HIS, EMR, and PACS, which are integrated with each other and operate within a workflow. CAPD systems, digital slide scanners, and slide IMS should participate in this integration so they can be easily utilized in a real-world workflow. The problem of CAPD systems being limited to specific data and tasks can be relieved by adding more data and more advanced AI technologies, including multi-task learning, continual learning, and reinforcement learning.

CONCLUSION

DP and CAP are revolutionary for pathology. If used properly, DP and CAP are expected to improve convenience and quality in pathology diagnosis and data management. However, a variety of challenges remain in implementation of DPS, and many aspects must be considered when applying CAP. Implementation is not limited to the pathology department and may involve the whole institution or even the entire healthcare system. CAP is becoming clinically available with the application of DL, but various limitations remain. The ability to overcome these limitations will determine the future of pathology.

ORCID

Soojeong Nam: https://orcid.org/0000-0001-9376-359X
Yosep Chong: https://orcid.org/0000-0001-8615-3064
Chan Kwon Jung: https://orcid.org/0000-0001-6843-3708
Tae-Yeong Kwak: https://orcid.org/0000-0001-9171-7258
Ji Youl Lee: https://orcid.org/0000-0001-6775-1157
Jihwan Park: https://orcid.org/0000-0002-4027-1038
Mi Jung Rho: https://orcid.org/0000-0002-9862-0122
Heounjeong Go: https://orcid.org/0000-0003-0412-8709

Author Contributions

Conceptualization: SN, YC, CKJ, TYK, HG.
Funding acquisition: JYL.
Investigation: SN, YC, CKJ, TYK, JYL, JP, MJR, HG.
Supervision: HG.
Writing—original draft: SN, YC, CKJ, TYK, HG.
Writing—review & editing: SN, YC, CKJ, TYK, HG.

Conflicts of Interest

C.K.J., the editor-in-chief and Y.C., contributing editor of the *Journal of Pathology and Translational Medicine*, were not involved in the editorial evaluation or decision to publish this article. All remaining authors have declared no conflicts of interest.

Funding

This work was supported by the Institute for Information & Communications Technology Promotion (IITP) grant funded by the Korean government (MSIT) (2018-2-00861, Intelligent SW Technology Development for Medical Data Analysis).

REFERENCES

1. Bera K, Schalper KA, Rimm DL, Velcheti V, Madabhushi A. Artificial intelligence in digital pathology: new tools for diagnosis and precision oncology. Nat Rev Clin Oncol 2019; 16: 703-15.
2. Abels E, Pantanowitz L, Aeffner F, et al. Computational pathology definitions, best practices, and recommendations for regulatory guidance: a white paper from the Digital Pathology Association. J Pathol 2019; 249: 286-94.
3. He J, Baxter SL, Xu J, Xu J, Zhou X, Zhang K. The practical implementation of artificial intelligence technologies in medicine. Nat Med 2019; 25: 30-6.
4. Evans AJ, Salama ME, Henricks WH, Pantanowitz L. Implementation of whole slide imaging for clinical purposes: issues to consider from the perspective of early adopters. Arch Pathol Lab Med 2017; 141: 944-59.
5. Mukhopadhyay S, Feldman MD, Abels E, et al. Whole slide imaging versus microscopy for primary diagnosis in surgical pathology: a multicenter blinded randomized noninferiority study of 1992 cases (pivotal study). Am J Surg Pathol 2018; 42: 39-52.
6. Niazi MK, Parwani AV, Gurcan MN. Digital pathology and artificial intelligence. Lancet Oncol 2019; 20: e253-61.
7. Hamet P, Tremblay J. Artificial intelligence in medicine. Metabolism 2017; 69S: S36-40.
8. Simon P. Too big to ignore: the business case for big data. Hoboken: John Wiley & Sons, 2013.
9. Yao X. Evolving artificial neural networks. Proc IEEE 1999; 87: 1423-47.
10. Deng L, Yu D. Deep learning: methods and applications. Found Trends Signal Process 2014; 7: 197-387.
11. Collobert R, Weston J. A unified architecture for natural language processing: deep neural networks with multitask learning. In: Proceedings of the 25th International Conference on Machine Learning; 2008 Jul 5-9; Helsinki, Finland. New York: Association for Computing Machinery, 2008; 160-7.
12. Wang S, Yang DM, Rong R, et al. Artificial intelligence in lung cancer pathology image analysis. Cancers (Basel) 2019; 11: E1673.
13. Garcia-Rojo M. International clinical guidelines for the adoption of digital pathology: a review of technical aspects. Pathobiology 2016; 83: 99-109.
14. Hanna MG, Reuter VE, Samboy J, et al. Implementation of digital pathology offers clinical and operational increase in efficiency and cost savings. Arch Pathol Lab Med 2019; 143: 1545-55.
15. Hanna MG, Pantanowitz L, Evans AJ. Overview of contemporary guidelines in digital pathology: what is available in 2015 and what still needs to be addressed? J Clin Pathol 2015; 68: 499-505.
16. Snead DR, Tsang YW, Meskiri A, et al. Validation of digital pathology imaging for primary histopathological diagnosis. Histopathology 2016; 68: 1063-72.
17. Irshad H, Veillard A, Roux L, Racoceanu D. Methods for nuclei detection, segmentation, and classification in digital histopathology: a review-current status and future potential. IEEE Rev Biomed Eng 2014; 7: 97-114.
18. Wang S, Yang DM, Rong R, Zhan X, Xiao G. Pathology image analysis using segmentation deep learning algorithms. Am J Pathol 2019; 189: 1686-98.
19. Gurcan MN, Pan T, Shimada H, Saltz J. Image analysis for neuroblastoma classification: segmentation of cell nuclei. Conf Proc IEEE Eng Med Biol Soc 2006; 1: 4844-7.
20. Ballaro B, Florena AM, Franco V, Tegolo D, Tripodo C, Valenti C. An automated image analysis methodology for classifying megakaryocytes in chronic myeloproliferative disorders. Med Image Anal 2008; 12: 703-12.
21. Korde VR, Bartels H, Barton J, Ranger-Moore J. Automatic segmentation of cell nuclei in bladder and skin tissue for karyometric analysis. Anal Quant Cytol Histol 2009; 31: 83-9.
22. Veta M, van Diest PJ, Kornegoor R, Huisman A, Viergever MA, Pluim JP. Automatic nuclei segmentation in H&E stained breast cancer histopathology images. PLoS One 2013; 8: e70221.
23. Ruifrok AC, Katz RL, Johnston DA. Comparison of quantification of histochemical staining by hue-saturation-intensity (HSI) transformation and color-deconvolution. Appl Immunohistochem Mol Morphol 2003; 11: 85-91.
24. Flanagan MB, Dabbs DJ, Brufsky AM, Beriwal S, Bhargava R. Histopathologic variables predict Oncotype DX recurrence score. Mod Pathol 2008; 21: 1255-61.
25. Hammond ME, Hayes DF, Dowsett M, et al. American Society of Clinical Oncology/College of American Pathologists guideline recommendations for immunohistochemical testing of estrogen and progesterone receptors in breast cancer (unabridged version). Arch Pathol Lab Med 2010; 134: e48-72.
26. Al-Kofahi Y, Lassoued W, Lee W, Roysam B. Improved automatic detection and segmentation of cell nuclei in histopathology images. IEEE Trans Biomed Eng 2010; 57: 841-52.
27. Stalhammar G, Fuentes Martinez N, Lippert M, et al. Digital image analysis outperforms manual biomarker assessment in breast cancer. Mod Pathol 2016; 29: 318-29.
28. Zarrella ER, Coulter M, Welsh AW, et al. Automated measurement of estrogen receptor in breast cancer: a comparison of fluorescent and chromogenic methods of measurement. Lab Invest 2016; 96: 1016-25.
29. Madabhushi A, Lee G. Image analysis and machine learning in

digital pathology: Challenges and opportunities. Med Image Anal 2016; 33: 170-5.
30. Williams BJ, Bottoms D, Treanor D. Future-proofing pathology: the case for clinical adoption of digital pathology. J Clin Pathol 2017; 70: 1010-8.
31. Kloppel G, La Rosa S. Ki67 labeling index: assessment and prognostic role in gastroenteropancreatic neuroendocrine neoplasms. Virchows Arch 2018; 472: 341-9.
32. Chai SM, Brown IS, Kumarasinghe MP. Gastroenteropancreatic neuroendocrine neoplasms: selected pathology review and molecular updates. Histopathology 2018; 72: 153-67.
33. Mok TS, Wu YL, Kudaba I, et al. Pembrolizumab versus chemotherapy for previously untreated, PD-L1-expressing, locally advanced or metastatic non-small-cell lung cancer (KEYNOTE-042): a randomised, open-label, controlled, phase 3 trial. Lancet 2019; 393: 1819-30.
34. Steven A, Fisher SA, Robinson BW. Immunotherapy for lung cancer. Respirology 2016; 21: 821-33.
35. Yang Y. Cancer immunotherapy: harnessing the immune system to battle cancer. J Clin Invest 2015; 125: 3335-7.
36. Khan AM, Rajpoot N, Treanor D, Magee D. A nonlinear mapping approach to stain normalization in digital histopathology images using image-specific color deconvolution. IEEE Trans Biomed Eng 2014; 61: 1729-38.
37. Bejnordi BE, Litjens G, Timofeeva N, et al. Stain specific standardization of whole-slide histopathological images. IEEE Trans Med Imaging 2016; 35: 404-15.
38. Vahadane A, Peng T, Sethi A, et al. Structure-preserving color normalization and sparse stain separation for histological images. IEEE Trans Med Imaging 2016; 35: 1962-71.
39. Zarella MD, Yeoh C, Breen DE, Garcia FU. An alternative reference space for H&E color normalization. PLoS One 2017; 12: e0174489.
40. Miyato T, Kataoka T, Koyama M, Yoshida Y. Spectral normalization for generative adversarial networks. Preprint at: https://arxiv.org/abs/1802.05957 (2018).
41. Shaban MT, Baur C, Navab N, Albarqouni S. StainGAN: stain style transfer for digital histological images. Preprint at: https://arxiv.org/abs/1804.01601 (2018).
42. Aeffner F, Zarella MD, Buchbinder N, et al. Introduction to digital image analysis in whole-slide imaging: a white paper from the Digital Pathology Association. J Pathol Inform 2019; 10: 9.
43. Campanella G, Hanna MG, Geneslaw L, et al. Clinical-grade computational pathology using weakly supervised deep learning on whole slide images. Nat Med 2019; 25: 1301-9.
44. Albarqouni S, Baur C, Achilles F, Belagiannis V, Demirci S, Navab N. AggNet: deep learning from crowds for mitosis detection in breast cancer histology images. IEEE Trans Med Imaging 2016; 35: 1313-21.
45. Irshad H, Montaser-Kouhsari L, Waltz G, et al. Crowdsourcing image annotation for nucleus detection and segmentation in computational pathology: evaluating experts, automated methods, and the crowd. Pac Symp Biocomput 2015: 294-305.
46. Aeffner F, Wilson K, Bolon B, et al. Commentary: roles for pathologists in a high-throughput image analysis Team. Toxicol Pathol 2016; 44: 825-34.
47. Tizhoosh HR, Pantanowitz L. Artificial intelligence and digital pathology: challenges and opportunities. J Pathol Inform 2018; 9: 38.
48. Serag A, Ion-Margineanu A, Qureshi H, et al. Translational AI and deep learning in diagnostic pathology. Front Med (Lausanne) 2019; 6: 185.
49. Chang HY, Jung CK, Woo JI, et al. Artificial intelligence in pathology. J Pathol Transl Med 2019; 53: 1-12.
50. Rashidi HH, Tran NK, Betts EV, Howell LP, Green R. Artificial intelligence and machine learning in pathology: the present landscape of supervised methods. Acad Pathol 2019; 6: 2374289519873088.
51. U.S. Food and Drug Administration. Artificial intelligence and machine learning in software as a medical device. Silverspring: U.S. Food and Drug Administration, 2019.
52. Molnar C. Interpretable machine learning [Internet]. The Author, 2018 [cited 2019 Nov 2]. Available from: https://christophm.github.io/interpretable-ml-book/.
53. Kahng M, Andrews PY, Kalro A, Polo Chau DH. ACTIVIS: visual exploration of industry-scale deep neural network models. IEEE Trans Vis Comput Graph 2018; 24: 88-97.
54. Lundberg SM, Lee SI. A unified approach to interpreting model predictions. In: Advances in Neural Information Processing Systems. Proceedings of the 31st Neural Information Processing Systems (NIPS 2017); 2017 Dec 4-9; Long Beach, CA, USA. Red Hook: Curran Associates Inc., 2017; 4765-74.
55. Selvaraju RR, Cogswell M, Das A, Vedantam R, Parikh D, Batra D. Grad-CAM: visual explanations from deep networks via gradient-based localization. Int J Comput Vision 2019 Oct 11 [Epub]. https://doi.org/10.1007/s11263-019-01228-7.
56. Ribeiro MT, Singh S, Guestrin C. Why should I trust you? Explaining the predictions of any classifier. New York: Association for Computing Machinery, 2016; 1135-44.
57. Ilse M, Tomczak JM, Welling M. Attention-based deep multiple instance learning. In: Proceedings of the 35th International Conference on Machine Learning; 2018 Jul 10-15; Stockholm, Sweden. Cambridge: Proceedings of Machine Learning Research, 2018; 3376-91.
58. Mothilal RK, Sharma A, Tan C. Explaining machine learning classi-

fiers through diverse counterfactual explanations. Preprint at: https://arxiv.org/abs/1905.07697 (2019).
59. Richter MM, Weber RO. Case-based reasoning: a textbook. Berlin: Springer-Verlag, 2013; 546.
60. Watson I, Marir F. Case-based reasoning: a review. Knowl Eng Rev 1994; 9: 327-54.
61. Keane MT, Kenny EM. How case based reasoning explained neural networks: an XAI survey of post-hoc explanation-by-example in ANN-CBR twins. Preprint at: https://arxiv.org/abs/1905.07186 (2019).
62. Hegde N, Hipp JD, Liu Y, et al. Similar image search for histopathology: SMILY. NPJ Digit Med 2019; 2: 56.

https://doi.org/10.4132/jptm.2019.12.31

JPTM
Journal of Pathology and Translational Medicine 2020; 54: 135-145
https://doi.org/10.4132/jptm.2019.11.06

ORIGINAL ARTICLE

Colorectal epithelial neoplasm associated with gut-associated lymphoid tissue

Yo Han Jeon, Ji Hyun Ahn, Hee Kyung Chang

Department of Pathology, Kosin University College of Medicine, Busan, Korea

Background: Colorectal epithelial neoplasm extending into the submucosal gut-associated lymphoid tissue (GALT) can cause difficulties in the differential diagnosis. Regarding GALT-associated epithelial neoplasms, a few studies favor the term "GALT carcinoma" while other studies have mentioned the term "GALT-associated pseudoinvasion/epithelial misplacement (PEM)". **Methods:** The clinicopathologic characteristics of 11 cases of colorectal epithelial neoplasm associated with submucosal GALT diagnosed via endoscopic submucosal dissection were studied. **Results:** Eight cases (72.7%) were in males. The median age was 59 years, and age ranged from 53 to 73. All cases had a submucosal tumor component more compatible with GALT-associated PEM. Eight cases (72.7%) were located in the right colon. Ten cases (90.9%) had a non-protruding endoscopic appearance. Nine cases (81.8%) showed continuity between the submucosal and surface adenomatous components. Nine cases showed (81.8%) focal defects or discontinuation of the muscularis mucosae adjacent to the submucosal GALT. No case showed hemosiderin deposits in the submucosa or desmoplastic reaction. No case showed single tumor cells or small clusters of tumor cells in the submucosal GALT. Seven cases (63.6%) showed goblet cells in the submucosa. No cases showed oncocytic columnar cells lining submucosal glands. **Conclusions:** Our experience suggests that pathologists should be aware of the differential diagnosis of GALT-associated submucosal extension by colorectal adenomatous neoplasm. Further studies are needed to validate classification of GALT-associated epithelial neoplasms.

Key Words: Humans; Colorectal neoplasms; Lymphoid tissue; Adenomatous polyps

Received: September 2, 2019 **Revised:** November 4, 2019 **Accepted:** November 5, 2019
Corresponding Author: Hee Kyung Chang, MD, Department of Pathology, Kosin University College of Medicine, 262 Gamcheon-ro, Seo-gu, Busan 49267, Korea
Tel: 82-51-990-6323, Fax: 82-51-241-7420, E-mail: changhkg@ns.kosinmed.or.kr

The gut-associated lymphoid tissue (GALT) system consists of scattered lymphoid cells in the lamina propria and organized lymphoid aggregates or follicles in the mucosa or submucosa [1-5]. GALT serves as part of both the immune system and the mucosal repair system of the gastrointestinal tract [1,6]. The association between GALT and various colorectal pathologic conditions-from inflammatory bowel disease to benign and malignant neoplasms-has been discussed [7-10]. Colorectal epithelial neoplasms located in the submucosa and surrounded by GALT may be encountered in daily practice and occasionally cause difficulties in differential diagnosis. The term "GALT carcinoma" has been suggested as a distinct malignancy arising from the GALT mucosal domain and representing the "third pathway of colorectal carcinogenesis". However, GALT carcinoma is not recognized as a distinct histologic subtype in current colorectal cancer classifications [2,11-28]. A few studies have suggested GALT-associated pseudoinvasion/epithelial misplacement (PEM) as a consideration in the differential diagnosis of GALT-associated tumors [11,12]. However, there are few studies in the Korean literature clarifying the pathologic nature of colorectal epithelial neoplasms located in submucosal GALT. Herein, we investigated the clinicopathologic characteristics of colorectal epithelial neoplasms associated with submucosal GALT.

MATERIALS AND METHODS

Case selection

Eleven cases of colorectal epithelial neoplasm, involving submucosal GALT, identified after endoscopic submucosal dissection, were studied from the pathologic archives of Kosin University Gospel Hospital (Busan, Korea), over a 7-year period from January 2012 to December 2018.

pISSN 2383-7837
eISSN 2383-7845

Clinicopathologic analysis

The following clinicopathologic features were extracted from the medical record: age, sex, location, endoscopic appearance. The location of the neoplasm was classified according to the International Classification of Diseases for Oncology classification [29] and was categorized into either right-sided colon (including cecum, ascending colon, hepatic flexure and transverse colon) or left-sided colon (including splenic flexure, descending colon, sigmoid colon, and rectum) [30].

The endoscopic appearance of the neoplasms were classified according to the Paris classification [31-35]. With regard to the distinction between sessile protruding type (0-Is) and slightly elevated non-protruding type (0-IIa), a more practical definition was applied instead of the definition using the cut-off value of 2.5mm or twice the thickness of surrounding normal colorectal mucosa: a superficial neoplastic lesion with the height more than one-third of the diameter was classified into protruding type [31,35].

Histopathologic evaluation

For each case, hematoxylin and eosin-stained slides were reviewed, and the pathologic diagnoses were reclassified by three pathologists (Y.H.J., J.H.A., and H.K.C.).

Submucosal GALT was defined as lymphoid aggregates or follicles located below the muscularis mucosae [3,6,8]. A colorectal epithelial neoplasm located in the submucosal GALT was defined as a colorectal epithelial neoplasm involving the submucosal GALT.

Conventional adenomas were classified into three subtypes based on the amount of villous component: tubular (villous component less than 25%), tubulovillous (villous component 25% to 75%), and villous adenoma (villous component more than 75%) [36].

Dysplasia was graded into either low-grade or high-grade. Non-complex architecture with elongated and pseudostratified nuclei was graded as low-grade dysplasia [36]. Complex architecture (markedly irregular, crowded, cribriform, or fused glands) with accompanying cytologic features (loss of nuclear polarity, pleomorphic nuclei) was graded as high-grade dysplasia [36]. Dysplastic glands without complex architecture were not considered high-grade dysplasia.

The following histologic features for PEM were evaluated: grade of dysplasia in submucosal glands, continuity of submucosal glands with surface adenomatous component, focal defect of muscularis mucosae adjacent to submucosal GALT, hemosiderin deposits in submucosa, contour of submucosal GALT, cystic dilation of submucosal glands, and admixture of submucosal glands with normal colonic epithelium [11,12,37-45].

The following histologic features suggesting frank invasion were evaluated: desmoplasia, single or small clusters of tumor cells, and lymphovascular invasion [46].

The following histologic features characteristic of GALT carcinoma were evaluated: oncocytic cytoplasm of submucosal glands and depletion of goblet cells in submucosal glands [13-28,47].

The size of the entire tumor was measured to the first digit after the decimal point (cm). The diameter of the largest isolated submucosal lymphoid aggregate or follicle involved by the neoplasm was measured to the second digit after the decimal point (cm).

Immunohistochemical study

To evaluate the muscularis mucosae, immunohistochemical staining for desmin was performed. Paraffin-embedded tissue sections with 5 μm thickness were deparaffinized in xylene and rehydrated by a graded series of ethyl alcohol concentrations. Heat-induced antigen retrieval was carried out in citrate buffer (pH 6.0). Sections were incubated with the primary antibody for desmin (1:200, D33, DAKO, Glostrup, UK) in a Bond-MAX automated immunostainer (Leica, Wetzlar, Germany) according to the manufacturer's protocols. Counterstaining with Mayer's hematoxylin was performed.

Statistical analysis

Clinical features including location (number 1 assigned for right-sided, number 2 assigned for left-sided), sex (number 1 assigned for male, number 2 assigned for female), and endoscopic appearance (number 1 assigned for protruding, number 2 assigned for non-protruding) were analyzed by single sample t test with a test value of 1.5.

The relationship between "the grade of dysplasia in the submucosal GALT" and pathologic features (including pathologic size of the entire lesion and largest diameter of isolated submucosal GALT involved) were analyzed by Mann-Whitney test.

The relationship between "the grade of dysplasia in the submucosal GALT" and the remaining clinicopathologic features (including those for PEM, frank invasion, and GALT carcinoma) were analyzed by chi-square test and Fisher exact probability test.

A p-value less than .05 was considered statistically significant. All statistics were analyzed using SPSS ver. 25.0 (IBM Corp., Armonk, NY, USA).

https://doi.org/10.4132/jptm.2019.11.06

Ethics statement

This retrospective study was approved by the Institutional Review Board of Kosin University Gospel Hospital with a waiver of informed consent (IRB No. 2019-08-009) and performed in accordance with the principles of the Declaration of Helsinki [48].

RESULTS

Clinical characteristics

In the 11 cases of colorectal neoplasms involving submucosal GALT, the median age was 59 years (ranging from 53 to 73 years). Eight cases (72.7%) occurred in males. Only one case (case 3) showed protruding or "dome-shaped" endoscopic appearance. The other 10 cases showed non-protruding endoscopic appearance. Eight cases (72.7%) were in the right-sided colon. Clinical characteristics of the 11 cases were summarized in Tables 1 and 2. With median follow-up duration of 17 months (ranging from 5 to 61 months), no recurrence was identified (data not shown in Tables 1 and 2).

Pathologic features

The pathologic diagnoses of the 11 cases included tubular adenoma with low grade dysplasia (n = 3, 27.3%) and tubular adenoma with high-grade dysplasia (n = 8, 72.7%). Three cases (27.3%) showed high-grade dysplasia in submucosal glands; the other eight cases (72.7%) showed low-grade dysplasia in submucosal glands. Nine cases (81.8%) showed continuity between submucosal and surface adenomatous components. Nine cases showed (81.8%) a focal defect or discontinuation of the muscularis mucosae adjacent to submucosal GALT (Fig. 1). No case showed hemosiderin deposition in the submucosa. Ten cases (90.9%) had rounded or lobular architecture of submucosal GALT involved in the glands; in the other case without rounded

Table 1. Clinicopathologic characteristics of colorectal neoplasm associated with submucosal GALT

	Case 1	Case 2	Case 3	Case 4	Case 5	Case 6	Case 7	Case 8	Case 9	Case 10	Case 11
Age (yr)	56	58	66	53	70	71	55	73	73	59	54
Sex	F	M	F	M	M	M	M	F	M	M	M
Location	Rectum	Ascending	Sigmoid	Ascending	Transverse	Ascending	Rectum	Transverse	Transverse	HF	Transverse
Endoscopic appearance[a]	0-IIa + Is	0-IIa	0-Is	0-IIa	0-IIa	0-IIa	0-IIc	0-IIa	0-IIa + Is	0-IIa	0-IIa
Pathologic diagnosis	TA w/ HGD	TA w/ HGD	TA w/ HGD	TA w/ HGD	TA w/ HGD	TA w/ LGD	TA w/ HGD	TA w/ HGD	TA w/ HGD	TA w/ LGD	TA w/ LGD
Dysplasia in the SM GALT	LGD	LGD	HGD	LGD	LGD	LGD	LGD	HGD	HGD	LGD	LGD
Continuity of SM glands with surface adenomatous component	+	−	+	+	+	+	−	+	+	+	+
Focal defect of MM adjacent to the SM GALT	+	−	+	+	+	+	−	+	+	+	−
Hemosiderin deposit in the SM	−	−	−	−	−	−	−	−	−	−	−
Rounded contour of involved SM GALT	+	+	−	+	+	+	+	+	+	+	+
Cystic dilatation of SM glands	+	−	+	−	−	−	−	−	−	−	+
Admixture of SM glands with normal colonic epithelium	−	−	−	−	−	−	−	−	−	−	+
Desmoplasia	−	−	−	−	−	−	−	−	−	−	−
Single or small clusters of tumor cells in the SM GALT	−	−	−	−	−	−	−	−	−	−	−
Lymphovascular invasion	−	−	−	−	−	−	−	−	−	−	−
Oncocytic cytoplasm of the SM glands	−	−	−	−	−	−	−	−	−	−	−
Goblet cells in the SM glands	+	+	−	−	+	−	+	+	+	−	+
Histologic size of the entire tumor (cm)	1.7	1.4	1.5	2.2	1.2	2.1	1.5	1.8	1.2	2.7	1.8
The largest diameter of isolated SM GALT (cm)	0.14	0.13	0.33	0.17	0.14	0.21	0.29	0.12	0.23	0.14	0.19

GALT, gut-associated lymphoid tissue; F, female; M, male; TA, tubular adenoma; w/, with; HGD, high-grade dysplasia; LGD, low-grade dysplasia; SM, submucosa or submucosal; 0-Is, protruding and sessile type; 0-IIa, flat elevated type; 0-IIc, slightly depressed type; +, present; −, absent; ±, inconspicuous.
[a]Endoscopic appearance was classified according to the Paris classification. 0-IIa+Is corresponds to "nodular mixed type of the granular laterally spreading tumor." 0-IIa corresponds to either "homogeneous type of granular laterally spreading tumor" or "flat elevated type of non-granular laterally spreading tumor."

Table 2. Summary of clinicopathologic characteristics of colorectal neoplasm associated with submucosal GALT and relationship with grade of dysplasia in submucosa

	Total (n=11)	HGD in the SM (n=3)	LGD in the SM (n=8)	p-value
Age (yr)	59 (53–73)	73 (66–73)	57 (53–71)	
Sex				.138
Male	8 (72.7)	1 (33.3)	7 (87.5)	
Female	3 (27.3)	2 (66.7)	1 (12.5)	
Endoscopic appearance[a]				.001
Protruding	1 (9.1)	1 (33.3)	0	
Non-protruding	10 (90.9)	2 (66.7)	8 (100)	
Location				.138
Right-sided	8 (72.7)	2 (66.7)	6 (75.0)	
Left-sided	3 (27.3)	1 (33.3)	2 (25.0)	
Pathologic diagnosis of entire ESD specimen				.491
HGD	8 (72.7)	3 (100)	5 (62.5)	
LGD	3 (27.3)	0	3 (37.5)	
Continuity of SM glands with surface adenomatous component				>.99
Continued	9 (81.8)	3 (100.0)	6 (75.0)	
Discontinued	2 (18.2)	0 (0.0)	2 (25.0)	
Focal defect of MM adjacent to SM GALT				>.99
Continued	2 (18.2)	0	2 (25.0)	
Discontinued	9 (81.8)	3 (100)	6 (75.0)	
Hemosiderin deposit in the SM				–
Present	0	0	0	
Absent	11 (100)	3 (100)	8 (100)	
Contour of involved SM GALT				.273
Rounded	10 (90.9)	2 (66.7)	8 (100)	
Irregular	1 (9.1)	1 (33.3)	0	
Cystic dilatation of SM glands				>.99
Present	3 (27.3)	1 (33.3)	2 (25.0)	
Absent	8 (72.7)	2 (66.7)	6 (75.0)	
Admixture of SM glands with normal colonic epithelium				>.99
Present	1 (9.1)	0	1 (12.5)	
Absent	10 (90.9)	3 (100)	7 (87.5)	
Desmoplasia				–
Present	0	0	0	
Absent	11 (100)	3 (100)	8 (100)	
Single or small clusters of tumor cells in the SM GALT				–
Present	0	0	0	
Absent	11 (100)	3 (100)	8 (100)	
Lymphovascular invasion				–
Present	0	0	0	
Absent	11 (100)	3 (100)	8 (100)	
Oncocytic cytoplasm of the SM glands				–
Present	0	0	0	
Absent	11 (100)	3 (100)	8 (100)	
Goblet cells in the SM glands				–
Present	7 (63.6)	2 (66.7)	5 (62.5)	
Absent	4 (36.4)	1 (33.3)	3 (37.5)	
Pathologic size of entire lesion (cm)	1.7 (1.2–2.7)	1.5 (1.2–1.8)	1.75 (1.2–2.7)	
The largest diameter of isolated SM GALT (cm)	0.17 (0.12 –0.33)	0.23 (0.12– 0.33)	0.155 (0.13–0.29)	

Values are presented as median (range) or number (%).
GALT, gut-associated lymphoid tissue; HGD, high-grade dysplasia; SM, submucosa or submucosal; LGD, low-grade dysplasia; ESD, endoscopic submucosal dissection.
[a]Endoscopic appearance was classified according to the Paris classification.

https://doi.org/10.4132/jptm.2019.11.06

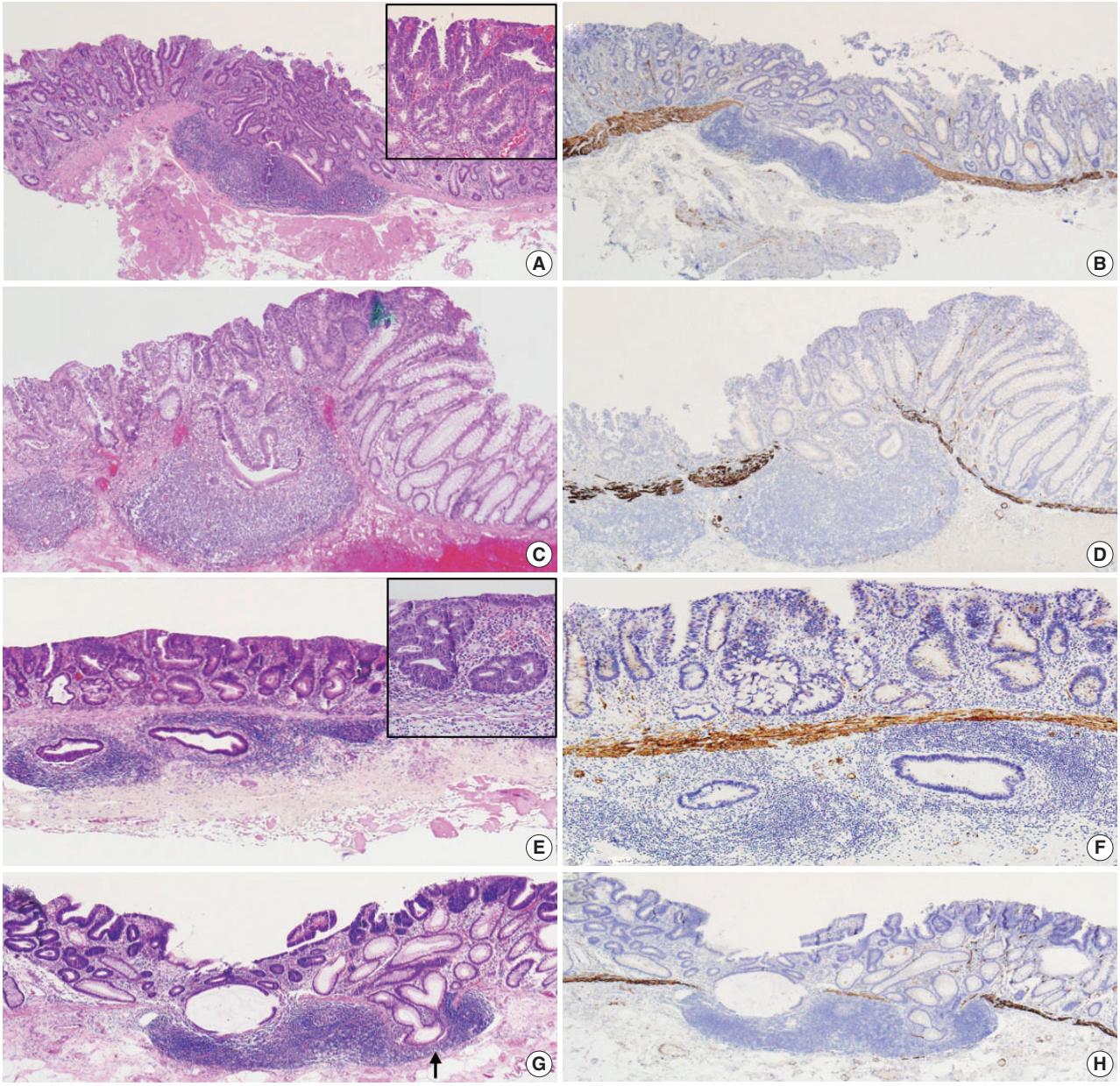

Fig. 1. Continuity of submucosal glands with surface adenomatous component and focal defect of muscularis mucosae adjacent to submucosal gut-associated lymphoid tissue (GALT). (A) Case 5. Tubular adenoma with high-grade dysplasia. Histologic continuity of submucosal glands with surface adenomatous component is seen. Submucosal glands with low-grade dysplasia show similar degree of differentiation compared with surface component. However, this neoplasm shows focal area of glands with complex architecture and corresponding high-grade cytologic features in surface mucosa elsewhere (depicted in inset). This case is more compatible with tubular adenoma with high-grade dysplasia than invasive adenocarcinoma, which usually shows less differentiated tumor cells in the deepest part of invasion. (B) Immunohistochemical (IHC) staining for desmin in case 5 shows focal defects of the muscularis mucosae with GALT-associated pseudoinvasion/epithelial misplacement (PEM). (C) Case 9. Tubular adenoma with high-grade dysplasia. Both surface adenomatous component and submucosal glands show high-grade dysplasia and histologic continuity across the muscularis mucosae. (D) IHC staining for desmin in case 9 highlights discontinuous muscularis mucosae. (E) Case 2. Tubular adenoma with high-grade dysplasia. In contrast to cases 5 and 9, no histologic continuity of submucosal glands with surface adenomatous component is seen. Inset depicts glands with high-grade dysplasia in surface mucosa. Narrow rim surrounding submucosal glands is not compatible with typical desmoplasia. Absence of single tumor cells/small clusters of tumor cells, poorly formed or back-to-back glands, solid tumor nests, or "true" desmoplasia favor diagnosis of tubular adenoma with high-grade dysplasia involving GALT (PEM) over adenocarcinoma with "true" submucosal invasion. (F) Intact muscularis mucosae with subjacent GALT of case 2 is identified with IHC staining for desmin. (G) Case 11. Tubular adenoma with low-grade dysplasia. Cystically dilated tumor glands cross through the muscularis mucosae. Note simultaneous crossing over by non-neoplastic glands (indicated by arrow). (H) IHC staining for desmin in case 11. PEM via GALT is accompanied by discontinuous muscularis mucosae rather than hypertrophy of muscularis mucosae.

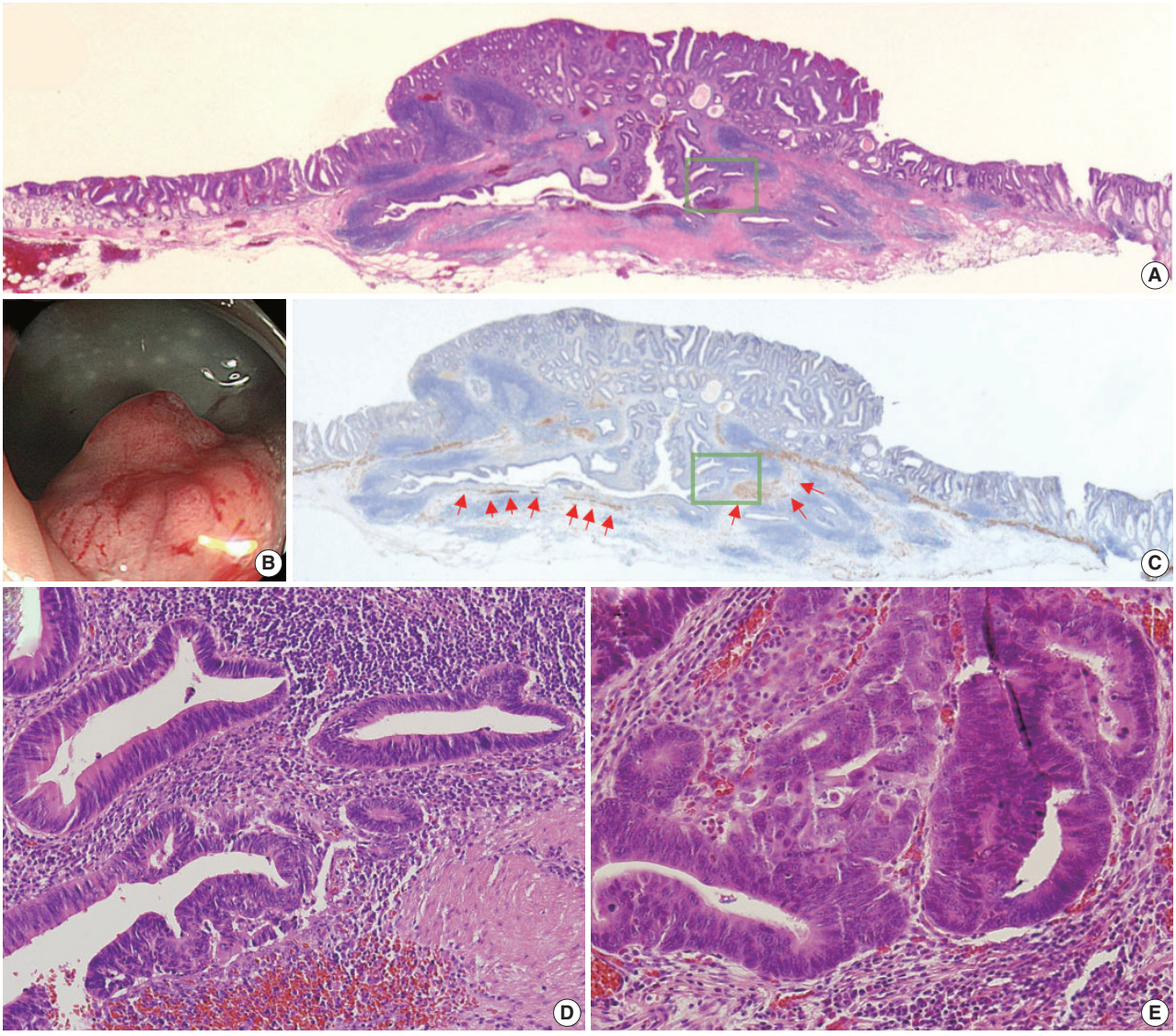

Fig. 2. Case 3. (A) Histologic continuity along with subtle rimming of muscularis mucosae in submucosa (so-called herniation pattern) favor diagnosis of tubular adenoma with high-grade dysplasia over invasive adenocarcinoma. Depth of neoplasm is more than twice the thickness of surrounding normal colorectal mucosa. (B) Endoscopic appearance of case 3. Exact measurement of neoplasm depth is not available for endoscopist. Superficial neoplastic lesion with height more than one-third of diameter is compatible with the protruding type. (C) Immunohistochemical staining for desmin in case 3. Rimming of muscularis mucosa is indicated by red arrows. (D) Glands with high-grade dysplasia are seen under imaginary line connecting adjacent muscularis mucosa beneath normal mucosa. Panel D corresponds to green boxes of panels A and C. (E) Glands of surface mucosal layer with high-grade dysplasia.

architecture (case 3), the tumor glands under the imaginary line connecting the adjacent muscularis mucosa beneath the normal mucosa were partly surrounded by submucosal GALT (Fig. 2). Three cases (27.3%) showed cystically dilated submucosal glands. Only one case (9.1%, case 11) showed an admixture of non-neoplastic glands and neoplastic glands in the submucosal GALT. No case showed a desmoplastic reaction. No case showed a single tumor cell or small clusters of tumor cells in the submucosal GALT. No case showed oncocytic cytoplasm of submucosal glands. Seven cases (63.6%) showed goblet cells in submucosal glands. The median value of the histologic size of the entire tumor was 1.7 cm (range, 1.2 to 2.7 cm). The median value of the largest diameter of the isolated submucosal GALT involved by epithelial neoplasm was 0.17 cm (range, 0.12 to 0.33 cm). Pathologic characteristics of the 11 cases were summarized in Tables 1 and 2.

All 11 cases of colorectal epithelial neoplasm involving submu-

https://doi.org/10.4132/jptm.2019.11.06

cosal GALT had a submucosal tumor component more compatible with PEM (Figs. 1, 2).

Clinicopathologic characteristics of colorectal neoplasm associated with submucosal GALT in relation to grade of dysplasia

No statistically significant difference in pathologic size of the entire lesion was identified between the two groups (high-grade dysplasia in submucosa versus low-grade dysplasia in submucosa). No statistically significant difference of the largest diameter of isolated submucosal GALT involved was identified between the two groups (high-grade dysplasia in the submucosa versus low-grade dysplasia in the submucosa) (Table 2).

No statistically significant relationship between grade of dysplasia in the submucosa (high-grade dysplasia versus low-grade dysplasia) and pathologic features (including pathologic features for PEM; continuity of submucosal glands with surface adenomatous component, focal defect of muscularis mucosae adjacent to submucosal GALT, hemosiderin deposit in the submucosa, contour of submucosal GALT, cystic dilation of submucosal glands, and admixture of submucosal glands with normal colonic epithelium; pathologic features for frank invasion; desmoplasia, single tumor cell or small clusters of tumor cells, and lymphovascular invasion; and pathologic features for GALT carcinoma; oncocytic cytoplasm of submucosal glands and depletion of goblet cells in submucosal glands) was identified (Table 2).

DISCUSSION

A consistent and close association between GALT, particularly organized lymphoid aggregates in the submucosa, and colorectal carcinogenesis, has been reported in rodent models despite scarce incidence of GALT in normal rat intestine [49-53]. However, the specific role of GALT in human colorectal carcinogenesis is not fully understood [6]. Herein, we analyzed the clinicopathologic features of eleven colorectal epithelial neoplasms involving submucosal GALT.

Eight cases (72.7%) were in males. However, validation with a larger number of cases is required to investigate the possible sex predilection of GALT-associated neoplasms. Fu et al. [8] reported significantly higher incidence of GALT in the early colorectal neoplasms of females compared to those of males.

Eight cases (72.7%) were located in the right-sided colon. Kealy [5] reported a more frequent incidence of GALT in the distal colon compared with the proximal colon. Langman and Rowland [4] reported similar relative abundance of GALT in the rectum, but the mean density of GALT in the normal human large intestine was approximately eight times higher than that of the previous report; the normal density of GALT in the proximal colon was not as low as that of previous data [54]. They attributed this gap to differences in the techniques used [4]. O'Leary and Sweeney [55] reported the greatest normal frequency of GALT in both the rectum and cecum, which has relatively abundant microflora [1]. Lee et al. [12] also reported the right side predilection of GALT-associated neoplasms ("tubular adenoma with pseudoinvasion" in their study).

Fu et al. [8] reported the different incidences of GALT according to different macroscopic types of colorectal neoplasm. They reported that neoplasms with depressed or flat macroscopic types showed significantly higher incidence of submucosal GALT than neoplasms with protruding macroscopic types [8]. In our study, 10 cases (90.9%) showed non-protruding endoscopic appearances; the endoscopic appearance of the one other case (case 3) was protruding type (0-Is according to Paris classification) [31]. Several reports have emphasized the non-protruding macroscopic appearance of GALT-associated colorectal neoplasms [2,22,56].

GALT carcinoma and GALT-associated PEM share some overlapping histopathologic features, including submucosal localization, well defined round contour with expansive growth, absence of desmoplasia, cystically dilated glands, and close association with submucosal GALT [12,13]. Most cases of GALT carcinoma reported so far were confined to the submucosal layer; only two of 23 cases reported as GALT carcinoma showed tumor extension beyond the submucosa [13,16,19,24]. Some prefer to use the term "pseudoinvasion" over "epithelial misplacement," emphasizing the expansive lobular growth pattern of tumor glands located in the submucosa after herniation [41]. In fact, the unique histologic features of GALT carcinoma had once been attributed to the result of PEM from overlying conventional adenomas. Thus, the term "lymphoid-associated neoplasia in the herniated colonic epithelium" was once presented [25,47]. One case report author used the term "adenomatous polyp," but other researchers have used the term "GALT carcinoma" [13,15].

The presence of lamina propria surrounding submucosal glandular structures strongly indicates PEM [11,12,37-45,57]. Absence of lamina propria surrounding submucosal glands along with discontinuity between surface adenomatous component and submucosal glands has been presented as a distinct feature of GALT carcinoma [13,18]. However, as normal lamina propria is occasionally occupied by GALT, a rim of lamina propria surrounding the submucosal glands can be obscured by

GALT. We are unable to suggest any specific reliable criteria with acceptable interobserver agreement regarding lamina propria rimming. Also, the absence of continuity between the surface adenomatous component and submucosal glands does not completely exclude the possibility of PEM, as shown in our study (cases 2 and 7).

Nevertheless, unique cytologic features that are distinctive of GALT carcinoma have been suggested, including submucosal glands lined by a single layer of columnar cells with oncocytic cytoplasm and lack of goblet cells. Both of these features are reminiscent of special cell types in follicle-associated epithelium [2]. In our study, seven cases (63.6%) showed goblet cells in the submucosa. No case showed submucosal glands lined by a single layer of oncocytic columnar cells. Hence, we insist that all 11 cases in this study have a submucosal tumor component more compatible with GALT-associated PEM.

Since their first description by Muto et al. [38], hemosiderin deposits in the submucosa, along with granulation tissue and fibroinflammatory reaction (so-called siderogenous desmoplasia), were considered characteristic histologic features of benign submucosal epithelium that are distinct from those of true invasive carcinoma [11,12,37-45,57]. The classic explanation is that repeated twisting or torsion of a long stalk of pedunculated polyp can cause epithelial misplacement into the submucosa to result in these histologic features. This is further supported by the preponderant occurrence in the sigmoid colon, where peristalsis is the most powerful [12,38,41]. However, in our study, no siderogenous desmoplasia indicating repeat tissue damage was identified. All eleven cases had the non-pedunculated macroscopic type and occurred both on the right-sided and left-sided of the colon. One possible explanation is that PEM in non-pedunculated colorectal neoplasms may be ascribed to a relative abundance of submucosal GALT. With respect to 'the microanatomical defect of muscularis mucosae' and 'the size of the submucosal GALT', Kealy [5] reported a positive correlation between maximum diameters of lymphoid nodules and gaps in the muscularis mucosae. In our study, the median value of the largest diameter of isolated submucosal GALT was 0.17 cm (range, 0.12 to 0.33 cm). Increased number and size of submucosal lymphoid follicles can result in microanatomic defects in the muscularis propria, eventually causing GALT-associated PEM [11,12].

The defining feature of colorectal cancer, in contrast to premalignant neoplasm, is invasion of the muscularis mucosae into the submucosa [36,58-61]. This definition of colorectal adenocarcinoma is partly based on histologic knowledge that there are no lymphatic vessels in normal colonic lamina propria. There is also a lack of clinicopathologic data showing intramucosal carcinoma with nodal metastasis, although 'the presence of lymphatic vessels in the colonic lamina propria of the pathologic states' and 'the presence of lymphovascular invasion in the colorectal intramucosal carcinoma' have been reported [62-65]. In certain circumstances, colorectal epithelial neoplasms can extend into the submucosa without histologic features of frank invasion.

Conventional cytologic features, such as anaplasia, loss of nuclear polarity, and nuclear-cytoplasmic ratio, have been used as criteria for the differential diagnosis of PEM versus true invasion, although this distinction is not widely accepted [57]. Adenomatous component showing high-grade dysplasia in the submucosa can mimic malignancy [40,41]. However, the grade of dysplasia in the submucosa itself may not match other pathologic parameters for the differential diagnosis of PEM. In our study, no statistical significance was identified in the relationship between "the grade of the dysplasia in the submucosa (high-grade dysplasia versus low-grade dysplasia)" and "the clinicopathologic features (including pathologic features for PEM, frank invasion, and GALT carcinoma)." Additionally, six cases showed similar grades of dysplasia between the submucosal component and surface component. The five other cases showed a less severe grade of dysplasia in the submucosa compared with that in the mucosa. No case showed high-grade dysplasia in the submucosa with low-grade dysplasia in the mucosa (Table 2, Fig. 1). Generally, invasive adenocarcinoma shows less differentiated tumor cells at the deepest part of invasion. However, adenoma with PEM shows a similar degree of differentiation between the surface component and the submucosal component [37,38,43].

Our experience suggests that pathologists should be aware of the interpretation of GALT-associated submucosal extension of colorectal adenomatous neoplasms. This study is limited due to the small number of cases. Thus, further investigation with a larger number of cases and validation of the classification criteria of GALT-associated colorectal neoplasm is recommended.

ORCID

Yo Han Jeon: https://orcid.org/0000-0002-0353-7255
Ji Hyun Ahn: https://orcid.org/0000-0002-3312-788X
Hee Kyung Chang: https://orcid.org/0000-0002-4843-5316

Author Contributions

Conceptularization: HKC.
Data curation: HKC, YHJ, JHA.

 https://doi.org/10.4132/jptm.2019.11.06

Formal Analysis: YHJ.
Investigation: YHJ, JHA, HKC.
Methodology: HKC.
Project administration: YHJ, JHA, HKC.
Resources: YHJ, JHA, HKC.
Software: YHJ.
Validation: HKC.
Visualization: YHJ.
Writing—original draft: YHJ.
Writing—review & editing: HKC, JHA.

Conflicts of Interest

The authors declare that they have no potential conflicts of interest.

Funding

No funding to declare.

REFERENCES

1. Neutra MR, Mantis NJ, Kraehenbuhl JP. Collaboration of epithelial cells with organized mucosal lymphoid tissues. Nat Immunol 2001; 2: 1004-9.
2. Rubio CA, Puppa G, de Petris G, Kis L, Schmidt PT. The third pathway of colorectal carcinogenesis. J Clin Pathol 2018; 71: 7-11.
3. Elmore SA. Enhanced histopathology of mucosa-associated lymphoid tissue. Toxicol Pathol 2006; 34: 687-96.
4. Langman JM, Rowland R. The number and distribution of lymphoid follicles in the human large intestine. J Anat 1986; 149: 189-94.
5. Kealy WF. Colonic lymphoid-glandular complex (microbursa): nature and morphology. J Clin Pathol 1976; 29: 241-4.
6. Sipos F, Muzes G. Isolated lymphoid follicles in colon: switch points between inflammation and colorectal cancer? World J Gastroenterol 2011; 17: 1666-73.
7. Nascimbeni R, Villanacci V, Mariani PP, et al. Aberrant crypt foci in the human colon: frequency and histologic patterns in patients with colorectal cancer or diverticular disease. Am J Surg Pathol 1999; 23: 1256-63.
8. Fu KI, Sano Y, Kato S, et al. Incidence and localization of lymphoid follicles in early colorectal neoplasms. World J Gastroenterol 2005; 11: 6863-6.
9. Shah N, Thakkar B, Shen E, et al. Lymphocytic follicles and aggregates are a determinant of mucosal damage and duration of diarrhea. Arch Pathol Lab Med 2013; 137: 83-9.
10. Rubio CA, Asmundsson J, Silva P, Illies C, Hartman J, Kis L. Lymphoid aggregates in Crohn's colitis and mucosal immunity. Virchows Arch 2013; 463: 637-42.
11. Shepherd NA, Griggs RK. Bowel cancer screening-generated diagnostic conundrum of the century: pseudoinvasion in sigmoid colonic polyps. Mod Pathol 2015; 28 Suppl 1: S88-94.
12. Lee HE, Wu TT, Chandan VS, Torbenson MS, Mounajjed T. Colonic adenomatous polyps involving submucosal lymphoglandular complexes: a diagnostic pitfall. Am J Surg Pathol 2018; 42: 1083-9.
13. McCarthy AJ, Chetty R. Gut-associated lymphoid tissue or so-called "dome" carcinoma of the colon: review. World J Gastrointest Oncol 2019; 11: 59-70.
14. Rubio CA, De Petris G, Puppa G. Gut-associated lymphoid tissue (GALT) carcinoma in ulcerative colitis. Anticancer Res 2018; 38: 919-21.
15. Zhou S, Ma Y, Chandrasoma P. Inverted lymphoglandular polyp in descending colon. Case Rep Pathol 2015; 2015: 646270.
16. Kannuna H, Rubio CA, Silverio PC, et al. DOME/GALT type adenocarcimoma of the colon: a case report, literature review and a unified phenotypic categorization. Diagn Pathol 2015; 10: 92.
17. Yamada M, Sekine S, Matsuda T. Dome-type carcinoma of the colon masquerading a submucosal tumor. Clin Gastroenterol Hepatol 2013; 11: A30.
18. Rubio CA, Befrits R, Ericsson J. Carcinoma in gut-associated lymphoid tissue in ulcerative colitis: Case report and review of literature. World J Gastrointest Endosc 2013; 5: 293-6.
19. Yamada M, Sekine S, Matsuda T, et al. Dome-type carcinoma of the colon; a rare variant of adenocarcinoma resembling a submucosal tumor: a case report. BMC Gastroenterol 2012; 12: 21.
20. Puppa G, Molaro M. Dome-type: a distinctive variant of colonic adenocarcinoma. Case Rep Pathol 2012; 2012: 284064.
21. Coyne JD. Dome-type colorectal carcinoma: a case report and review of the literature. Colorectal Dis 2012; 14: e360-2.
22. Rubio CA, Lindh C, Björk J, Törnblom H, Befrits R. Protruding and non-protruding colon carcinomas originating in gut-associated lymphoid tissue. Anticancer Res 2010; 30: 3019-22.
23. Stewart CJ, Hillery S, Newman N, Platell C, Ryan G. Dome-type carcinoma of the colon. Histopathology 2008; 53: 231-4.
24. Asmussen L, Pachler J, Holck S. Colorectal carcinoma with dome-like phenotype: an under-recognised subset of colorectal carcinoma? J Clin Pathol 2008; 61: 482-6.
25. Rubio CA, Talbot I. Lymphoid-associated neoplasia in herniated colonic mucosa. Histopathology 2002; 40: 577-9.
26. Jass JR, Constable L, Sutherland R, et al. Adenocarcinoma of colon differentiating as dome epithelium of gut-associated lymphoid tissue. Histopathology 2000; 36: 116-20.
27. Clouston AD, Clouston DR, Jass JR. Adenocarcinoma of colon differentiating as dome epithelium of gut-associated lymphoid tissue.

Histopathology 2000; 37: 567.
28. De Petris G, Lev R, Quirk DM, Ferbend PR, Butmarc JR, Elenitoba-Johnson K. Lymphoepithelioma-like carcinoma of the colon in a patient with hereditary nonpolyposis colorectal cancer. Arch Pathol Lab Med 1999; 123: 720-4.
29. Fritz A, Percy C, Jack A, Shanmugaratnam K, Sobin LH, Parkin MD. International Classification of Diseases for Oncology (ICD-O). 3rd ed. Geneva: World Health Organization, 2013.
30. Stintzing S, Tejpar S, Gibbs P, Thiebach L, Lenz HJ. Understanding the role of primary tumour localisation in colorectal cancer treatment and outcomes. Eur J Cancer 2017; 84: 69-80.
31. The Paris endoscopic classification of superficial neoplastic lesions: esophagus, stomach, and colon: November 30 to December 1, 2002. Gastrointest Endosc 2003; 58(6 Suppl): S3-43.
32. Vleugels JLA, Hazewinkel Y, Dekker E. Morphological classifications of gastrointestinal lesions. Best Pract Res Clin Gastroenterol 2017; 31: 359-67.
33. Endoscopic Classification Review Group. Update on the paris classification of superficial neoplastic lesions in the digestive tract. Endoscopy 2005; 37: 570-8.
34. Kudo S, Lambert R, Allen JI, et al. Nonpolypoid neoplastic lesions of the colorectal mucosa. Gastrointest Endosc 2008; 68(4 Suppl): S3-47.
35. Schlemper RJ, Hirata I, Dixon MF. The macroscopic classification of early neoplasia of the digestive tract. Endoscopy 2002; 34: 163-8.
36. Lokuhetty D, White VA, Watanabe R, Cree IA, Organizacion Mundial de la Salud; International Agency for Research on Cancer. WHO classification of tumours. Vol. 1. Digestive system tumours. 5th ed. Lyon: IARC Press, 2019.
37. Fenoglio-Preiser CM, Noffsinger AE, Stemmermann GN, Lantz PE, Isaacson PG. Gastrointestinal pathology: an atlas and text. 3rd ed. Philadelphia: Wolters Kluwer Health/Lippincott Williams & Wilkins, 2008; 926-31.
38. Muto T, Bussey HJ, Morson BC. Pseudo-carcinomatous invasion in adenomatous polyps of the colon and rectum. J Clin Pathol 1973; 26: 25-31.
39. Dirschmid K, Kiesler J, Mathis G, Beller S, Stoss F, Schobel B. Epithelial misplacement after biopsy of colorectal adenomas. Am J Surg Pathol 1993; 17: 1262-5.
40. Yantiss RK, Bosenberg MW, Antonioli DA, Odze RD. Utility of MMP-1, p53, E-cadherin, and collagen IV immunohistochemical stains in the differential diagnosis of adenomas with misplaced epithelium versus adenomas with invasive adenocarcinoma. Am J Surg Pathol 2002; 26: 206-15.
41. Tanizawa T, Seki T, Nakano M, Kamiyama R. Pseudoinvasion of the colorectal polypoid tumors: serial section study of problematic cases. Pathol Int 2003; 53: 584-90.
42. Molavi D, Argani P. Distinguishing benign dissecting mucin (stromal mucin pools) from invasive mucinous carcinoma. Adv Anat Pathol 2008; 15: 1-17.
43. Loughrey MB, Shepherd NA. The pathology of bowel cancer screening. Histopathology 2015; 66: 66-77.
44. Panarelli NC, Somarathna T, Samowitz WS, et al. Diagnostic challenges caused by endoscopic biopsy of colonic polyps: a systematic evaluation of epithelial misplacement with review of problematic polyps from the bowel cancer screening program, United Kingdom. Am J Surg Pathol 2016; 40: 1075-83.
45. Ferreira da Silva MJ, Pinho R, Wen X, Tente D, Leite S, Carvalho J. Adenoma with pseudoinvasion: s crucial differential diagnosis for invasive adenocarcinoma. Gastroenterol Hepatol 2017; 40: 96-8.
46. Chang HJ, Park CK, Kim WH, et al. A standardized pathology report for colorectal cancer. Korean J Pathol 2006; 40: 193-203.
47. Rubio CA. Ectopic colonic mucosa in ulcerative colitis and in Crohn's disease of the colon. Dis Colon Rectum 1984; 27: 182-6.
48. World Medical Association. World Medical Association Declaration of Helsinki: ethical principles for medical research involving human subjects. JAMA 2013; 310: 2191-4.
49. Nauss KM, Locniskar M, Pavlina T, Newberne PM. Morphology and distribution of 1,2-dimethylhydrazine dihydrochloride-induced colon tumors and their relationship to gut-associated lymphoid tissue in the rat. J Natl Cancer Inst 1984; 73: 915-24.
50. Carter JW, Lancaster HK, Hardman WE, Cameron IL. Distribution of intestine-associated lymphoid tissue, aberrant crypt foci, and tumors in the large bowel of 1,2-dimethylhydrazine-treated mice. Cancer Res 1994; 54: 4304-7.
51. Hardman WE, Cameron IL. Colonic crypts located over lymphoid nodules of 1,2-dimethylhydrazine-treated rats are hyperplastic and at high risk of forming adenocarcinomas. Carcinogenesis 1994; 15: 2353-61.
52. Rubio CA, Shetye J, Jaramillo E. Non-polypoid adenomas of the colon are associated with subjacent lymphoid nodules: an experimental study in rats. Scand J Gastroenterol 1999; 34: 504-8.
53. Rubio CA. The histogenesis of the third pathway of colonic carcinogenesis in rats. Anticancer Res 2017; 37: 1039-42.
54. Dukes C, Bussey HJ. The number of lymphoid follicles of the human large intestine. J Pathol Bacteriol 1926; 29: 111-6.
55. O'Leary AD, Sweeney EC. Lymphoglandular complexes of the colon: structure and distribution. Histopathology 1986; 10: 267-83.
56. Rubio CA, Schmidt PT. Gut-associated lymphoid tissue (GALT) carcinoma or dome carcinoma? Anticancer Res 2016; 36: 5385-7.
57. Greene FL. Epithelial misplacement in adenomatous polyps of the colon and rectum. Cancer 1974; 33: 206-17.
58. Fenoglio-Preiser CM, Lantz P, Listrom M, Noffsinger A, Riker F,

Stemmermann G. Gastrointestinal pathology: an atlas and text. 2nd ed. Philadelphia: Lippincott-Raven, 1999.
59. Schlemper RJ, Itabashi M, Kato Y, et al. Differences in the diagnostic criteria used by Japanese and Western pathologists to diagnose colorectal carcinoma. Cancer 1998; 82: 60-9.
60. Risio M. The natural history of pT1 colorectal cancer. Front Oncol 2012; 2: 22.
61. Quirke P, Risio M, Lambert R, von Karsa L, Vieth M. Quality assurance in pathology in colorectal cancer screening and diagnosis-European recommendations. Virchows Arch 2011; 458: 1-19.
62. Lewin MR, Fenton H, Burkart AL, Sheridan T, Abu-Alfa AK, Montgomery EA. Poorly differentiated colorectal carcinoma with invasion restricted to lamina propria (intramucosal carcinoma): a follow-up study of 15 cases. Am J Surg Pathol 2007; 31: 1882-6.
63. Kenney BC, Jain D. Identification of lymphatics within the colonic lamina propria in inflammation and neoplasia using the monoclonal antibody D2-40. Yale J Biol Med 2008; 81: 103-13.
64. Fenoglio CM, Kaye GI, Lane N. Distribution of human colonic lymphatics in normal, hyperplastic, and adenomatous tissue. Its relationship to metastasis from small carcinomas in pedunculated adenomas, with two case reports. Gastroenterology 1973; 64: 51-66.
65. Hashimoto H, Horiuchi H, Kurata A, et al. Intramucosal colorectal carcinoma with lymphovascular invasion: clinicopathological characteristics of nine cases. Histopathology 2019; 74: 1055-66.

JPTM
Journal of Pathology and Translational Medicine 2020; 54: 146-153
https://doi.org/10.4132/jptm.2019.11.12

ORIGINAL ARTICLE

Double cocktail immunostains with high molecular weight cytokeratin and GATA-3: useful stain to discriminate in situ involvement of prostatic ducts or acini from stromal invasion by urothelial carcinoma in the prostate

Junghye Lee[1], Youngeun Yoo[1], Sanghui Park[1], Min-Sun Cho[1], Sun Hee Sung[1], Jae Y. Ro[2]

[1]Department of Pathology, Ewha Womans University College of Medicine, Seoul, Korea;
[2]Department of Pathology and Genomic Medicine, Houston Methodist Hospital and Weill Medical College of Cornell University, Houston, TX, USA

Background: Distinguishing prostatic stromal invasion (PSI) by urothelial carcinoma (UC) from in situ UC involving prostatic ducts or acini with no stromal invasion (in situ involvement) may be challenging on hematoxylin and eosin stained sections. However, the distinction between them is important because cases with PSI show worse prognosis. This study was performed to assess the utility of double cocktail immunostains with high molecular weight cytokeratin (HMWCK) and GATA-3 to discriminate PSI by UC from in situ UC involvement of prostatic ducts or acini in the prostate. **Methods:** Among 117 radical cystoprostatectomy specimens for bladder UCs, 25 cases showed secondary involvement of bladder UC in prostatic ducts/acini only or associated stromal invasion and of these 25 cases, seven cases revealed equivocal PSI. In these seven cases with equivocal PSI, HMWCK, and GATA-3 double immunohistochemical stains were performed to identify whether this cocktail stain is useful to identify the stromal invasion. **Results:** In all cases, basal cells of prostate glands showed strong cytoplasmic staining for HMWCK and UC cells showed strong nuclear staining for GATA-3. In cases with stromal invasion of UC, GATA-3-positive tumor cells in the prostatic stroma without surrounding HMWCK-positive basal cells were highlighted and easily recognized. Among seven equivocal cases, two cases showed PSI and five in situ UC in the prostate. In two cases, the original diagnoses were revised. **Conclusions:** Our study suggested that HMWCK and GATA-3 double stains could be utilized as an adjunct method in the distinction between PSI by UC from in situ UC involving prostatic ducts or acini.

Key Words: Urothelial carcinoma; Prostatic stromal invasion; High molecular weight cytokeratin; GATA-3

Received: July 31, 2019 **Revised:** October 18, 2019 **Accepted:** November 12, 2019
Corresponding Author: Sanghui Park, MD, PhD, Department of Pathology, Ewha Womans University College of Medicine, 1071 Anyangcheon-ro, Yangcheon-gu, Seoul 07985, Korea
Tel: +82-2-2650-5044, Fax: +82-2-2650-2879, E-mail: spark0430@ewha.ac.kr
Corresponding Author: Min-Sun Cho, MD, PhD, Department of Pathology, Ewha Womans University College of Medicine, 25 Magokdong-ro 2-gil, Gangseo-gu, Seoul 07084, Korea
Tel: +82-2-6986-3422, Fax: +82-2-6986-7013, E-mail: mcho1124@ewha.ac.kr

Primary urothelial carcinoma (UC) of the prostate is rare, representing only about 1% to 4% of all prostate malignancies [1-3]. In contrast, secondary involvement of primary bladder UC is relatively common with an incidence of 12% in an early report [4]. However, the true incidence of prostatic involvement is more common. In several studies using whole-mount prostate sectioning technique, the incidence of prostatic involvement has been reported up to 48% (average, 35.5%) [5-9]. The incidence of prostatic stromal invasion (PSI) ranges from 7.6% to 16.6% [4,6,9-13]. In 7th American Joint Committee on Cancer (AJCC) staging system, primary bladder UCs with PSI are classified as pT4a and correlated with worse prognosis [14]. However, the staging of continuous subepithelial PSI from in situ carcinoma was not designated properly. The 8th AJCC staging system clarified the staging of PSI according to the mode of invasion: primary bladder UCs with direct PSI via transmural route is designated as T4a while continuous subepithelial PSI from in situ carcinoma is now classified as T2 [15]. Although the presence of PSI does not affect the current 8th AJCC staging of muscle-invasive primary bladder UCs (≥T2), it is still important to distinguish PSI from in situ UC because PSI is associated with poor prognosis [16]. Therefore, the correct identification of PSI with primary bladder UC is of paramount importance for accurate staging and predicting patients' prognoses. However, the

pISSN 2383-7837
eISSN 2383-7845

distinction between PSI by UCs from only in situ UC involvement of prostatic ducts or acini in the prostate can be challenging on hematoxylin and eosin (H&E) stained slides examination alone in some cases.

In this study, double cocktail immunostains with high molecular weight cytokeratin (HMWCK) and GATA-3 were performed to determine its usefulness for detecting PSI.

MATERIALS AND METHODS

Cases selection

Surgical pathology files of our institute from 2000 to 2012 were searched for radical cystectomy cases of prostatic involvement by primary bladder UCs with available tissue blocks. Among 164 radical cystectomy cases for primary bladder UCs, 140 were males and concomitant prostatectomy was performed in 117 cases (117/140, 83.6%). Among 117 radical cystoprostatectomy specimens for bladder UCs, 25 cases (21.4%) showed secondary involvement of bladder UC in prostatic ducts/acini only or associated stromal invasion, and of these 25 cases, seven cases revealed equivocal PSI. The remaining 18 cases revealed unequivocal prostatic involvement with either in situ only or PSI. PSI was considered equivocal at H&E level when one of the following features was present: (1) in situ UC in prostatic ducts with irregular and blurred outlines and a basal layer that was not well defined (pattern 1) and (2) in situ UC in prostatic ducts surrounded by desmoplastic stroma with or without inflammatory infiltrate (pattern 2). Slides were re-reviewed independently by two experienced pathologists (S.P. and M.S.C.). They had concordant interpretation in 18 cases and had discordant interpretation in seven cases due to equivocal stromal invasion.

Double immunohistochemistry

Double immunohistochemical stains were performed with

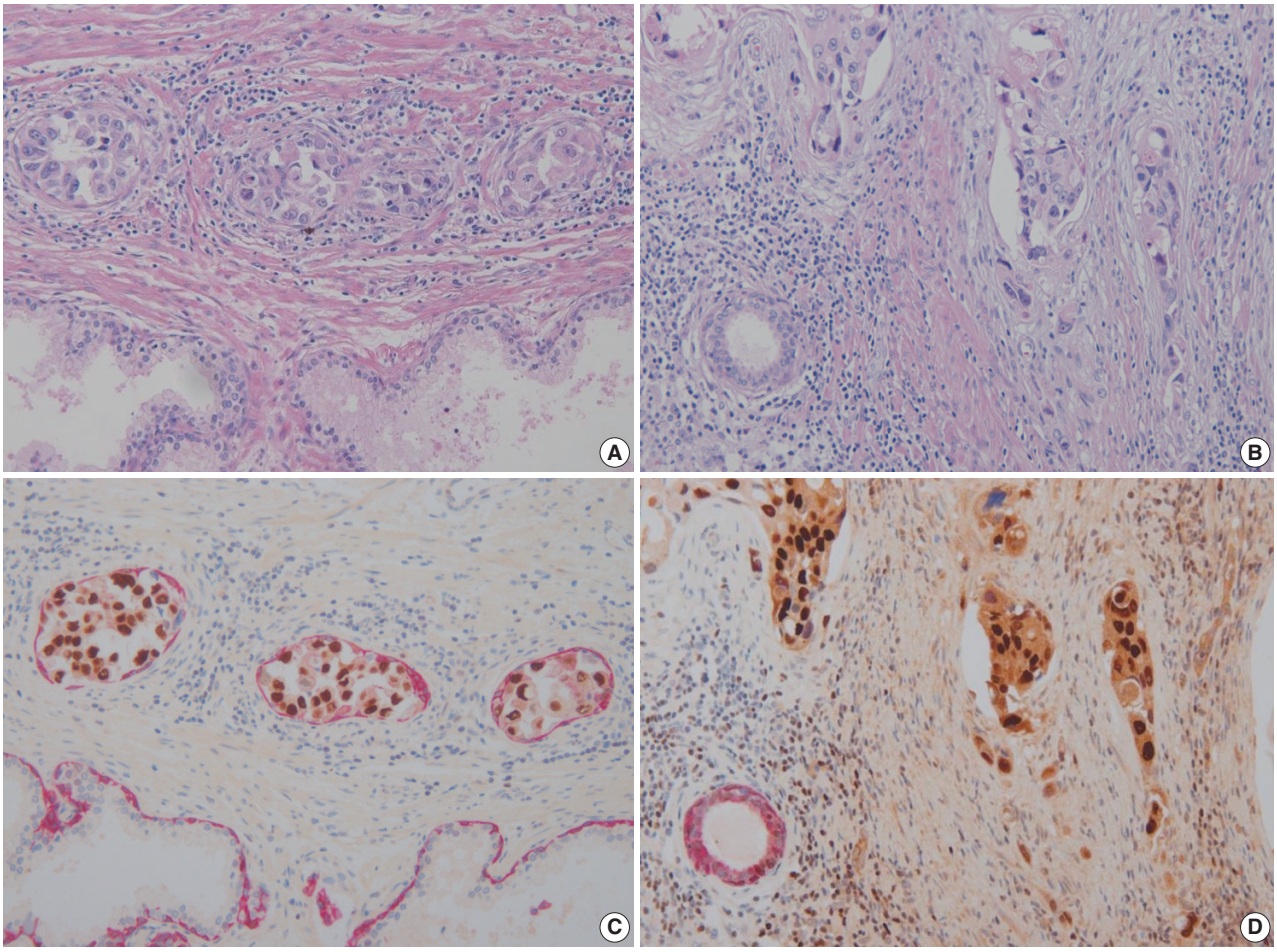

Fig. 1. (A) Urothelial carcinoma in situ involving prostatic ducts. (B) Urothelial carcinoma with prostatic stromal invasion. (C) Urothelial carcinoma in situ involving prostatic ducts surrounded by basal cells (double immunohistochemical stain). (D) Urothelial carcinoma with prostatic stromal invasion without surrounding basal cells (double immunohistochemical stain).

mouse monoclonal antibodies against human HMWCK (1:200 dilution, 34βE12 clone, Novocastra, Newcastle upon Tyne, UK) and GATA-3 (1:100 dilution, L50-823 clone, Cell Marque, Rocklin, CA, USA) using formalin-fixed paraffin-embedded tissue blocks of tumors with adjacent benign prostatic tissue. Four-μm sections were dried at 55°C for 3 hours, then subjected to heat-induced epitope retrieval, 30 minutes for HMWCK and 20 minutes for GATA-3, at pH 9.0 on a Leica-Bond Autostainer (Leica Biosystems, Newcastle upon Tyne, UK). Bond Polymer Refine Detection Kit was used and the sections were counterstained with hematoxylin. Subsequently, double-stain combinations using HMWCK and GATA-3 were tested in some cases using different combinations of brown and red chromogens. Bond Polymer Refine Brown Detection Kit (Leica Biosystems) was used for detection of GATA-3 and Bond Polymer Refine Red Detection Kit for detection of HMWCK. All cases contained foci of UC with colonization of prostatic ducts and acini that were used as GATA-3 positive control. Adjacent benign prostatic glands were used as an internal control for HMWCK stain (Fig. 1). Pancytokeratin stain (1:200 dilution, AE1/AE3, Novocastra) was performed for case 6.

Ethics statement

All procedures performed in the current study were approved by the international review board at Ewha Womans University Hospital (2016-09-020) in accordance with the 1964 Helsinki declaration and its later amendments. Formal written informed consent was not required with a waiver by the IRB.

RESULTS

Clinicopathological data on these seven patients with equivocal PSI are summarized in Table 1. The patients' mean age was of 73.3 years at diagnosis (range, 60 to 93 years). Among seven cases, six showed conventional muscle invasive high-grade UC and one showed diffuse and multifocal UC in situ throughout the bladder (case 1). Six showed conventional high-grade UC morphology, but one case (case 4) showed several different histologic features (squamous, glandular and neuroendocrine differentiations). Lymphovascular invasion was identified in three cases. Five cases were free of tumor at margins and two showed positive margins, one in left ureter and the other in the urethra.

In these seven cases, UC involvement was seen in prostatic ducts and acini with equivocal PSI. Four cases revealed pattern 1 equivocal invasion (Fig. 2A) and three cases pattern 2 equivocal invasion (Figs. 2B, 3A, B). Originally, two cases, both with pattern 2 equivocal invasion, were diagnosed as having PSI and the remaining five cases, four pattern 1 and one pattern 2 cases, with equivocal invasion were diagnosed as no PSI.

In these seven cases, double cocktail immunostains were performed. Prostatic basal cells surrounding in situ UC stained positively for HMWCK and UC cells stained for GATA-3 (Fig. 1A, C). In all cases, UC cells stained positively for GATA-3 (7/7, 100%). The combination of HMWCK (red)/GATA-3 (brown) easily distinguish in situ from invasive tumor (Fig. 1B, D). Among seven equivocal cases, two cases showed PSI and five cases in situ UC in the prostate. Based on these stain results, cases 5 and 6 were revised according to the 7th AJCC staging system and

Table 1. Clinicopathologic features in patients with equivocal prostatic stromal invasion

Case No.	Age/Sex	Histology (variant)	LVI	Margin status	Equivocal pattern	PSI, original (H&E)	PSI, revised (IHC)	AJCC 7th T (original)	AJCC 7th T (revised)	AJCC 8th T	Treatment	F/U (mo)
1	M/71	UC in situ (C)	Absent	Negative	1	No	No	Tis	Tis	Tis	TURBT, RCP	LTF
2	M/61	UC, HG (C)	Absent	Negative	1	No	No	T1	T1	T1	TURBT, BCG, neoadjuvant CTx, RCP	AWD (56)
3	M/93	UC, HG (C)	Absent	Negative	1	No	No	T3	T3	T3	TURBT, RCP	DOD (10)
4	M/79	UC, HG, (S, G, N)	Present	Negative	1	No	No	T3	T3	T3	TURBT, neoadjuvant CTx, RCP, adjuvant CTx	DOD (2)
5	M/60	UC, HG (C)	Absent	Positive, left ureter	2	Yes	No	T4a	T1	T1	TURBT, BCG, RCP	AWD (54)
6	M/85	UC, HG (C)	Present	Negative	2	No	Yes	T3	T4a	T3	TURBT, RCP, adjuvant CTx	DOD (16)
7	M/64	UC, HG (C)	Present	Positive, urethra	2	Yes	Yes	T4a	T4a	T2	TURBT, BCG, neoadjuvant CTx, RCP, adjuvant CTx	AWD (58)

LVI, lymphovascular invasion; PSI, prostatic stromal invasion; H&E, hematoxylin and eosin; IHC, immunohistochemistry; AJCC, American Joint Committee on Cancer; F/U, follow-up; M, male; UC, urothelial carcinoma; C, conventional; TURBT, transurethral resection of bladder tumor; RCP, radical cystoprostatectomy; LTF, loss to follow up; HG, high grade; BCG, bacillus Calmette-Guerin; CTx, chemotherapy; AWD, alive with disease; DOD, died of disease; S, squamous differentiation; G, glandular differentiation; N, neuroendocrine differentiation.

https://doi.org/10.4132/jptm.2019.11.12

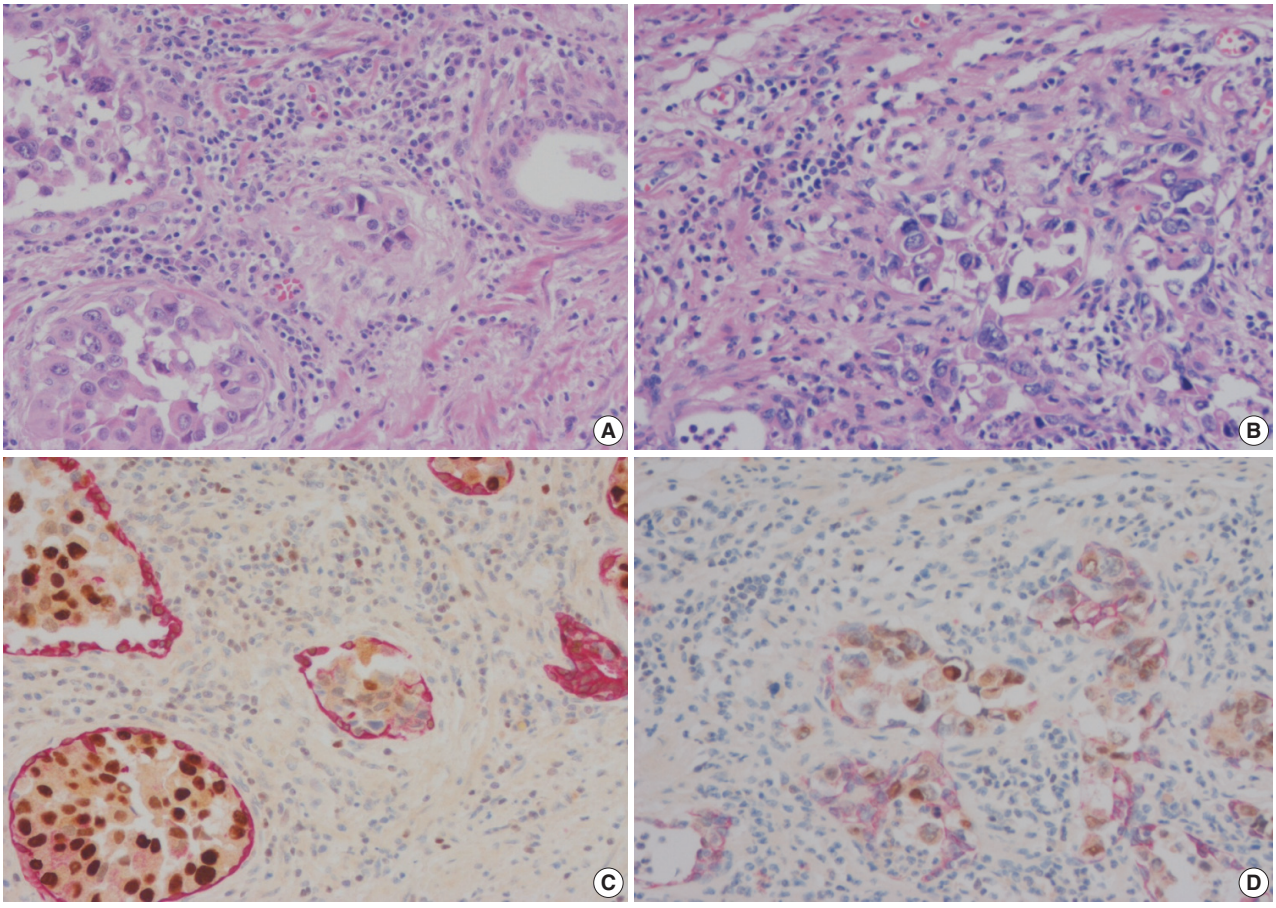

Fig. 2. (A) Urothelial carcinoma in situ with equivocal stromal invasion (equivocal pattern 1). (B) Urothelial carcinoma in situ with equivocal stromal invasion (equivocal pattern 2). (C) Urothelial carcinoma in situ with intact surrounding basal cells (double immunohistochemical stain). (D) Urothelial carcinoma in situ with disrupted but sustained basal cells (double immunohistochemical stain).

cases 5 and 7 were revised according to the 8th AJCC system. In one case, the original T4a classification was revised as T1 and in the other case, the original T3 classification was revised to T4a according to the 7th AJCC staging system. According to the 8th AJCC staging system, one case classified originally as T4a was revised as T1, and the other T4a case was revised as T2.

All patients received radical cystoprostatectomy after transurethral resection of bladder tumor and additional treatments such as bacillus Calmette-Guerin (BCG) instillation, neoadjuvant chemotherapy and adjuvant chemotherapy were given as needed. Three patients (cases 1, 7, and 5) are alive with disease at 21, 26, and 54 months, respectively. Other three patients (cases 4, 3, and 6) died of disease at 2-, 10-, and 16-month follow-up, respectively, and the remaining one patient (case 2) was lost to follow up.

In equivocal cases with pattern 1, GATA-3–positive tumor cells in prostatic ducts/acini were surrounded by HMWCK-positive basal cells (Fig. 2C). In three equivocal cases with pattern 2, two cases were revised after performing double immunohistochemistry (IHC). In one case, double IHC revealed the presence of preserved basal cells with continuous, linear and focally weak staining pattern of HMWCK at the periphery of the involved prostatic ducts/acini (case 5) (Fig. 2D). This case, originally signed out as PSI, was revised as in situ UC involving prostatic ducts/acini without PSI. In the other case (case 6), intense aggregates of inflammatory cells were identified adjacent to prostatic ducts (Fig. 3A, B). GATA-3–positive and HMWCK-negative singly scattered invasive tumor cells were present within the periductal inflammatory area (Fig. 3C). Singly scattered tumor cells were also highlighted by pancytokeratin stain, supporting invasive UC cells (Fig. 3D). This case, originally signed out as in situ UC involving prostatic ducts, was revised as having PSI.

DISCUSSION

It is well-known that UCs with extensive PSI has a poor prog-

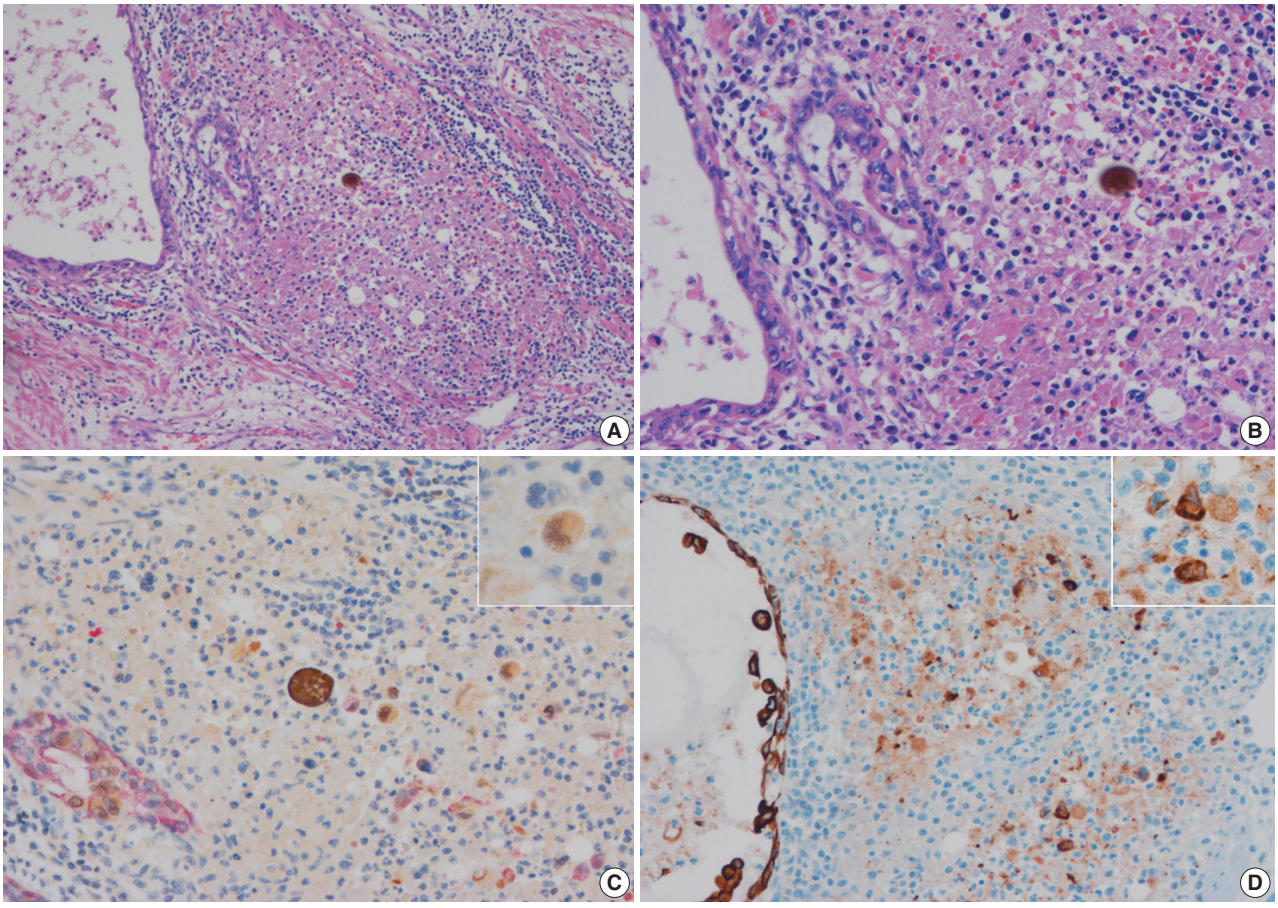

Fig. 3. (A) Periductal inflammatory infiltrates within prostatic stroma. (B) Inflammatory infiltrates with no discernible tumor cells. (C) GATA-3–positive, high molecular weight cytokeratin–negative scattered tumor cells in inflammatory infiltrates (double immunohistochemical stain). (D) Scattered tumor cells are also positive for pancytokeratin stain.

nosis, but even a few cases with focal PSI may have similarly poor prognosis [16,17]. Therefore, it is essential to find even focal areas of PSI for proper classification. In 7th AJCC staging system, primary bladder UCs invading prostatic stroma through spreading to the prostatic urethra are classified as T4a. However, in the new 8th AJCC staging system [15], only those cases with primary bladder UCs directly invading prostatic stroma through the bladder wall are classified as T4a. Continuous subepithelial PSI from in situ UC is now categorized as T2 and does not affect the staging of primary bladder muscle-invasive UC (> T2). Yet distinguishing continuous subepithelial PSI of in situ UC (T2) from involvement of in situ UC (Tis) in non-muscle invasive primary bladder UCs (Tis or T1) are still important for patients who underwent early radical cystoprostatectomy because overall tumor stage can be upstaged because of the presence of PSI. Also, even though the impact of a concurrent continuous subepithelial PSI on the prognosis of muscle-invasive primary bladder UCs (> T2) is still unclear, the presence of PSI itself is reported to be associated with poor prognosis regardless of the mode of invasion [16].

Therefore, the significance of PSI needs to be re-evaluated. In most cases with PSI, stromal invasion can be easily detected on H&E slides because PSI is usually associated with single isolate cell invasion, desmoplastic stromal reaction, acute and/or chronic inflammatory response, and retraction artifact around tumor cells [18]. However, the determination of PSI is somewhat subjective and may be impossible in some cases because they lack these characteristic histologic features on H&E slides. Perrino et al. [19] showed 11.1% (4/36) discordant interpretations of PSI between original report and review using double immunostains with cytokeratin (CK) 7/CK5 and p53/CK5 [20]. The main distinction between in situ UC from PSI is to identify tumor cells in the prostatic stroma without surrounding prostatic basal cells.

In this study, we evaluated the utility of HMWCK and GATA-3 double IHC in determining stromal invasion of primary bladder UC in the prostate. We classified equivocal PSI cases into two

https://doi.org/10.4132/jptm.2019.11.12

patterns on H&E. In all cases with pattern 1 invasion, the diagnoses based on H&E and on IHC were concordant. However, in cases showing pattern 2, the concordance rate was low with two of three cases being misdiagnosed on H&E. Singly scattered tumor cells were present in inflammatory stroma in those two cases. The singly scattered tumor cells were positive for pancytokeratin as well as GATA-3 but negative for HMWCK. Based on these findings, we recommend pancytokeratin and GATA-3 IHC stains in the prostate with pattern 2 equivocal PSI.

In previous two studies, various combinations of double stains were used to differentiate in situ UC from PSI in the prostate [18,20]. Chastain et al. [18] demonstrated that p63 and HMWCK double stains are useful in differentiating PSI. Even though this combination of double IHC is useful when p63-positive tumor cells are present in the prostatic stroma without surrounding HMWCK-positive basal cells, it has a limitation because not all tumor cells are positive for p63. In all cases, basal cells showed strong staining for both p63 and HMWCK, but only 50% and 41% of cases showed no or weak expression in tumor cells, respectively [18]. In the other study, Fichtenbaum et al. [20] reported that double stains with CK7/CK5 and p53/CK5 discriminated in situ vs. invasive urothelial cancer in the prostate. These combinations of double stains are also a good method to discriminate in situ vs. PSI and can be utilized in a routine practice because CK5 is a very sensitive and specific marker for basal cells (100%) and CK7 and p53 are very sensitive markers for tumor cells with 100% and 83% positivity, respectively [20]. CK7 is very specific for UCs in differentiating commonly encountered adenocarcinomas such as prostatic adenocarcinoma and metastatic colonic adenocarcinoma because the expression of CK7 is not usually seen in these adenocarcinomas [21,22]. However, even though rare, other metastatic adenocarcinomas including pulmonary adenocarcinoma, ovarian serous adenocarcinoma, endometrial adenocarcinoma, gastric adenocarcinoma, cholangiocarcinoma, invasive ductal carcinoma, that can be found in the prostate also may express CK7 [21,22]. Moreover, high grade UC may be negative for CK7 occasionally [23]. In our study, we used GATA-3 stain for UCs and HMWCK for prostatic basal cells. GATA-3 is a recently described immunohistochemical marker that is specific and sensitive for UCs and breast cancers [24,25]. When GATA-3–positive tumor cells are present in the prostatic stroma, PSI by UCs is highly suggested in the proper clinical context.

There are several limitations in this study. First, selective limited prostate sectioning technique was applied to this study. If whole-mount step sections of the prostate were selected, more cases with prostatic involvement might have been detected. Second, the number of subjects, especially the number of cases with equivocal PSI, was rather small. Third, GATA-3 also stains lymphocytes. GATA-3-positive atypical cells were present in the inflammatory stroma (case 6). Even though GATA-3–positive atypical cells in the inflammatory stroma were confirmed as epithelial cells by pancytokeratin staining, they might be keratin-positive debris such as disrupted normal epithelium or disrupted prostatic ducts or glands, especially in post-BCG status. However, BCG instillation was not performed in this case. Fourth, GATA-3 is recently reported to show aberrant diffuse nuclear staining in both luminal and basal cells of benign prostate glands with radiation atypia as well as in the basal cells of non-irradiated benign prostate glands [26]. UC and benign prostate glands can be distinguished based on their morphology, but certain variants of UCs, especially UC with glandular differentiation can cause a diagnostic problem. Fifth, even though GATA-3 is a novel immunohistochemical marker for UC, GATA-3 expression differed among UC variants [27]. Especially, GATA-3 is reported to be weakly or rarely expressed in sarcomatoid and small cell carcinoma variants of UC and squamous cell carcinomas [27]. Thus, GATA-3 immunostain may have only limited diagnostic value in such cases. Lastly, strong HMWCK positivity is reported in 50% to 91.7% of UCs [18,28].

In the current study, weak GATA3 positivity in basal cells of benign prostatic glands was observed in two out of seven cases (28.6%) while HMWCK positivity in UCs was found in five out of seven (71.4%). Such expression pattern could cause diagnostic confusion for pathologists in irradiated specimens which often accompany radiation atypia in benign prostatic glands. However, none of the patients in the current study had received previous irradiation therapy. Also, even though some benign prostatic glands expressed GATA3 positivity, the staining intensity was much weaker than that observed in UCs. Furthermore, none of GATA3 positive benign prostatic cells in the current study showed cytologic atypia.

The double staining for GATA-3 and HMWCK may enable us to distinguish PSI from equivocal in situ lesions. In rare cases in which GATA-3 is aberrantly expressed in prostatic glands, the presence of HMWCK staining and the architectural and cytological findings on H&E can aid in the correct interpretation. Another advantage of the double staining method is convenience. Compared to switching between GATA-3 and HMWCK stains individually to spot the equivocal lesion under microscopic examination, assessing a single slide is more convenient. Lastly, the equivocal PSI lesions tend to be subtle and minute in size.

Double immunostain method reduces the possible loss of the lesion during multiple sections for different markers.

Differentiating cases of UC with PSI from in situ UC involving prostatic ducts or acini is critical for subsequent patients' prognosis even though the significance of focal PSI is still controversial and PSI itself is not considered as pT4a any longer in 8th AJCC staging system. However, one patient with PSI (case 6, original T3 [7th]→revised to T4a [7th], T3 [8th]) died with only 16 months follow-up after cystoprostatectomy. On the contrary, the other patient without PSI (case 5, original T4a [7th]→revised to T1 [7th], T1 [8th]) is still alive for 54 months. In these equivocal cases, one case (case 5) was misdiagnosed as PSI and subsequently T4a (7th AJCC) was assigned in the original diagnosis. The presence of basal cells around tumor nests, as demonstrated by double IHC, led to the final diagnosis of in situ UC involving prostatic ducts in this case. The other case (case 6) was diagnosed as in situ involving only prostatic ducts without PSI in the original diagnosis; therefore, pT3 was based on the perivesical fat invasion of the primary bladder UC. However, PSI besides in situ prostatic duct involvement was diagnosed because scattered infiltrating tumor cells with positive GATA3 and pancytokeratin positivity with lack of HMWCK stain within the inflammatory infiltrates and subsequently pT4a was re-assigned in this case. Another patient with PSI (case 7, original T4a [7th]→revised to T4a [7th], T2 [8th]) is also alive for 58 months. In this case, the primary bladder UC was non-muscle invasive and the concurrent urethral PSI determined the staging.

In conclusion, we demonstrated that GATA-3 and HMWCK double IHC is useful in discriminating PSI by UC from in situ UC involving prostatic ducts or acini especially in cases with pattern 2 equivocal PSI.

ORCID

Junghye Lee: https://orcid.org/0000-0001-8454-4360
Youngeun Yoo: https://orcid.org/0000-0003-4855-3870
Sanghui Park: https://orcid.org/0000-0003-3837-8677
Min-Sun Cho: https://orcid.org/0000-0001-8772-9686
Sun Hee Sung: https://orcid.org/0000-0001-9345-1131
Jae Y. Ro: https://orcid.org/0000-0002-4158-3658

Author Contributions

Conceptualization: SP, JYR.
Data curation: SP, YY, JL.
Formal analysis: JL, SP.
Investigation: JL, SP.
Methodology: SP.
Project administration: SP.
Resources: SP, SHS, MSC.
Supervision: SP.
Validation: SP, SHS, MSC.
Visualization: JL, SP.
Writing—original draft: JL, SP.
Writing—review & editing: JL, SP.

Conflicts of Interest

The authors declare that they have no potential conflicts of interest.

Funding

No funding to declare.

REFERENCES

1. Bates HR Jr. Transitional cell carcinoma of the prostate. J Urol 1969; 101: 206-7.
2. Rubenstein AB, Rubnitz ME. Transitional cell carcinoma of the prostate. Cancer 1969; 24: 543-6.
3. Wolfe JH, Lloyd-Davies RW. The management of transitional cell carcinoma in the prostate. Br J Urol 1981; 53: 253-7.
4. Schellhammer PF, Bean MA, Whitmore WF Jr. Prostatic involvement by transitional cell carcinoma: pathogenesis patterns and prognosis. J Urol 1977; 118: 399-403.
5. Pettus JA, Al-Ahmadie H, Barocas DA, et al. Risk assessment of prostatic pathology in patients undergoing radical cystoprostatectomy. Eur Urol 2008; 53: 370-5.
6. Reese JH, Freiha FS, Gelb AB, Lum BL, Torti FM. Transitional cell carcinoma of the prostate in patients undergoing radical cystoprostatectomy. J Urol 1992; 147: 92-5.
7. Revelo MP, Cookson MS, Chang SS, Shook MF, Smith JA Jr, Shappell SB. Incidence and location of prostate and urothelial carcinoma in prostates from cystoprostatectomies: implications for possible apical sparing surgery. J Urol 2004; 171(2 Pt 1): 646-51.
8. Shen SS, Lerner SP, Muezzinoglu B, Truong LD, Amiel G, Wheeler TM. Prostatic involvement by transitional cell carcinoma in patients with bladder cancer and its prognostic significance. Hum Pathol 2006; 37: 726-34.
9. Wood DP Jr, Montie JE, Pontes JE, VanderBrug Medendorp S, Levin HS. Transitional cell carcinoma of the prostate in cystoprostatectomy specimens removed for bladder cancer. J Urol 1989; 141: 346-9.

10. Coutts AG, Grigor KM, Fowler JW. Urethral dysplasia and bladder cancer in cystectomy specimens. Br J Urol 1985; 57: 535-41.
11. Herr HW, Donat SM. Prostatic tumor relapse in patients with superficial bladder tumors: 15-year outcome. J Urol 1999; 161: 1854-7.
12. Njinou Ngninkeu B, Lorge F, Moulin P, Jamart J, Van Cangh PJ. Transitional cell carcinoma involving the prostate: a clinicopathological retrospective study of 76 cases. J Urol 2003; 169: 149-52.
13. Pagano F, Bassi P, Ferrante GL, et al. Is stage pT4a (D1) reliable in assessing transitional cell carcinoma involvement of the prostate in patients with a concurrent bladder cancer? A necessary distinction for contiguous or noncontiguous involvement. J Urol 1996; 155: 244-7.
14. Edge SB, Byrd DR, Compton CC, et al. AJCC cancer staging manual. 7th ed. New York: Springer, 2010.
15. Amin MB, Edge S, Greene F, et al. AJCC cancer staging manual. Chicago: Springer, 2017.
16. Ayyathurai R, Gomez P, Luongo T, Soloway MS, Manoharan M. Prostatic involvement by urothelial carcinoma of the bladder: clinicopathological features and outcome after radical cystectomy. BJU Int 2007; 100: 1021-5.
17. Oliva IV, Smith SL, Chen Z, Osunkoya AO. Urothelial carcinoma of the bladder with transmural and direct prostatic stromal invasion: does extent of stromal invasion significantly impact patient outcome? Hum Pathol 2011; 42: 51-6.
18. Chastain EC, Oliva IV, Osunkoya AO. Utility of p63 and high molecular weight cytokeratin in the distinction between urothelial carcinoma with prostatic stromal invasion and urothelial carcinoma with colonisation of prostatic ducts and acini. Pathology 2012; 44: 199-203.
19. Perrino CM, Fichtenbaum EJ, Pohar KS, Zynger DL. Challenges in the pathological reporting of urothelial carcinoma involving prostatic transurethral resection specimens within a single institution. Pathology 2013; 45: 664-9.
20. Fichtenbaum EJ, Marsh WL Jr, Zynger DL. CK5, CK5/6, and double-stains CK7/CK5 and p53/CK5 discriminate in situ vs invasive urothelial cancer in the prostate. Am J Clin Pathol 2012; 138: 190-7.
21. Kim DH, Joo JE, Kim EK, Lee HJ, Lee WM. The Expressions of Cytokeratin 7 and 20 in Epithelial Tumors: A Survey of 91 Cases. Cancer Res Treat 2003; 35: 355-63.
22. Seipel AH, Samaratunga H, Delahunt B, Wiklund P, Clements M, Egevad L. Immunohistochemistry of ductal adenocarcinoma of the prostate and adenocarcinomas of non-prostatic origin: a comparative study. APMIS 2016; 124: 263-70.
23. Downes MR, Torlakovic EE, Aldaoud N, Zlotta AR, Evans AJ, van der Kwast TH. Diagnostic utility of androgen receptor expression in discriminating poorly differentiated urothelial and prostate carcinoma. J Clin Pathol 2013; 66: 779-86.
24. Higgins JP, Kaygusuz G, Wang L, et al. Placental S100 (S100P) and GATA3: markers for transitional epithelium and urothelial carcinoma discovered by complementary DNA microarray. Am J Surg Pathol 2007; 31: 673-80.
25. Liu H, Shi J, Wilkerson ML, Lin F. Immunohistochemical evaluation of GATA3 expression in tumors and normal tissues: a useful immunomarker for breast and urothelial carcinomas. Am J Clin Pathol 2012; 138: 57-64.
26. Tian W, Dorn D, Wei S, et al. GATA3 expression in benign prostate glands with radiation atypia: a diagnostic pitfall. Histopathology 2017; 71: 150-5.
27. Liang Y, Heitzman J, Kamat AM, Dinney CP, Czerniak B, Guo CC. Differential expression of GATA-3 in urothelial carcinoma variants. Hum Pathol 2014; 45: 1466-72.
28. Chuang AY, DeMarzo AM, Veltri RW, Sharma RB, Bieberich CJ, Epstein JI. Immunohistochemical differentiation of high-grade prostate carcinoma from urothelial carcinoma. Am J Surg Pathol 2007; 31: 1246-55.

JPTM
Journal of Pathology and Translational Medicine 2020; 54: 154-164
https://doi.org/10.4132/jptm.2019.11.13

ORIGINAL ARTICLE

Programmed death-ligand 1 expression and its correlation with clinicopathological parameters in gallbladder cancer

Ji Hye Kim[1], Kyungbin Kim[1], Misung Kim[1], Young Min Kim[1,2], Jae Hee Suh[1,2], Hee Jeong Cha[1,2], Hye Jeong Choi[1,2]

[1]Department of Pathology, Ulsan University Hospital, Ulsan; [2]University of Ulsan College of Medicine, Ulsan, Korea

Background: Immunomodulatory therapies targeting the interaction between programmed cell death protein 1 and programmed death-ligand 1 (PD-L1) have become increasingly important in anticancer treatment. Previous research on the subject of this immune response has established an association with tumor aggressiveness and a poor prognosis in certain cancers. Currently, scant information is available on the relationship between PD-L1 expression and gallbladder cancer (GBC). **Methods:** We investigated the expression of PD-L1 in 101 primary GBC cases to determine the potential association with prognostic impact. PD-L1 expression was immunohistochemically assessed using a single PD-L1 antibody (clone SP263). Correlations with clinicopathological parameters, overall survival (OS), or progression-free survival (PFS) were analyzed. **Results:** PD-L1 expression in tumor cells at cutoff levels of 1%, 10%, and 50% was present in 18.8%, 13.8%, and 7.9% of cases. Our study showed that positive PD-L1 expression at any cutoff was significantly correlated with poorly differentiated histologic grade and the presence of lymphovascular invasion ($p<.05$). PD-L1 expression at cutoff levels of 10% and 50% was significantly positive in patients with perineural invasion, higher T categories, and higher pathologic stages ($p<.05$). Additionally, there was a significant association noted between PD-L1 expression at a cutoff level of 50% and worse OS or PFS ($p=.049$ for OS, $p=.028$ for PFS). Other poor prognostic factors included histologic grade, T category, N category, pathologic stage, lymphovascular invasion, perineural invasion, growth pattern, and margin of resection ($p<.05$). **Conclusions:** The expression of PD-L1 in GBC varies according to cutoff level but is valuably associated with poor prognostic parameters and survival. Our study indicates that the overexpression of PD-L1 in GBC had a negative prognostic impact.

Key Words: Gallbladder neoplasm; Programmed death-ligand 1; Prognosis

Received: September 2, 2019 **Revised:** November 8, 2019 **Accepted:** November 12, 2019

Corresponding Author: Hye Jeong Choi, MD, PhD, Department of Pathology, Ulsan University Hospital, University of Ulsan College of Medicine, 877 Bangeojinsunwhando-ro, Dong-gu, Ulsan 05505, Korea
Tel: +82-52-250-7264, Fax: +82-52-252-3024, E-mail: thanksg@uuh.ulsan.kr

Gallbladder cancer (GBC) is a rare biliary tract malignancy seen in most developed countries, widespread with extensive geographic and ethnic variance [1]. Annually, GBC affects less than two out of 100,000 individuals but is more commonly observed in India, Chile, Japan, and Korea than in Western countries [2,3]. Most patients present with an advanced stage at diagnosis and the 5-year survival rate is < 10% [4]. In Korea, the overall incidence of GBC from 2009 to 2013 was 2.96 of 100,000 people among males and 2.79 of 100,000 people among females [5]. The 5-year survival rate is 30% and the median survival is 10.7 months [6]. Ulsan, where the hospital in this study is located, showed the highest incidence during 2009 to 2013 (4.31/100,000 in men and 4.09/100,000 in women) as compared with the national incidence [5,6].

In recent years, research on various tumor entities has increasingly focused on immunomodulatory drugs than directly cytotoxic cancer therapies. Genomic sequencing studies have identified a host of genetic aberrations that are potentially targetable in GBC [7,8]. In particular, the immunomodulatory therapy approach targeting the interaction between programmed cell death protein 1 (PD-1) and programmed death-ligand 1 (PD-L1) has become increasingly significant. The aberrant expression of PD-L1 allows for tumor cells to escape the host immune system and continue to proliferate. Previous research has demonstrated the association of PD-L1 with tumor aggressiveness and poor prognosis in gastric, esophageal, and hepatocellular carcinoma as well as colonic and lung cancers [9,10]. It is expected that the therapeutic agents known as immune checkpoint inhibitors will

pISSN 2383-7837
eISSN 2383-7845

be a key emerging strategy in treating the subgroup of advanced GBC.

Throughout the published literature, scant information is available on the use of PD-L1 as a prognostic marker in GBC. Existing research by Neyaz et al. [11] and Lin et al. [12] has reported inconsistent and contradictory results. Furthermore, although the possibility of immunotherapy has been studied, relevant information in this area is also very limited so far [13,14]. This study aimed to investigate the expression of PD-L1 and determine the potential association with prognostic impact in GBC. We also reviewed associations with clinicopathological parameters and survival.

MATERIALS AND METHODS

Specimens and patient selection

Formalin-fixed, paraffin-embedded (FFPE) primary GBC tissues were derived from 101 patients at Ulsan University Hospital (UUH) between January 2013 and December 2018. Clinical data were recorded from the UUH electronic medical records, including age, sex, size, location, risk factors (e.g., gallstone, cholecystitis, diabetes mellitus, hypertension), margin of tumor resection, histologic grade, TNM stage, lymph node involvement, lymphovascular invasion or perineural invasion by tumor, adjuvant chemotherapy, and follow-up time in months. Follow-up was completed on April 8, 2019. Overall survival (OS) was the interval either between the initial diagnosis and death or between the initial diagnosis and the last observation among surviving patients, respectively. Progression-free survival (PFS) was the interval between the initial diagnosis and progressive changes in the typical imaging appearance on computed tomography and/or magnetic resonance imaging. No patient underwent chemotherapy before surgery. The pathologic diagnosis was confirmed according to the eighth edition of the American Joint Committee on Cancer staging system [15] and the World Health Organization classification systems.

Automated immunohistochemistry

A representative paraffin block from each specimen was chosen for immunohistochemical analysis. We immunohistochemically analyzed PD-L1 expression on 3- to 5-μm tissue sections of FFPE specimens. The primary PD-L1 antibody (rabbit monoclonal antibody clone SP263; Roche Holding AG, Basel, Switzerland) was used in all cases in a concentration of approximately 1.61 μg/mL. A negative control for all cases was also developed using the same antibody to control for potential false-positive staining. Placental tissues served as positive controls. Immunohistochemistry assays were performed on a VENTANA BenchMark ULTRA instrument (Roche Holding AG) according to the manufacturer's instructions.

Evaluation of immunohistochemistry

The PD-L1 expression proportion score was assessed as the percentage of positive membranous expression on tumor cells, whereas cytoplasmic expression was regarded as negative. Tumor cells with any membranous staining intensity were judged to be positive. Various PD-L1 antibodies and cutoff levels were used in different studies. We assessed PD-L1 expression using the cutoff levels of 1%, 10%, and 50% (Fig. 1).

Statistical analysis

SPSS ver. 24.0 (IBM Corp., Armonk, NY, USA) was used to conduct statistical analyses. To determine the association between two or more variables and PD-L1 expression, Pearson's chi-square test or Fisher exact test where appropriate were applied, with statistical significance at $p < .05$. The univariable analysis of OS and PFS was completed using the Kaplan-Meier method and log-rank test.

Ethics statement

This study was approved by the institutional review board (IRB) of UUH, who granted a waiver of the need for informed consent (IRB No. 2019-08-017). This study was performed in accordance with the principles of the Declaration of Helsinki.

RESULTS

Clinicopathological characteristics

The study group included 101 primary GBC cases, with a female predominance (56.4%). The mean age of the included patients was 68.0 years (range, 40 to 90 years) and 97 patients (96.0%) were aged older than 45 years. Fifty-two patients (51.5%) were diagnosed via simple cholecystectomy specimens and 10 of these underwent further surgery after diagnosis. Risk factors included gallstone (28.7%), cholecystitis (91.0%), hypertension (28.7%), and diabetes (32.7%). The majority of cases showed adenocarcinoma not otherwise specified (n = 82, 81.2%), and the most common type was well-differentiated (n = 45, 44.6%). Although subtype-specific components accompanying adenocarcinoma were present, no cases were diagnosed as either undifferentiated carcinoma, squamous cell carcinoma, adenosquamous cell carcinoma, or neuroendocrine carcinoma. This

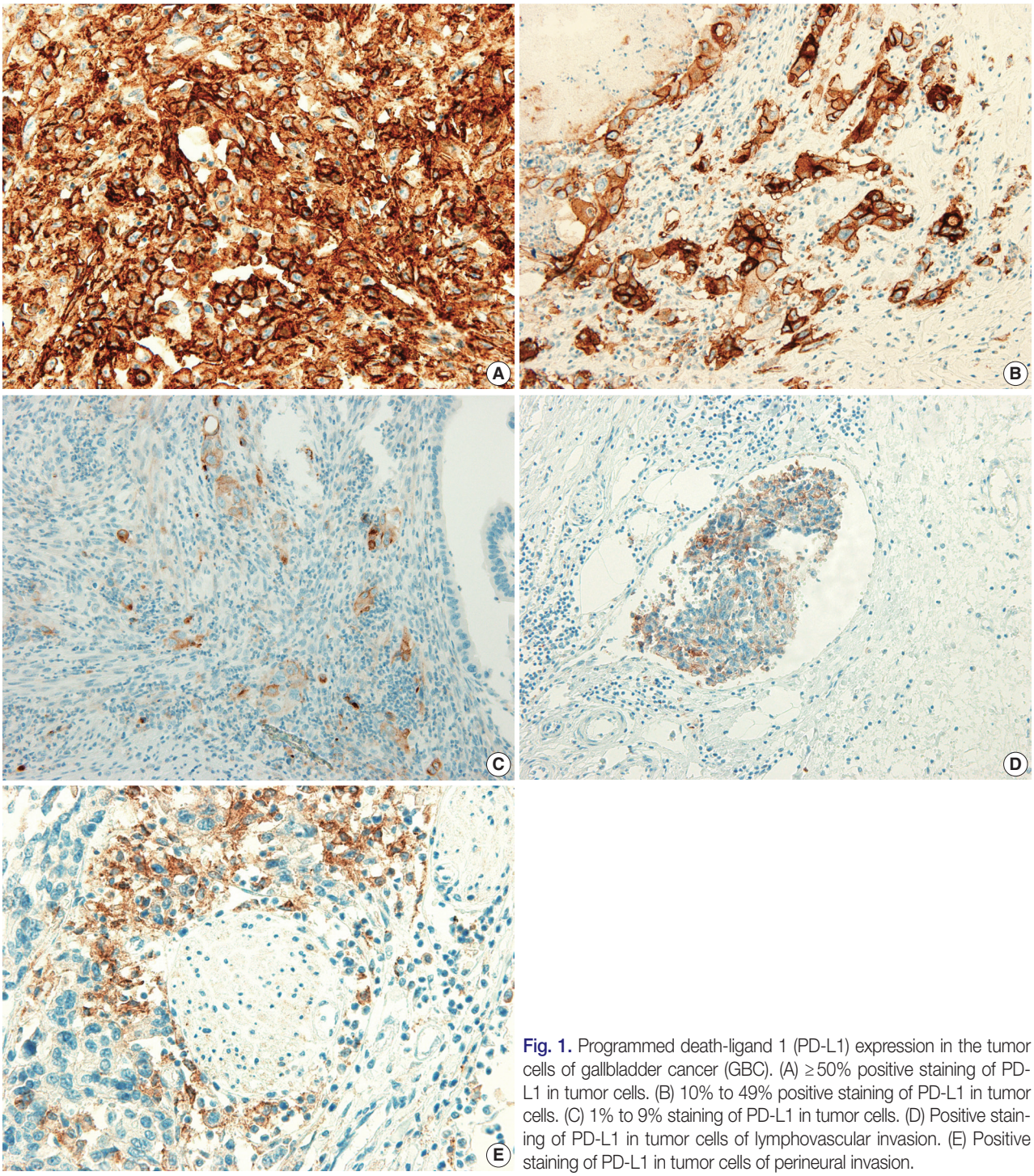

Fig. 1. Programmed death-ligand 1 (PD-L1) expression in the tumor cells of gallbladder cancer (GBC). (A) ≥50% positive staining of PD-L1 in tumor cells. (B) 10% to 49% positive staining of PD-L1 in tumor cells. (C) 1% to 9% staining of PD-L1 in tumor cells. (D) Positive staining of PD-L1 in tumor cells of lymphovascular invasion. (E) Positive staining of PD-L1 in tumor cells of perineural invasion.

cohort included mostly patients with early stages of disease; 84 patients (83.2%) presented with pT1 or pT2 category. Among 72 patients eligible for the evaluation of pathologic stage status, 37 (51.4%) presented with stage I or stage II disease. The clinicopathological characteristics of our GBC patients are shown in Table 1.

Correlation of clinicopathological parameters with PD-L1 expression

PD-L1 expression in tumor cells was observed in 19 patients (18.8%) with a cutoff level of 1%, 14 patients (13.8%) with a cutoff level of 10%, and eight patients (7.9%) with a cutoff level of 50%. The finding of any positive PD-L1 expression was sig-

https://doi.org/10.4132/jptm.2019.11.13

Table 1. Clinicopathological characteristics in gallbladder cancer patients

Clinicopathological variable	No. (%)
Age, mean (range, yr)	68.0 (40–90)
Sex	
Male	44 (43.6)
Female	57 (56.4)
Histological type	
Adenocarcinoma NOS	82 (81.2)
MANEC	3 (3.0)
ICPN with associated invasive carcinoma	5 (5.0)
Adenocarcinoma with undifferentiated carcinoma	3 (3.0)
Adenocarcinoma with squamous differentiation	3 (3.0)
Adenocarcinoma with sarcomatoid differentiation and sarcomatoid carcinoma	2 (2.0)
Adenocarcinoma with signet cell component and signet ring cell carcinoma	2 (2.0)
Mucinous carcinoma	1 (1.0)
Histologic grade	
Well differentiated	45 (44.6)
Moderately differentiated	34 (33.7)
Poorly differentiated	18 (17.8)
Undifferentiated	1 (1.0)
Others (SRC, MUC, SARC)	3 (3.0)
T category	
pT1a	15 (14.9)
PT1b	14 (13.9)
pT2a	47 (46.5)
pT2b	8 (7.9)
pT3	15 (14.9)
pT4	2 (2.0)
N category	
Nx	31 (30.7)
N0	37 (36.6)
N1	28 (27.7)
N2	5 (5.0)
M category	
M0	98 (97.0)
M1	3 (3.0)
Pathologic stage (total=72)	
I	18 (25.0)
IIA	16 (22.2)
IIB	3 (4.2)
IIIA	2 (2.8)
IIIB	26 (36.1)
IVA	1 (1.4)
IVB	6 (8.3)
Operation	
Simple cholecystectomy	43 (42.6)
Radical cholecystectomy	55 (54.4)
Pylorus resecting pancreatoduodenectomy with hepatectomy	2 (2.0)
Pylorus preserving pancreatoduodenectomy with hepatectomy	1 (1.0)
Complete resection	
Yes	92 (91.1)
No	19 (9.9)
Adjuvant chemotherapy	
Not received	71 (70.3)
Received	30 (29.7)
Gallstone	
No	72 (71.3)
Yes	29 (28.7)
Cholecystitis	
No	9 (9.0)
Yes	92 (91.0)
Hypertension	
No	72 (71.3)
Yes	29 (28.7)
Diabetes	
No	68 (67.3)
Yes	33 (32.7)
Tumor location	
Fundus	36 (35.6)
Body	40 (39.6)
Neck, cystic duct	14 (13.9)
More than 2 portions	11 (10.9)
Size, median (range, cm)	2.7 (0.1–6.9)
Growth pattern	
Polypoid	53 (52.5)
Nonpolypoid, ulcerative	48 (47.5)
Lymphovascular invasion	
Absent	62 (61.4)
Present	39 (38.6)
Perineural invasion	
Absent	65 (64.4)
Present	36 (35.6)
PD-L1 expression (%)	
<1	82 (81.2)
1–9	5 (5.0)
10–49	6 (5.9)
≥50	8 (7.9)

Values are presented as number (%).
NOS, not otherwise specified; MANEC, mixed adenoneuroendocrine carcinoma; ICPN, intracholecystic papillary neoplasm; SRC, signet ring cell carcinoma; MUC, mucinous carcinoma; SARC, sarcomatoid carcinoma; PD-L1, programmed death-ligand 1.

nificantly correlated with poorer and other differentiation (1% cutoff: p = .001; 10% cutoff: p < .001; 50% cutoff: p < .001) and the presence of lymphovascular invasion (1% cutoff, p = .015; 10% cutoff, p = .001; 50% cutoff, p = .005). Positive PD-L1 expression with cutoff levels of 10% and 50% was associated with the presence of perineural invasion (10% cutoff, p = .032; 50% cutoff, p = .023), higher T category (10% cutoff, p = .012; 50% cutoff, p = .026), and higher pathologic stage (10% cutoff, p = .045; 50% cutoff, p = .010). In addition, positive PD-L1 expression with 1% and 10% cutoff levels was correlated with larger tumor size (1% cutoff, p = .040; 10% cutoff, p = .007). No significant differences were observed with regard to sex; age; tumor

Table 2. Correlation of clinicopathological parameters with PD-L1 expression in GBC

Clinicopathological parameter	PD-L1		p-value	PD-L1		p-value	PD-L1		p-value
	<1%	≥1%		<10%	≥10%		<50%	≥50%	
Sex			.887			.270			>.99[a]
Male	36 (43.9)	8 (42.1)		36 (41.4)	8 (57.1)		41 (44.1)	3 (37.5)	
Female	46 (56.1)	11 (57.9)		51 (58.6)	6 (42.9)		52 (55.9)	5 (62.5)	
Age (yr)			.259			.302			.716[a]
<68	42 (51.2)	7 (36.8)		44 (50.6)	5 (35.7)		46 (49.5)	3 (37.5)	
≥68	40 (48.8)	12 (63.2)		43 (49.4)	9 (64.3)		47 (50.5)	5 (62.5)	
Histologic type			.132[a]			.004[a]			.306[a]
Adenocarcinoma NOS, ICPN with associated invasive carcinoma	73 (89.0)	14 (73.7)		79 (90.8)	8 (57.1)		81 (87.1)	6 (75.0)	
Adenocarcinoma with other component, others	9 (11.0)	5 (26.3)		8 (9.2)	6 (42.9)		12 (12.9)	2 (25.0)	
Histologic grade			.001			<.001[a]			<.001[a]
Well differentiated	42 (51.2)	3 (15.8)		44 (50.6)	1 (7.1)		45 (48.4)	0	
Moderately differentiated	28 (34.1)	6 (31.6)		31 (35.6)	3 (21.4)		33 (35.5)	1 (12.5)	
Poorly differentiated, undifferentiated, others	12 (14.6)	10 (52.6)		12 (13.8)	10 (71.4)		15 (16.1)	7 (87.5)	
T category			.304[a]			.012[a]			.026[a]
pT1+pT2	70 (85.4)	14 (73.7)		76 (87.4)	8 (57.1)		80 (86.0)	4 (50.0)	
pT3+pT4	12 (14.6)	5 (26.3)		11 (12.6)	6 (42.9)		13 (14.0)	4 (50.0)	
N category			.260			.137			.093[a]
N0	31 (56.4)	6 (40.0)		33 (56.9)	4 (33.3)		36 (56.3)	1 (16.7)	
N1+N2	24 (43.6)	9 (60.0)		25 (43.1)	8 (66.7)		28 (43.8)	5 (83.3)	
Pathologic stage			.116			.045			.010[a]
I+II	32 (56.1)	5 (33.3)		34 (56.7)	3 (25.0)		37 (56.1)	0	
III+IV	25 (43.9)	10 (66.7)		26 (43.3)	9 (75.0)		29 (43.9)	6 (100)	
Growth pattern			.315			.437			>.99[a]
Polypoid	45 (54.9)	8 (42.1)		47 (54.0)	6 (42.9)		49 (52.7)	4 (50.0)	
Nonpolypoid (ulcerative)	37 (45.1)	11 (57.9)		40 (46.0)	8 (57.1)		44 (47.3)	4 (50.0)	
Lymphovascular invasion			.015			.001			.005[a]
No	55 (67.1)	7 (36.8)		59 (67.8)	3 (21.4)		61 (65.6)	1 (12.5)	
Yes	27 (32.9)	12 (63.2)		28 (32.2)	11 (78.6)		32 (34.4)	7 (87.5)	
Perineural invasion			.086			.032[a]			.023[a]
No	56 (68.3)	9 (47.4)		60 (69.0)	5 (35.7)		63 (67.7)	2 (25.0)	
Yes	26 (31.7)	10 (52.6)		27 (31.0)	9 (64.3)		30 (32.3)	6 (75.0)	
Tumor location			.487[a]			.079[a]			.060[a]
Fundus	30 (36.6)	6 (31.6)		31 (35.6)	5 (35.7)		35 (37.6)	1 (12.5)	
Body	33 (40.2)	7 (36.8)		35 (40.2)	5 (35.7)		36 (38.7)	4 (50.0)	
Neck, cystic duct	12 (14.6)	2 (10.5)		14 (16.1)	0		14 (15.1)	0	
More than 2 portions	7 (8.5)	4 (21.1)		7 (8.0)	4 (28.6)		8 (8.6)	3 (37.5)	
Tumor size (cm)			.040			.007			.062[a]
<2.7	43 (52.4)	5 (26.3)		46 (52.9)	2 (14.3)		47 (50.5)	1 (12.5)	
≥2.7	39 (47.6)	14 (73.7)		41 (47.1)	12 (85.7)		46 (49.5)	7 (87.5)	
Complete resection			.676[a]			>.99[a]			.539[a]
Yes	75 (91.5)	17 (89.5)		79 (90.8)	13 (92.9)		85 (91.4)	7 (87.5)	
No	7 (8.5)	2 (10.5)		8 (9.2)	1 (7.1)		8 (8.6)	1 (12.5)	
Adjuvant chemotherapy			.720			.344[a]			.233[a]
No or refuse	57 (69.5)	14 (73.7)		63 (72.4)	8 (57.1)		67 (72.0)	4 (50.0)	
Yes	25 (30.5)	5 (26.3)		24 (27.6)	6 (42.9)		26 (28.6)	4 (50.0)	
Gallstone			.798			.339[a]			.433[a]
No	58 (70.7)	14 (73.7)		60 (69.0)	12 (85.7)		65 (69.9)	7 (87.5)	
Yes	24 (29.3)	5 (26.3)		27 (31.0)	2 (14.3)		28 (30.1)	1 (12.5)	
Cholecystitis			.228			.727			>.99
No	21 (91.3)	2 (8.7)		21 (91.3)	2 (8.7)		21 (91.3)	2 (8.7)	
Yes	61 (78.2)	17 (21.8)		67 (85.9)	11 (14.1)		72 (92.3)	6 (7.7)	
Diabetes			.512			.137[a]			.268[a]
No	54 (65.9)	14 (73.7)		56 (64.4)	12 (85.7)		61 (65.6)	7 (87.5)	
Yes	28 (34.1)	5 (26.3)		31 (35.6)	2 (14.3)		32 (34.4)	1 (12.5)	
Hypertension			.729			.346			.255[a]
No	51 (62.2)	11 (57.9)		55 (63.2)	7 (50.0)		59 (63.4)	3 (37.5)	
Yes	31 (37.8)	8 (42.1)		32 (36.8)	7 (50.0)		34 (36.6)	5 (62.5)	

Values are presented as number (%).
Statistical analysis method: Pearson chi-square test.
PD-L1, programmed death-ligand 1; GBC, gallbladder cancer; NOS, not otherwise specified; ICPN, intracholecystic papillary neoplasm; Others, mixed adenoneuroendocrine carcinoma, signet ring cell carcinoma, mucinous carcinoma, sarcomatoid carcinoma.
[a]Fisher exact test.

https://doi.org/10.4132/jptm.2019.11.13

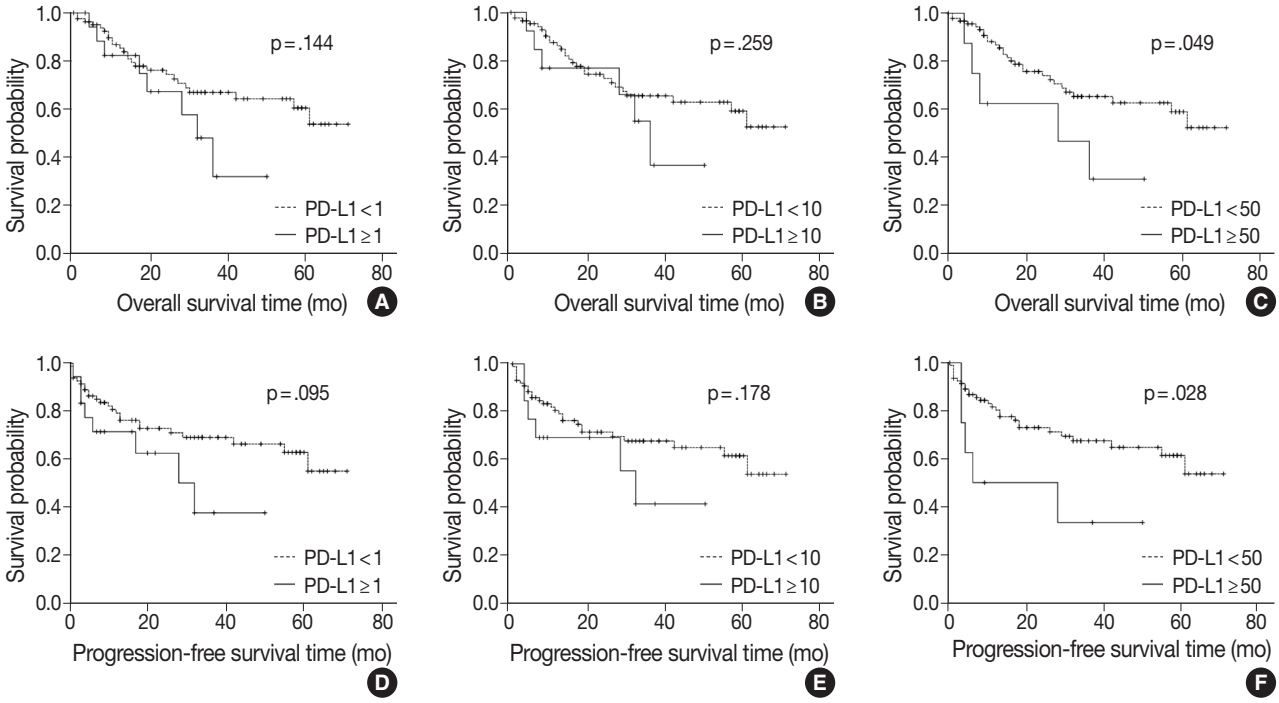

Fig. 2. Kaplan-Meier plots for overall survival or progression-free survival of gallbladder cancer according to programmed death-ligand 1 (PD-L1) expression (A, 1% cutoff; B, 10% cutoff; C, 50% cutoff; D, 1% cutoff; E, 10% cutoff; F, 50% cutoff).

location; margin of tumor resection; adjuvant chemotherapy; or primary risk factors for GBC such as gallstones, cholecystitis, diabetes, and hypertension. The associations between PD-L1 expression in tumor cells and clinicopathological characteristics of GBC patients are shown in Table 2.

Survival analysis

At the time of analysis, the median OS was 14 months (range, 0 to 71 months). Thirty-three patients (32.6%) died during the follow-up period. Meanwhile, a total of 24 patients showed disease progression, and 19 of these patients died. Survival analysis using Kaplan-Meier analysis was performed to evaluate the prognostic impact of PD-L1 expression and other parameters. OS was significantly associated with histologic grade ($p = .003$), T category ($p < .001$), N category ($p < .001$), pathologic stage ($p < .001$), lymphovascular invasion ($p < .001$), perineural invasion ($p < .001$), growth pattern ($p = .019$), and resection margin ($p = .006$). Worse mean survival was observed in histologic grade progressing from well-differentiated to poorly differentiated, undifferentiated, or other. The patients with higher T categories, nodal metastasis, higher pathologic stages, presence of lymphovascular invasion, and presence of perineural invasion showed poorer OS, whereas those with a polypoid growth pattern and complete resection showed better OS. These parameters were more significantly associated with PFS. Significant differences in both OS and PFS according to PD-L1 expression were seen only at the 50% cutoff statistically (1% cutoff: $p = .14$; 10% cutoff: $p = .259$; 50% cutoff: $p = .049$ for OS and 1% cutoff: $p = .095$; 10% cutoff: $p = .178$; 50% cutoff: $p = .028$ for PFS) (Fig. 2). We observed a high expression of PD-L1 correlated with poor prognostic significance of both survival types, especially PFS. Old age (≥68 years) was correlated with poor OS and larger tumor size (≥2.7 cm) was correlated with poor PFS, respectively. No significant associations with sex, histologic type, adjuvant chemotherapy, gallstone status, cholecystitis, diabetes, or hypertension were evident. Correlations between OS or PFS and clinicopathological parameters are shown in Table 3.

DISCUSSION

Immune checkpoint inhibitors targeting the PD-1–PD-L1 pathway have exhibited potent efficacy in some cancers such as triple-negative breast cancer, renal cell carcinoma, and non-small cell lung cancer [16-20]. Clinical benefits were strongly correlated with high PD-L1 expression and certain drugs have been approved for use in conjunction [20,21]. While PD-L1 expression significantly correlates with poor prognosis in gastric cancer, hepatocellular carcinoma, and esophageal cancer, both better

Table 3. Correlation of clinicopathological parameters with OS or PFS in GBC

Clinicopathological parameter	OS (mo)	p-value	PFS (mo)	p-value
Sex		.632		.694
Male	50.61±4.57		49.90±4.82	
Female	45.90±3.78		45.21±3.97	
Age (yr)		.044		.070
<68	52.37±3.65		51.07±3.99	
≥68	42.52±4.61		41.30±4.85	
Histologic type		.385		.349
Adenocarcinoma NOS, ICPN with associated invasive carcinoma	49.57±3.27		49.04±3.42	
Adenocarcinoma with other component, others	38.81±6.30		36.73±6.74	
Histologic grade		.003		.002
Well differentiated	59.50±3.62		59.02±3.79	
Moderately differentiated	40.43±4.59		39.81±4.87	
Poorly differentiated, undifferentiated, others	33.07±5.16		30.12±5.63	
T category		<.001		<.001
pT1+pT2	53.37±3.17		52.98±3.28	
pT3+pT4	25.05±5.41		19.64±6.02	
N category		<.001		<.001
N0	62.85±3.28		62.31±3.46	
N1+N2	34.51±5.05		32.62±5.75	
Pathologic stage		<.001		<.001
I+II	62.53±3.25		62.43±3.31	
III+IV	34.86±4.92		33.03±5.54	
Lymphovascular invasion		<.001		<.001
No	58.03±3.26		57.79±3.33	
Yes	31.38±4.34		28.17±4.89	
Perineural invasion		<.001		<.001
No	55.46±3.00		55.17±3.10	
Yes	31.91±5.06		29.65±5.59	
Tumor location		.050		.094
Fundus	42.46±4.07		42.17±4.44	
Body	48.36±4.42		47.67±4.61	
Neck, cystic duct	57.13±6.88		55.27±7.91	
More than 2 portions	24.73±6.50		24.64±6.82	
Tumor size (cm)		.058		.042
<2.7	54.65±4.14		54.16±4.29	
≥2.7	41.27±3.85		39.84±4.15	
Growth pattern		.019		.015
Polypoid	55.12±3.77		54.68±3.90	
Nonpolypoid, ulcerative	37.52±3.89		35.82±4.35	
Complete resection		.006		.005
Yes	25.63±8.72		22.98±9.38	
No	50.67±3.12		49.98±3.28	
Adjuvant chemotherapy		.488		.322
No	48.58±3.43		48.08±3.54	
Yes	45.27±5.46		43.02±6.11	
Gallstone		.066		.095
No	50.26±3.28		49.54±3.47	
Yes	38.78±5.63		38.31±5.87	
Cholecystitis		.668		.694
No	47.70±4.54		47.02±4.85	
Yes	47.78±3.64		47.45±3.78	
Diabetes		.270		.222
No	50.89±3.72		50.38±3.90	
Yes	42.10±4.57		40.50±4.86	

(Continued to the next page)

https://doi.org/10.4132/jptm.2019.11.13

Table 3. Continued

Clinicopathological parameter	OS (mo)	p-value	PFS (mo)	p-value
Hypertension		.615		.619
No	45.93±3.55		44.93±3.78	
Yes	51.21±4.96		51.02±5.07	
PD-L1 expression				
PD-L1<1%	50.53±3.29	.144	49.95±3.43	.095
PD-L1≥1%	31.35±4.42		28.75±5.17	
PD-L1<10%	49.80±3.24	.259	49.27±3.38	.178
PD-L1≥10%	32.89±5.03		30.31±5.75	
PD-L1<50%	50.13±3.14	.049	49.48±3.29	.028
PD-L1≥50%	27.88±6.69		23.33±7.47	

Values are presented as mean±standard error.
Statistical analysis method: survival analysis by Kaplan-Meier method and log-rank test.
OS, overall survival; PFS, progression-free survival; GBC, gallbladder cancer; NOS, not otherwise specified; ICPN, intracholecystic papillary neoplasm; others, mixed adenoneuroendocrine carcinoma, signet ring cell carcinoma, mucinous carcinoma,sarcomatoid carcinoma; PD-L1, programmed death-ligand 1.

and worse results have been observed in lung cancer, colorectal cancer, and melanoma [22]. PD-L1 expression has been suggested as an important prognostic factor, but few studies have evaluated the expression levels of PD-L1 in GBC patients and there are no consistent results regarding its value as a predictor.

Various studies suggest that PD-L1 expression is associated with poor prognostic factors or survival in different tumor types. These studies observed that tumors with poor differentiation, vascular invasion, nodal metastasis, higher stage, adenocarcinoma histology, and lower survival rate were correlated with higher PD-L1 expression. Table 4 summarizes recent studies covering the prognostic value of PD-L1 [11,12,23-32].

In patients with advanced cholangiocarcinoma or gallbladder adenocarcinoma, results from phase I KEYNOTE-028 and phase II KEYNOTE-158 research indicated that pembrolizumab, a humanized monoclonal antibody against PD-1, constitutes a possible treatment option regardless of PD-L1 expression [14]. The PD-L1 antibody (22C3) and a 1% cutoff level were used in these trials. Elsewhere, Ha et al. [33] found a high level of soluble PD-L1 in the serum represents a negative prognostic factor in advanced cholangiocarcinoma and GBC patients who received palliative chemotherapy. Recently, two other studies evaluated the predictive value of PD-L1 expression using immunohistochemistry in GBC tissues. Neyaz et al. [11] examined the relationship between PD-L1 expression in tumor cells and tumor-infiltrating lymphocytes (TILs) at cutoff levels of 1%, 10%, and 50% and clinicopathological characteristics or OS. Their study ultimately showed significant correlations existed in terms of histologic type, histologic grade, TIL density, and stage of disease at all cutoff levels but did not find any significant correlations in conjunction with OS. Lin et al. [12] evaluated the expression of PD-L1, PD-L2, and the density of $CD8^+$ TIL in association with OS, PFS, and risk factors in gallbladder adenocarcinoma by analyzing PD-L1 expression at a 5% cutoff level and performing four subgroup analyses according to PD-L1 expression and $CD8^+$ TILs. According to the results, there were no correlations observed with PD-L1 expression in tumor cells alone except for regarding $CD8^+$ TIL density and worse OS. Instead, the study demonstrated the coevaluation of CD8 TIL and PD-L1 had the significant prognostic value, and patients with high TILs and/or PD-L1 positivity had the worst PFS and OS.

Based on the above studies, PD-L1 expression in tumor cells as a predictive marker is controversial in GBC. In this study, we evaluated the expression of PD-L1 in 101 GBC cases and investigated the relationship between PD-L1 expression and various clinicopathological parameters or survival. A standard positive cutoff level or biomarker for PD-L1 has not been established [34-36]. Different antibodies (e.g., SP263, SP142, 22C3, 22-8, and E1L3N clones) and cutoff levels (e.g., 1%, 5%, 25%, and 50%) are used in various studies; we used the monoclonal antibody SP263 and the 1%, 10%, and 50% cutoff levels in our investigation. Our study showed a strong positive correlation in poor histologic grade and lymphovascular invasion at any cutoff level of PD-L1 expression. Also, other unfavorable parameters such as perineural invasion, higher T category, and higher pathologic stage of disease showed a significant correlation with PD-L1 expression at the 10% and 50% cutoff levels. Our final aim was to evaluate the prognostic impact of the clinicopathological parameters in survival. In this study, the association between PD-L1 expression at the 50% cutoff level and OS or PFS achieved statistical significance. Other parameters including the presence of lymphovascular invasion and perineural invasion; incomplete resection; higher histologic grade; higher T category, N category, and pathologic stage; and nonpolypoid growth pat-

http://jpatholtm.org/

Table 4. PD-L1 expression in tumor cells in various tumors

Disease	No.	Detection specimen; detection antibody	PD-L1 expression cutoff (%)	Other clinicopathological parameters associated with PD-L1 expression	Survival with PD-L1 expression	Study
Gallbladder cancer	174	FFPE tissue; anti–PD-L1 (clone SP263)	1, 10, 50	Significant positive association with histologic type (squamous cell carcinoma, adenosquamous cell carcinoma, undifferentiated carcinoma), histologic grade (progressed from WD to PD), nuclear grade, stage 3 and 4, TIL (0 to 3+)	OS was not associated with PD-L1 expression	Neyaz et al. [11]
Gallbladder adenocarcinoma	66	FFPE tissue; anti–PD-L1 (E1L3N)	5	PD-L1 positive alone was not correlated with any clinicopathological or pathological parameters except for $CD8^+$ TIL density and worse median OS	Combination of CD8 high with negative expression of PD-L1 serves as prognostic factor for improved OS and PFS	Lin et al. [12]
Gastric adenocarcinoma	240	FFPE tissue; anti–PD-L1 (E1L3N)	10	Patients with poor tumor differentiation had a higher positive rate of PD-L1 expression on tumor cells	Positive PD-L1 expression on TILs had a shorter OS; However, PD-L1 expression on tumor cells was not associated with OS	Fang et al. [23]
Gastric cancer	107	FFPE tissue; anti–PD-L1 (polyclonal anti-human PD-L1/CD274 antibody)	Not applicable	Positive rate of PD-L1 expression is much higher in depth of invasion, high differentiation, lymph node metastasis, and higher T category	PD-L1–positive gastric cancers were significantly associated with a poor prognosis	Qing et al. [24]
Esophageal cancer	41	Frozen tissue; anti–PD-L1 (MIH1, mouse IgG1)	10	Effect of PD-L1 status was more distinct in the advanced stage of tumor with lymph node metastasis and distinct metastasis	Overall survival of patients with tumors positive for both PD-L1 and PD-L2 was significantly worse than that with tumors negative for both	Ohigashi et al. [25]
Colorectal cancer	143	FFPE tissue; anti–PD-L1 (Abcam, ab58810)	Strong and moderate immunostaining intensity	PD-L1 was significantly associated with cell differentiation status and TNM stage	Positive PD-L1 expression showed a trend shorter survival time; as an independent predictor of prognosis	Shi et al. [26]
Lung adenocarcinoma	163	FFPE tissue; anti–PD-L1 (Proteintech Group Inc., Chicago, IL, USA)	5	PD-L1 had higher positive results in tumors with higher grade differentiation and vascular invasion	PD-L1 expression correlated with better RFS	Yang et al. [27]
Lung non-small cell carcinoma	819	FFPE tissue; anti–PD-L1 (22C3)	50	Lower PD-L1 positivity correlated with lower stage and squamous cell carcinoma than adenocarcinoma	Not assessed	Skov et al. [28]
Extrahepatic cholangiocarcinoma	69	FFPE tissue; anti–PD-L1 (E1L3N)	Not applicable	Significant correlations of PD-L1 expression with venous invasion and poor differentiation of the tumor were observed	PD-L1 expression was not correlated with patient OS, but combined high PDL1 expression on tumor cells and low infiltration of CD3+ TILs showed poor OS	Walter D et al. [29]
Hepatocellular carcinoma	240+ additional 125	FFPE tissue; anti–PD-L1 (eBioscience)	High vs. low	PD-L1 expression was an independent prognostic factor for tumor vascular invasion, encapsulation, and TNM stage	PD-L1–positive (high expression) patients had significantly poorer DFS and OS	Gao et al. [30]
Hepatocellular carcinoma	448	FFPE tissue; anti–PD-L1 (E1L3N)	1, 5	No significant difference in PD-L1 expression was detected	Survival analysis showed that 5% PD-L1 expression was significantly correlated with improved rates of OS and RFS	Chen et al. [31]
Uveal melanoma	67	FFPE tissue; anti–PD-L1 (E1L3N)	5	Significant association of PD-L1 expression to a decreased number of TIL	PD-L1 expression is associated with metastasis-free survival	Zoroquiain et al. [32]

PD-L1, programmed death-ligand 1; FFPE, formalin-fixed, paraffin-embedded; WD, well-differentiated; PD, poorly differentiated; TIL, tumor-infiltrating lymphocyte; OS, overall survival; PFS, progression-free survival.

https://doi.org/10.4132/jptm.2019.11.13

tern were also significantly associated with poor OS and PFS.

In summary, although opposite results have been reported regarding the use of PD-L1 expression as a predictive parameter in GBC, our results supported the negative clinical impact of PD-L1 expression as described by Lin et al. [12]. We found that GBC cases with high PD-L1 expression were significantly associated with poor clinicopathological parameters and survival at the 50% cutoff level. Interestingly, although a significant association with PD-L1 expression was found in the two studies using E1L3N and SP263, SP263 did not display any such significance in the previous study by Neyaz et al. [11]. We have to consider the following reasons for discrepancies in PD-L1 expression: dissimilar cutoff levels and anti-PD-L1 antibodies, heterogeneity of tumor, interobserver and intra-observer variability, and the influence of relationships with other indicators such as PD-L1 expression in TILs. Future research with larger study populations focused on elucidating detailed evaluation criteria and identifying the benefit of PD-L1–inhibiting immunomodulating therapies should be conducted.

ORCID

Ji Hye Kim: https://orcid.org/0000-0001-7160-8601
Kyungbin Kim: https://orcid.org/0000-0001-5430-4235
Misung Kim: https://orcid.org/0000-0002-7317-324X
Young Min Kim: https://orcid.org/0000-0001-8266-4553
Jae Hee Suh: https://orcid.org/0000-0001-7032-0294
Hee Jeong Cha: https://orcid.org/0000-0001-8744-5747
Hye Jeong Choi: https://orcid.org/0000-0002-5124-8589

Author Contributions

Conceptualization: JHK, HJC (Hye Jeong Choi).
Data curation: JHK.
Formal analysis: JHK, MK.
Investigation: JHK.
Methodology: JHK, KK, MK, HJC (Hee Jeong Cha), YMK, JHS, HJC (Hye Jeong Choi).
Project administration: HJC (Hye Jeong Choi).
Resources: HJC (Hye Jeong Choi).
Supervision: HJC (Hye Jeong Choi).
Validation: JHK, KK, MK, HJC (Hee Jeong Cha), YMK, HJC (Hye Jeong Choi).
Visualization: JHK, HJC (Hye Jeong Choi).
Writing—original draft: JHK, HJC (Hye Jeong Choi).
Writing—review & editing: KK, MK, HJC (Hee Jeong Cha), YMK, JHS.

Conflicts of Interest

The authors declare that they have no potential conflicts of interest.

Funding

No funding to declare.

Acknowledgments

This work was supported by the Medical Information Center of Ulsan University Hospital in statistical analyses.

REFERENCES

1. Shaffer EA. Gallbladder cancer: the basics. Gastroenterol Hepatol (N Y) 2008; 4: 737-41.
2. Goldin RD, Roa JC. Gallbladder cancer: a morphological and molecular update. Histopathology 2009; 55: 218-29.
3. Albores-Saavedra J, Kloppel G, Adsay NV, et al. Carcinoma of the gallbladder and extrahepatic bile ducts. In: Bosman FT, Carneiro F, Hruban RH, Theise ND, eds. WHO classification of tumours of the digestive system. 4th ed. Lyon: IARC Press, 2010; 266-73.
4. Aloia TA, Jarufe N, Javle M, et al. Gallbladder cancer: expert consensus statement. HPB (Oxford) 2015; 17: 681-90.
5. Wi Y, Woo H, Won YJ, Jang JY, Shin A. Trends in gallbladder cancer incidence and survival in Korea. Cancer Res Treat 2018; 50: 1444-51.
6. Kim BW, Oh CM, Choi HY, Park JW, Cho H, Ki M. Incidence and overall survival of biliary tract cancers in South Korea from 2006 to 2015: using the National Health Information Database. Gut Liver 2019; 13: 104-13.
7. Jiao Y, Pawlik TM, Anders RA, et al. Exome sequencing identifies frequent inactivating mutations in *BAP1*, *ARID1A* and *PBRM1* in intrahepatic cholangiocarcinomas. Nat Genet 2013; 45: 1470-3.
8. Javle MM, Rashid A, Kar SP, et al. Identification of unique somatic mutations with functional relevance through genetic characterization of gallbladder cancer (GB ca). J Clin Oncol 2013; 31(4 Suppl): 214.
9. Wu P, Wu D, Li L, Chai Y, Huang J. PD-L1 and survival in solid tumors: a meta-analysis. PLoS One 2015; 10: e0131403.
10. Pyo JS, Kang G, Kim JY. Prognostic role of PD-L1 in malignant solid tumors: a meta-analysis. Int J Biol Markers 2017; 32: e68-74.
11. Neyaz A, Husain N, Kumari S, et al. Clinical relevance of PD-L1 expression in gallbladder cancer: a potential target for therapy. Histopathology 2018; 73: 622-33.
12. Lin J, Long J, Wan X, et al. Classification of gallbladder cancer by assessment of CD8(+) TIL and PD-L1 expression. BMC Cancer 2018; 18: 766.

13. Takahashi R, Yoshitomi M, Yutani S, et al. Current status of immunotherapy for the treatment of biliary tract cancer. Hum Vaccin Immunother 2013; 9: 1069-72.
14. Bang YJ, Ueno M, Malka D, et al. Pembrolizumab (pembro) for advanced biliary adenocarcinoma: results from the KEYNOTE-028 (KN028) and KEYNOTE-158 (KN158) basket studies. J Clin Oncol 2019; 37(15 Suppl): 4079.
15. Amin MB, Edge S, Greene F, et al. AJCC cancer staging manual. New York: Springer, 2017.
16. Schmid P, Adams S, Rugo HS, et al. Atezolizumab and Nab-paclitaxel in advanced triple-negative breast cancer. N Engl J Med 2018; 379: 2108-21.
17. Motzer RJ, Penkov K, Haanen J, et al. Avelumab plus axitinib versus sunitinib for advanced renal-cell carcinoma. N Engl J Med 2019; 380: 1103-15.
18. Giroux Leprieur E, Dumenil C, Julie C, et al. Immunotherapy revolutionises non-small-cell lung cancer therapy: results, perspectives and new challenges. Eur J Cancer 2017; 78: 16-23.
19. Carretero-González A, Lora D, Ghanem I, et al. Analysis of response rate with ANTI PD1/PD-L1 monoclonal antibodies in advanced solid tumors: a meta-analysis of randomized clinical trials. Oncotarget 2018; 9: 8706-15.
20. Zhao B, Zhang W, Yu D, Xu J, Wei Y. The benefit and risk of nivolumab in non-small-cell lung cancer: a single-arm meta-analysis of noncomparative clinical studies and randomized controlled trials. Cancer Med 2018; 7: 1642-59.
21. Reck M, Rodriguez-Abreu D, Robinson AG, et al. Pembrolizumab versus chemotherapy for PD-L1-positive non-small-cell lung cancer. N Engl J Med 2016; 375: 1823-33.
22. Wang X, Teng F, Kong L, Yu J. PD-L1 expression in human cancers and its association with clinical outcomes. Onco Targets Ther 2016; 9: 5023-39.
23. Fang W, Chen Y, Sheng J, et al. Association between PD-L1 expression on tumour-infiltrating lymphocytes and overall survival in patients with gastric cancer. J Cancer 2017; 8: 1579-85.
24. Qing Y, Li Q, Ren T, et al. Upregulation of PD-L1 and APE1 is associated with tumorigenesis and poor prognosis of gastric cancer. Drug Des Devel Ther 2015; 9: 901-9.
25. Ohigashi Y, Sho M, Yamada Y, et al. Clinical significance of programmed death-1 ligand-1 and programmed death-1 ligand-2 expression in human esophageal cancer. Clin Cancer Res 2005; 11: 2947-53.
26. Shi SJ, Wang LJ, Wang GD, et al. B7-H1 expression is associated with poor prognosis in colorectal carcinoma and regulates the proliferation and invasion of HCT116 colorectal cancer cells. PLoS One 2013; 8: e76012.
27. Yang CY, Lin MW, Chang YL, Wu CT, Yang PC. Programmed cell death-ligand 1 expression in surgically resected stage I pulmonary adenocarcinoma and its correlation with driver mutations and clinical outcomes. Eur J Cancer 2014; 50: 1361-9.
28. Skov BG, Rorvig SB, Jensen TH, Skov T. The prevalence of programmed death ligand-1 (PD-L1) expression in non-small cell lung cancer in an unselected, consecutive population. Mod Pathol 2020; 33: 109-17.
29. Walter D, Herrmann E, Schnitzbauer AA, et al. PD-L1 expression in extrahepatic cholangiocarcinoma. Histopathology 2017; 71: 383-92.
30. Gao Q, Wang XY, Qiu SJ, et al. Overexpression of PD-L1 significantly associates with tumor aggressiveness and postoperative recurrence in human hepatocellular carcinoma. Clin Cancer Res 2009; 15: 971-9.
31. Chen CL, Pan QZ, Zhao JJ, et al. PD-L1 expression as a predictive biomarker for cytokine-induced killer cell immunotherapy in patients with hepatocellular carcinoma. Oncoimmunology 2016; 5: e1176653.
32. Zoroquiain P, Esposito E, Logan P, et al. Programmed cell death ligand-1 expression in tumor and immune cells is associated with better patient outcome and decreased tumor-infiltrating lymphocytes in uveal melanoma. Mod Pathol 2018; 31: 1201-10.
33. Ha H, Nam AR, Bang JH, et al. Soluble programmed death-ligand 1 (sPDL1) and neutrophil-to-lymphocyte ratio (NLR) predicts survival in advanced biliary tract cancer patients treated with palliative chemotherapy. Oncotarget 2016; 7: 76604-12.
34. Diggs LP, Hsueh EC. Utility of PD-L1 immunohistochemistry assays for predicting PD-1/PD-L1 inhibitor response. Biomark Res 2017; 5: 12.
35. Festino L, Botti G, Lorigan P, et al. Cancer treatment with anti-PD-1/PD-L1 agents: is PD-L1 expression a biomarker for patient selection? Drugs 2016; 76: 925-45.
36. O'Malley DP, Yang Y, Boisot S, et al. Immunohistochemical detection of PD-L1 among diverse human neoplasms in a reference laboratory: observations based upon 62,896 cases. Mod Pathol 2019; 32: 929-42.

 https://doi.org/10.4132/jptm.2019.11.13

JPTM
Journal of Pathology and Translational Medicine 2020; 54: 165-170
https://doi.org/10.4132/jptm.2020.02.04

ORIGINAL ARTICLE

Adjunctive markers for classification and diagnosis of central nervous system tumors: results of a multi-center neuropathological survey in Korea

Yoon Jin Cha[1]*, Se Hoon Kim[1]*, Na Rae Kim[2], The Neuropathology Study Group of the Korean Society of Pathologists

[1]Department of Pathology, Yonsei University College of Medicine, Seoul;
[2]Department of Pathology, Gachon University Gil Medical Center, Incheon, Korea

Background: The revised 4th 2016 World Health Organization (WHO) classification of tumors of the central nervous system (CNS) classification has adopted integrated diagnosis encompassing the histology and molecular features of CNS tumors. We aimed to investigate the immunohistochemistry, molecular testing, and testing methods for diagnosis of CNS tumors in pathological labs of tertiary centers in Korea, and evaluate the adequacy of tests for proper diagnosis in daily practice. **Methods:** A survey, composed of eight questions concerning molecular testing for diagnosis of CNS tumors, was sent to 10 neuropathologists working in tertiary centers in Korea. **Results:** For diagnosis of astrocytic and oligodendroglial tumors, all 10 centers performed isocitrate dehydrogenase mutations testing and 1p/19q loss of heterozygosity. For glioneuronal tumors, immunohistochemistry (IHC) assays for synaptophysin (n=9), CD34 (n=7), BRAF(VE1) (n=5) were used. For embryonal tumors, particularly in medulloblastoma, four respondents used IHC panel (growth factor receptor bound protein 2-associated protein 1, filamin A, and yes-associated protein 1) for molecular subclassification. Regarding meningioma, all respondents performed Ki-67 IHC and five performed telomerase reverse transcriptase promoter mutation. **Conclusions:** Most tertiary centers made proper diagnosis in line with 2016 WHO classification. As classification of CNS tumors has evolved to be more complex and more ancillary tests are required, these should be performed considering the effect of necessity and justification.

Key Words: World Health Organization; Central nervous system; Neoplasms; Molecular testing; Korea

Received: January 7, 2020 **Revised:** January 29, 2020 **Accepted:** February 4, 2020
Corresponding Author: Na Rae Kim, MD, Department of Pathology, Gachon University Gil Medical Center, 21 Namdong-daero 774beon-gil, Namdong-gu, Incheon 21565, Korea
Tel: +82-32-460-3073, Fax: +82-32-460-2394, E-mail: clara_nrk@gilhospital.com

*Yoon Jin Cha and Se Hoon Kim contributed equally to this work.

The 4th revised World Health Organization (WHO) classification of tumors of the central nervous system (CNS) highlights the importance of integrated diagnosis of CNS tumors [1]. In addition to histological features, molecular signatures are now mandatory for diagnosis, as well as patient management in neuro-oncological aspects. Molecularly different tumors could have different biological behavior and treatment response to therapeutic agents. The 2016 update of WHO classification suggests well-established molecular parameters in diagnostic algorithms of diffuse gliomas. For appropriate integrated diagnosis of diffuse gliomas, one needs to examine the isocitrate dehydrogenase (IDH) mutation and 1p/19q status. In this study, we investigated current adjuvant examination being performed in Korea for diagnosis of brain tumors.

MATERIALS AND METHODS

The survey was distributed to the members of the Korean Society of Neuropathology (n = 12) from May to June 2017 (30 days). We expected that most institutions would have prepared for the new diagnostic criteria proposed by the revised WHO classification.

Survey questionnaires included the number of neuropathological specimens per year, ancillary tests being performed for brain tumor diagnosis, and the type of methods for the ancillary tests. The results were analyzed after receiving answers to the survey.

Ethics statement

This study did not involve human subjects and was approved

pISSN 2383-7837
eISSN 2383-7845

by the Institutional Review Board of Gachon University Gil Medical Center with a waiver of informed consent (GFIRB2018-266).

RESULTS

The survey questions were answered by 10 of the 12 neuropathologists who received the survey questionnaires. All 10 respondents were neuropathologists working in tertiary centers capable of neurosurgery and neuropathological diagnosis. The total number of neuropathological cases for a year, including tumor, non-tumor, muscle, and peripheral nerve biopsy, was more than 300 cases in five centers (average, 906; range, 392 to 1,900), 200–300 cases in one center, 100–200 cases in another, 50–100 in two, and less than 50 cases in two others. All 10 centers make the diagnosis based on the 4th revised 2016 WHO classification.

Immunohistochemical stainings in gliomas

For diagnosis of astrocytic and oligodendroglial tumors, immunohistochemistry (IHC) for glial fibrillary acidic protein (GFAP), oligodendrocyte transcription factor 2 (OLIG2), α-thalassemia/mental retardation syndrome X-linked (ATRX), IDH1, BRAF (VE1), Ki-67, p53, S-100, vimentin, epidermal growth factor receptor (EGFR), synaptophysin, H3.3K27M, and H3.3K27me3 was used. Depending on the centers, three to 11 markers were used for diagnosis. The most commonly used IHC markers were IDH1, ATRX, p53, and Ki-67 (Fig. 1A).

In pilocytic astrocytomas and pleomorphic xanthoastocytomas (PXAs), most IHC markers were overlapped with the items mentioned above (Supplementary Fig. S1).

For diagnosis of ependymomas, GFAP, epithelial membrane

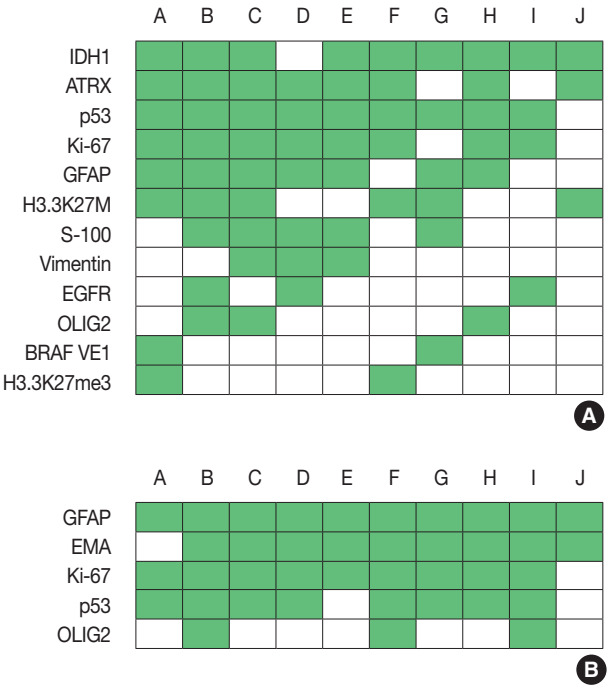

Fig. 1. Immunohistochemistry markers used in glioma (A) and ependymoma (B). Alphabet A–J represents respondents. IDH1, isocitrate dehydrogenase 1; ATRX, α-thalassemia/mental retardation syndrome X-linked; GFAP, glial fibrillary acidic protein; EGFR, epidermal growth factor receptor; OLIG2, oligodendrocyte transcription factor 2; EMA, epithelial membrane antigen.

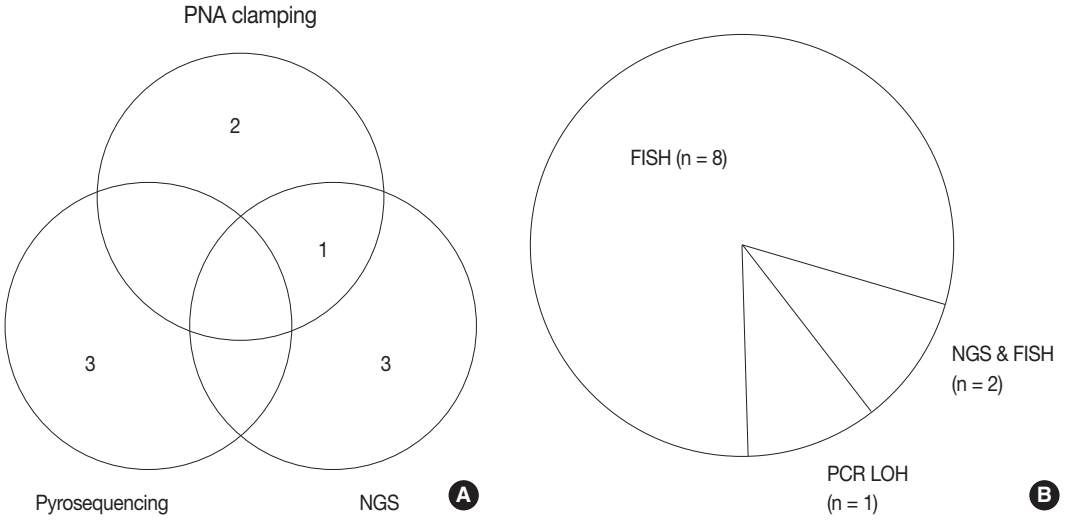

Fig. 2. Current methods for isocitrate dehydrogenase (IDH) mutation test (A) and 1p/19q status (B) among respondents. PNA, peptide nucleic acid; NGS, next-generation sequencing; FISH, fluorescence in situ hybridization; PCR, polymerase chain reaction; LOH, loss of heterozygosity.

https://doi.org/10.4132/jptm.2020.02.04

antigen, Ki-67, and p53 were most frequently used, followed by CD99 and OLIG2 (Fig. 1B).

Molecular testing in gliomas

Regarding astrocytic and oligodendroglial tumors, IDH mutation tests (including *IDH1* and *IDH2*) (n = 9) and 1p/19q loss of heterozygosity (LOH) (n = 10) were performed before making a final diagnosis. Next-generation sequencing (NGS) (n = 4), pyrosequencing (n = 3), peptide nucleic acid (PNA) clamping method (n = 3), and Sanger sequencing (n = 1) methods were used for IDH mutation testing (Fig. 2A). One center performs both NGS and PNA clamping methods for IDH mutation test whereas the other one uses only IDH1 IHC. While most of the centers used fluorescence in situ hybridization (FISH) to evaluate the 1p/19q status, two centers conducted NGS in addition to FISH, for evaluating the 1p/19q status. One center used polymerase chain reaction–based LOH analysis (Fig. 2B)

Additional molecular testing included *MGMT* (O^6-methylguanine–DNA methyltransferase) methylation test (n = 8), and telomerase reverse transcriptase (*TERT*) promoter mutation (n = 8; four single test, four NGS). *BRAF* mutation test and NGS test, for V600E, were performed in eight centers. One center separately performed *BRAF* mutation test in all astrocytic and oligodendroglial tumors. Two centers performed *BRAF* mutation test in all infiltrating gliomas except oligodendroglioma.

For pilocytic astrocytomas and PXAs, most molecular testings were overlapped with the items mentioned above (Supplementary Fig. S2).

For ependymomas, three centers performed NGS and one center performed an additional FISH test for 1q gain.

Ganglioglioma and dysembryoplastic neuroepithelial tumor

Regarding glioneuronal tumors, the survey focused on gangliogliomа and dysembryoplastic neuroepithelial tumor (DNET), as they comprised the majority of glioneuronal tumors. In cases of ganglioglioma, the most commonly used IHC markers were GFAP, Ki-67, and synaptophysin, followed by NeuN and CD34 (Fig. 3A), whereas for DNET, synaptophysin, GFAP, Ki-67, CD34, and NeuN were the most commonly used (Fig. 3B). Regarding molecular testing, one center performed the same molecular tests as in gliomas. In some centers, IDH mutation test (n = 3 in ganglioglioma, n = 2 in DNET), *BRAF* V600E test (n = 1 in ganglioglioma, n = 2 in DNET), and *MGMT* methylation test (n = 2 in ganglioglioma, n=3 in DNET) were performed. NGS was performed for ganglioglioma in three centers and DNET in one. Five centers did not perform further molecular testing in ganglioglioma and DNET.

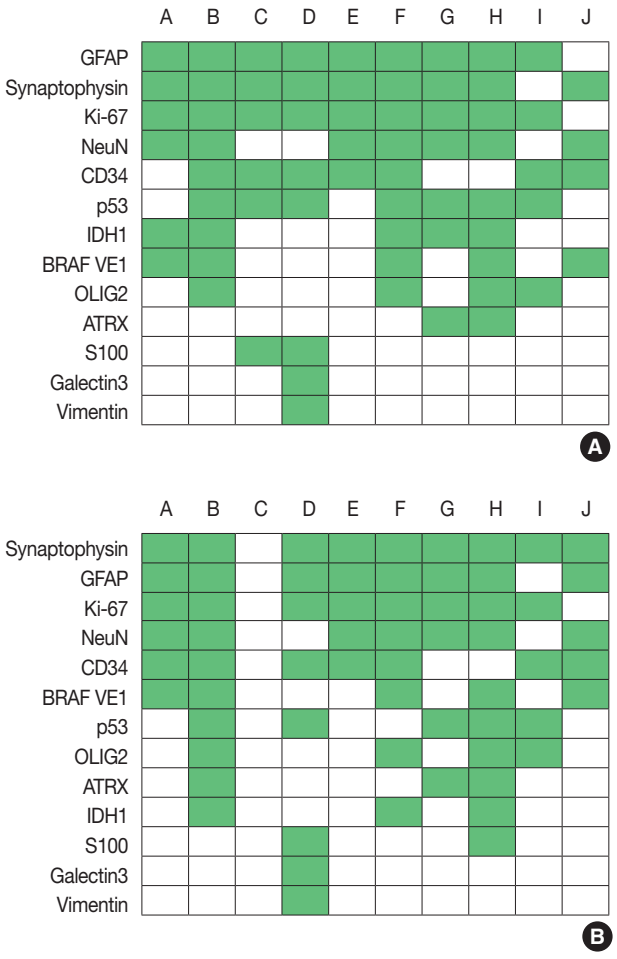

Fig. 3. Immunohistochemistry markers used in ganglioglioma (A) and dysembryoplastic neuroepithelial tumor (B). Alphabet A–J represents respondents. GFAP, glial fibrillary acidic protein; IDH1, isocitrate dehydrogenase 1; OLIG2, oligodendrocyte transcription factor 2; ATRX, α-thalassemia/mental retardation syndrome X-linked.

Embryonal tumors

p53 (n = 9), Ki-67 (n = 9), and synaptophysin (n=8) were the most commonly used IHC markers in medulloblastoma, followed by GFAP. For molecular classification, surrogate IHC markers, including growth factor receptor bound protein 2-associated protein 1 (GAB1; n = 5), β-catenin (n = 1), filamin A (n = 4), and yes-associated protein 1 (YAP1) (n = 4), were used. All 10 centers performed integrase interactor 1 IHC for atypical teratoid rhabdoid tumors and one center performed additional BRG2 IHC. LIN28A IHC was used for embryonal tumors in three centers. Three centers performed NGS for embryonal tumors.

Meningioma

All 10 centers performed Ki-67 IHC for meningioma, and additional phosphohistone H3 IHC was used in six centers. Three centers separately examined the *TER*T promoter mutation. Two centers performed NGS for meningioma, which included *TERT* in NGS panel.

DISCUSSION

We conducted surveys in 10 pathology labs in tertiary centers in Korea to investigate the current status of adjunctive examination for CNS tumor diagnosis. The 4th revised 2016 WHO classification adopted layered diagnosis encompassing histological and molecular features, which can precisely classify CNS tumors, thus allowing for more accurate predictions, regarding treatment response and prognosis [1]. In particular, IDH mutation and 1p/19q status are the most important diagnostic discriminators of astrocytic and oligodendroglial tumors.

We found that the majority of tertiary centers examined IDH mutation and 1p/19q status before development of final diagnosis in glial tumors. Particularly, IDH1 IHC is included in routine IHC panel in most centers and appears to be a very helpful surrogate marker for IDH mutation, because approximately over 90% of IDH mutation is *IDH1* [2]. Although *ATRX* is not essential in diagnosis of glial tumors based on the current WHO classification, 80% of respondents routinely used ATRX IHC.

The *ATRX* gene is a telomere maintenance-related gene that functions in chromatic remodeling and maintains genomic stability incorporating H3.3 histone proteins into telomeres [3,4]. *ATRX* gene inactivation is correlated with the alternative lengthening of telomeres. A subset of gliomas harboring *ATRX* mutation is characterized by IDH mutation and 1p/19q intact [5-7]. Loss of nuclear expression by IHC is a highly sensitive and specific feature of *ATRX* alteration [4] and can be used as a surrogate marker for *ATRX* mutation. Combining IHC panel with IDH1 and ATRX helps to predict astrocytic tumors in cases of those lacking ATRX expression [8].

MGMT methylation and *TERT* promoter mutation are not required for diagnosis, but impact patient prognosis and treatment response [9-11]. Promoter methylation of *MGMT* induces epigenetic silencing of the *MGMT* gene, restoring alkylated DNA. Temozolomide is an alkylating agent used in glioblastoma and the benefits of temozolomide treatment have been shown in patients with *MGMT* methylation [10]. *TERT* promoter mutation increases telomerase activity and is frequently found in glioblastomas and oligodendrogliomas [12]. Previous study classified gliomas into molecular groups based on IDH mutation, 1p/19q, and *TERT* mutation status [9]. Results showed higher survival rate in *TERT* and IDH mutation groups in grade II and III gliomas, whilst single *TERT* mutation showed the worst survival rate of all gliomas [9]. *MGMT* methylation and *TERT* promoter mutation tests were conducted in 80% of the respondents, and four centers obtained *TERT* promoter mutation results by NGS.

NGS has been evolving rapidly and is being adopted in many tertiary centers in Korea. NGS uses targeted gene panels to analyze hundreds of genes. In Korea, there are essential genes such as *HER2*, *EGFR*, *ALK*, *KRAS*, *NRAS*, *BRAF*, *BRCA1*, *BRCA2*, *KIT*, *PDGFRA*, *IDH1*, *IDH2*, *MYC (C-myc)*, and *N-myc (MYCN)* for non-hereditary solid tumors, that should be included in said panels. Most tertiary centers running NGS use gene panels with 50–300 genes. For gliomas, only one of the respondents was using a separate neuropathology gene panel, and the remaining were using a common panel for solid tumors. For infiltrating gliomas, NGS was routinely performed in six centers. In addition to *EGFR*, *BRAF*, *IDH1*, and *IDH2* which are essential panel genes, six respondents had *TERT*, *TP53*, and *SMARCB1* also in their panels, and one institution substituted FISH with 1p/19q LOH (by evaluation of microsatellite loci) by NGS.

For the diagnosis of glioneuronal tumors, CD34 and synaptophysin IHC were the most commonly performed assays. Synaptophysin is a marker for presynaptic vesicle, and is widely used to detect neuron or neuronal differentiation. DNET and gangliogliomas are the most common glioneuronal tumors and the differential diagnosis between these two is important, because DNET is a benign tumor but gangliogliomas could undergo malignant transformation [13,14]. Expression of CD34 is the one characteristic feature that favors gangliogliomas diagnosis over DNET [13]. *BRAF* V600E mutation could be found variably in glioneuronal tumors including DNET, gangliogliomas, and PXA [15,16] and could be used as a diagnostic and targetable marker.

For meningioma, all respondents performed Ki-67 IHC routinely. Although Ki-67 labeling index (LI) is not included in the current grading system, Ki-67 LI is correlated with mitosis and tumor recurrence [17,18]. In previous studies, tumors with more than 3% proliferative index, showed a shorter recurrence time after resection [19]. *TERT* mutation also has been reported in meningiomas, especially in recurrent and high grade (grades II and III) tumors [20]. Although an overall incidence of *TERT* mutation is low (around 5%) in meningioma, *TERT* mutation

 https://doi.org/10.4132/jptm.2020.02.04

predicted more aggressive behavior and poor prognosis in meningioma [21,22].

Medulloblastoma is one of the most common embryonal tumors and the second most common CNS tumor in children. Medulloblastoma is considered a heterogeneous group that can be classified into four molecular subgroups based on Sonic hedgehog (SHH) and WNT status. In daily practice, using three (GAB1, filamin A, and YAP1) or four IHC (GAB1, filamin A, YAP1, and β-catenin) panel could discriminate SHH, WNT, and non-SHH/WNT subgroups [23]. Moreover, *TP53* mutation can designate the WNT type, IHC of p53 in mutant pattern could help to limitedly predict the molecular subtype [24]. Five respondents (50%) used GAB1 and four used a panel composed of GAB1, filamin A, and YAP1, and nine respondents used Ki-67 and p53 as routine IHC panel in medulloblastoma.

NGS can evaluate clinically significant variants across hundreds of targeted genes. In Korea, CNS tumor is classified under non-genetic solid tumor category. Among the essentially required 14 genes, *EGFR*, *BRAF*, *IDH1*, and *IDH2* are relevant to CNS tumors. In the present survey, almost all tertiary centers except one used commercial panels and platforms from the same manufacturers, which also meets the government's minimum requirements. NGS is an accurate and sensitive tool for detection of additional genetic alteration with much less amount of DNA or RNA compared to the conventional techniques, which require more amount of tissue and only detect one alteration in one test. However, in daily practice, NGS is still an expensive ancillary test as it has a 2–4 week-turnaround time. For prompt diagnosis and subsequent proper treatment, IDH mutation and 1p/19q LOH are being examined separately to achieve more rapid final diagnosis.

In conclusion, we found that most tertiary centers handling neuropathological specimens were making diagnosis according to the 2016 WHO classification. However, a limitation is still present because present survey could not encompass every single pathology lab in Korea. Although most CNS tumors in Korea are expected to be managed in tertiary centers that participated in this survey, there is a possibility that some cases that are not handled in tertiary centers may not be properly examined for the basic molecular status such as IDH mutation. For the sake of proper diagnosis, the first line of ancillary tests composed of IHC and simple molecular tests should be established. The second line of ancillary tests should encompass NGS assay and other further tests that can cover the detailed analysis of CNS tumors.

Supplementary Materials

The Data Supplement is available with this article at https://doi.org/10.4132/jptm.2020.02.04.

ORCID

Yoon Jin Cha: https://orcid.org/0000-0002-5967-4064
Se Hoon Kim: https://orcid.org/0000-0001-7516-7372
Na Rae Kim: https://orcid.org/0000-0003-2793-6856

Author Contributions

Conceptualization: NRK, SHK.
Data curation: YJC.
Formal analysis: YJC.
Funding acquisition: NRK.
Investigation: YJC, SHK, NRK.
Methodology: SHK.
Supervision: SHK, NRK.
Validation: YJC.
Writing—original draft: YJC, SHK.
Writing—review & editing: YJC, SHK, NRK.

Conflicts of Interest

S.H.K., contributing editor of the *Journal of Pathology and Translational Medicine*, was not involved in the editorial evaluation or decision to publish this article. All remaining authors have declared no conflicts of interest.

Funding

This research was supported by 2015 The Korean Society of Pathologists Grant.

Acknowledgments

We have to express our appreciation to the participants who generously shared their time, experience, and materials for the purposes of this project. All the products of this work would not be possible without their support and participation: Sung-Hye Park, Seoul National University Hospital; Youn Soo Lee, Seoul ST. Mary's Hospital; Mi Jung Kwon, Hallym University Sacred Heart Hospital; Sang Pyo Kim, Keimyung University Dongsan Medical Center; Eun Deok Chang, Uijeongbu ST. Mary's Hospital; Kyung Hwa Lee, Chonnam National University Hwasun Hospital; So Dug Lim, Konkuk University Medical Center; Soo Jeong Nam, Asan Medical Center.

REFERENCES

1. Louis DN, Ohgaki H, Wiestler OD, Cavenee WK. WHO classifica-

tion of tumours of the central nervous system. 4th rev. ed. Lyon: IARC Press, 2016.
2. Yan H, Parsons DW, Jin G, et al. *IDH1* and *IDH2* mutations in gliomas. N Engl J Med 2009; 360: 765-73.
3. Pekmezci M, Rice T, Molinaro AM, et al. Adult infiltrating gliomas with WHO 2016 integrated diagnosis: additional prognostic roles of ATRX and TERT. Acta Neuropathol 2017; 133: 1001-16.
4. Heaphy CM, de Wilde RF, Jiao Y, et al. Altered telomeres in tumors with *ATRX* and DAXX mutations. Science 2011; 333: 425.
5. Kannan K, Inagaki A, Silber J, et al. Whole-exome sequencing identifies *ATRX* mutation as a key molecular determinant in lower-grade glioma. Oncotarget 2012; 3: 1194-203.
6. Leeper HE, Caron AA, Decker PA, Jenkins RB, Lachance DH, Giannini C. IDH mutation, 1p19q codeletion and *ATRX* loss in WHO grade II gliomas. Oncotarget 2015; 6: 30295-305.
7. Liu XY, Gerges N, Korshunov A, et al. Frequent *ATRX* mutations and loss of expression in adult diffuse astrocytic tumors carrying *IDH1/IDH2* and *TP53* mutations. Acta Neuropathol 2012; 124: 615-25.
8. Karsy M, Guan J, Cohen AL, Jensen RL, Colman H. New molecular considerations for glioma: IDH, ATRX, BRAF, TERT, H3 K27M. Curr Neurol Neurosci Rep 2017; 17: 19.
9. Eckel-Passow JE, Lachance DH, Molinaro AM, et al. Glioma groups based on 1p/19q, *IDH*, and *TERT* promoter mutations in tumors. N Engl J Med 2015; 372: 2499-508.
10. Hegi ME, Diserens AC, Gorlia T, et al. *MGMT* gene silencing and benefit from temozolomide in glioblastoma. N Engl J Med 2005; 352: 997-1003.
11. Stupp R, Hegi ME, Mason WP, et al. Effects of radiotherapy with concomitant and adjuvant temozolomide versus radiotherapy alone on survival in glioblastoma in a randomised phase III study: 5-year analysis of the EORTC-NCIC trial. Lancet Oncol 2009; 10: 459-66.
12. Arita H, Narita Y, Fukushima S, et al. Upregulating mutations in the *TERT* promoter commonly occur in adult malignant gliomas and are strongly associated with total 1p19q loss. Acta Neuropathol 2013; 126: 267-76.
13. Blumcke I, Wiestler OD. Gangliogliomas: an intriguing tumor entity associated with focal epilepsies. J Neuropathol Exp Neurol 2002; 61: 575-84.
14. Luyken C, Blumcke I, Fimmers R, Urbach H, Wiestler OD, Schramm J. Supratentorial gangliogliomas: histopathologic grading and tumor recurrence in 184 patients with a median follow-up of 8 years. Cancer 2004; 101: 146-55.
15. Chappe C, Padovani L, Scavarda D, et al. Dysembryoplastic neuroepithelial tumors share with pleomorphic xanthoastrocytomas and gangliogliomas *BRAF*(V600E) mutation and expression. Brain Pathol 2013; 23: 574-83.
16. Schindler G, Capper D, Meyer J, et al. Analysis of *BRAF* V600E mutation in 1,320 nervous system tumors reveals high mutation frequencies in pleomorphic xanthoastrocytoma, ganglioglioma and extra-cerebellar pilocytic astrocytoma. Acta Neuropathol 2011; 121: 397-405.
17. Lanzafame S, Torrisi A, Barbagallo G, Emmanuele C, Alberio N, Albanese V. Correlation between histological grade, MIB-1, p53, and recurrence in 69 completely resected primary intracranial meningiomas with a 6 year mean follow-up. Pathol Res Pract 2000; 196: 483-8.
18. Ozen O, Demirhan B, Altinors N. Correlation between histological grade and MIB-1 and p53 immunoreactivity in meningiomas. Clin Neuropathol 2005; 24: 219-24.
19. Oya S, Kawai K, Nakatomi H, Saito N. Significance of Simpson grading system in modern meningioma surgery: integration of the grade with MIB-1 labeling index as a key to predict the recurrence of WHO Grade I meningiomas. J Neurosurg 2012; 117: 121-8.
20. Goutagny S, Nault JC, Mallet M, Henin D, Rossi JZ, Kalamarides M. High incidence of activating *TERT* promoter mutations in meningiomas undergoing malignant progression. Brain Pathol 2014; 24: 184-9.
21. Spiegl-Kreinecker S, Lotsch D, Neumayer K, et al. *TERT* promoter mutations are associated with poor prognosis and cell immortalization in meningioma. Neuro Oncol 2018; 20: 1584-93.
22. Sahm F, Schrimpf D, Olar A, et al. TERT promoter mutations and risk of recurrence in meningioma. J Natl Cancer Inst 2016; 108: djv377.
23. Ellison DW, Dalton J, Kocak M, et al. Medulloblastoma: clinicopathological correlates of SHH, WNT, and non-SHH/WNT molecular subgroups. Acta Neuropathol 2011; 121: 381-96.
24. Ramaswamy V, Remke M, Bouffet E, et al. Risk stratification of childhood medulloblastoma in the molecular era: the current consensus. Acta Neuropathol 2016; 131: 821-31.

 https://doi.org/10.4132/jptm.2020.02.04

JPTM
Journal of Pathology and Translational Medicine 2020; 54: 171-178
https://doi.org/10.4132/jptm.2019.12.03

ORIGINAL ARTICLE

Contribution of cytologic examination to diagnosis of poorly differentiated thyroid carcinoma

Na Rae Kim[1], Jae Yeon Seok[1], Yoo Seung Chung[2], Joon Hyop Lee[2], Dong Hae Chung[1]

[1]Department of Pathology, [2]Division of Thyroid Clinic, Department of General Surgery, Gil Medical Center, Gachon University College of Medicine, Incheon, Korea

Background: The cytologic diagnosis of poorly differentiated thyroid carcinoma (PDTC) is difficult because it lacks salient cytologic findings and shares cytologic features with more commonly encountered neoplasms. Due to diverse cytologic findings and paucicellularity of PDTC, standardization of cytologic diagnostic criteria is limited. The purpose of this study is to investigate and recognize diverse thyroid findings of fine needle aspiration (FNA) cytology and frozen smear cytology in diagnosis of this rare but aggressive carcinoma. **Methods:** The present study included six cases of FNA cytology and frozen smears of histologically diagnosed PDTCs. **Results:** PDTC showed cytologic overlap with well-differentiated thyroid carcinomas (WDTCs). Five of six cases showed dedifferentiation arising from well differentiated thyroid carcinomas. Only one de novo PDTC showed highly cellular smears composed of discohesive small cells, high nuclear/cytoplasmic (N/C) ratio, prominent micronucleoli, and irregular nuclei. Retrospectively reviewed, these findings are highly suspicious for PDTC. Cytologic findings of nuclear atypia, pleomorphism, and irregularity were frequently found, whereas scattered small cells were seen only in the de novo case. **Conclusions:** Heterogeneous cytologic findings of PDTCs are shared with those of WDTCs and contribute to difficult preoperative cytologic diagnoses. Most PDTCs show dedifferentiation from WDTCs. Albeit rare, de novo PDTC should be considered with cytology showing discohesive small cells with high N/C ratio. This will enable precise diagnosis and prompt treatment of this aggressive malignancy.

Key Words: Cytology; Biopsy, fine-needle; Poorly differentiated thyroid carcinoma; Frozen sections

Received: August 9, 2019 **Revised:** November 13, 2019 **Accepted:** December 3, 2019
Corresponding Author: Dong Hae Chung, MD, Department of Pathology, Gil Medical Center, Gachon University College of Medicine, 21 Namdong-daero 774beon-gil, Namdong-gu, Incheon 21565, Korea
Tel: +82-32-460-3073, Fax: +82-32-460-2394, E-mail: dhchung@gilhospital.com

Poorly differentiated thyroid carcinoma (PDTC) was first described by Sakamoto et al. [1] as an aggressive thyroid malignancy with morphology and biological behavior between those of well differentiated follicular or papillary thyroid carcinoma and undifferentiated anaplastic thyroid carcinoma (ATC). Recent genetic alterations may be helpful for predicting the biologic behavior of PDTC. Mutations in the promoter region of telomerase reverse transcriptase are detected in up to 40% of PDTCs, which is intermediate between mutation rates reported for well differentiated thyroid carcinoma (WDTC) and undifferentiated ATC [2]. Because PDTC requires additional chemoradiotherapy after surgical resection to prevent recurrence and metastasis, exact diagnosis is important [3].

PDTC is diagnosed using histologic criteria [4,5]. Unfortunately, most cases are diagnosed after surgical resection and not by preoperative fine needle aspiration (FNA) cytology [6]. PDTC is usually diagnosed from thyroidectomy specimens. According to the recent World Health Organization (WHO) classification, PDTC can only be definitively diagnosed histopathologically, but we believe that the Turin criteria applied to FNA specimens can aid in differentiation of PDTC from anaplastic carcinoma in clinically advanced cases. This was also described by Bongiovanni et al. [7]. The use of thyroid core needle biopsy is increasing, but FNA cytology remains the most commonly used first-line diagnostic tool for evaluating thyroid nodules [8]. Prompt preoperative diagnosis is important for planning multimodality treatment because PDTC has a greater propensity for recurrence or distant metastasis than differentiated thyroid carcinoma. However, presumptive cytologic diagnosis via FNA is challenging due to the rarity of PDTC and its overlapping features with various follicular neoplasms of the thyroid. Here, we describe and review cytologic findings of PDTCs.

pISSN 2383-7837
eISSN 2383-7845

MATERIALS AND METHODS

Six cases of PDTC treated between from January 2015 to November 2018 at Gachon University Gil Medical Center, Incheon, South Korea were retrospectively analyzed. The thyroid FNA smears of all six cases were histologically diagnosed as PDTCs according to histologic criteria agreed upon at the Turin consensus conference held in 2006 [5]. Hematoxylin and eosin stained cytologic smears and liquid based cytology (ThinPrep Pap test, Cytyc Corporation, Boxborough, MA, USA) were evaluated. Diagnostic cytologic categorization of FNA was conducted using the six-level diagnostic scheme described in the Bethesda System for Reporting Thyroid Cytopathology (TBSRTC) [7]. Core needle biopsy performed in one case was classified based on the reporting procedure proposed by the Korean Endocrine Pathology Thyroid Core Needle Biopsy Study Group (2015) [9]. TNM staging was evaluated by the American Joint Committee on Cancer [10].

Ethics statement

Study approval was obtained from our Institutional Review Board (No. GCIRB 2019-106) with a waiver of informed consent.

RESULTS

Clinical summary

Case 1 was a 55-year-old man transferred from our neurology center due to an abnormal thyroid ultrasound during regular follow up. FNA was performed on a 3.3 cm oval hypoechoic mass. Six months later, the mass had increased to 4.4 cm. Core needle biopsy gave the impression of a follicular neoplasm, and total thyroidectomy was performed after frozen cytology and frozen section examination. The patient received radioactive iodine treatment and was free of recurrence at 7 months after surgery. Case 2 was a 35-year-old woman with an incidentally identified thyroid mass. On thyroid ultrasound, the mass was 4.9 cm sized, ill-defined, oval, hypoechoic, and located in the right lobe. FNA cytology was performed. Frozen cytology and frozen section findings were highly suspicious for insular carcinoma, and total thyroidectomy was performed. The case was diagnosed as PDTC with no nodal metastasis. High dose radioactive iodine treatment was planned. Three months after surgery, the patient was free of recurrence. Case 3 was a 65-year-old man diagnosed with papillary thyroid carcinoma at an outside hospital. Enhanced head and neck computed tomography showed a large mass measuring 6.8 cm at the right lobe and 4.7 cm at the isthmus. After FNA slides prepared at the outside hospital were reviewed, right lobectomy was performed. The patient refused further treatment, including total thyroidectomy, and was lost to follow up. Case 4 was a 39-year-old man who presented with an incidentally identified thyroid mass. Thyroid ultrasound showed a 1.8-cm-sized indeterminate mass in the right lobe. FNA followed by total thyroidectomy and radioactive iodine (150 mCi) treatment were performed. During 11 months of follow up, the patient was free of recurrence. Case 5 was a 73-year-old woman who presented with an incidental thyroid mass. Thyroid ultrasound showed a 5.5 cm predominantly solid heterogeneous mass in the left lobe. After FNA and total thyroidectomy, ^{131}I radioactive iodine (150 mCi) was administered. During 45 months of follow up, she remained free of recurrence and continues to be followed every 6 months. Case 6 was a 66-year-old woman who presented with a long-standing left thyroid mass that replaced the mid and lower poles of the left thyroid. Preoperative FNA and intraoperative frozen cytology with frozen sections were performed and followed by total thyroidectomy. During 22 months of follow up, there was no evidence of tumor recurrence or lymph node metastasis.

Pathologic findings

Cytologic findings

FNA of case 1 showed a small amount of follicular cells with no mitosis or necrosis. The initial diagnosis was categorized as atypia of undetermined significance requiring the differential diagnoses of follicular neoplasm and follicular pattern-predominant papillary carcinoma (Fig. 1A). FNA cytology in case 2 revealed scattered, highly cellular, small round cells (Fig. 1C, D) and no evidence of nuclear inclusions, grooves, or necrosis. Initially, a follicular neoplasm was suspected. Because of the small scattered cells, a nodular form of lymphoid malignancy was also suspected. Frozen cytology and frozen sections raised a high level of suspicion for PDTC (Fig. 1E). FNA of case 3 revealed cellular clusters of atypical follicular cells with irregular vesicular nuclei; initial diagnosis was suspicious for papillary carcinoma, i.e. category V (Fig. 1F). FNA of case 4 showed a few scattered clusters of follicular cells with mild irregular nuclei in a hemorrhagic background (Fig. 1G) and was classified as category IIII, follicular lesion of undetermined significance. FNA of case 5 revealed paucicellular bloody smears (Fig. IH) suggestive of a benign follicular nodule. On retrospective review, aspirated smears were scant. Intraoperative frozen imprint smears revealed a few papillary structures in many singly scattered small cells showing

 https://doi.org/10.4132/jptm.2019.12.03

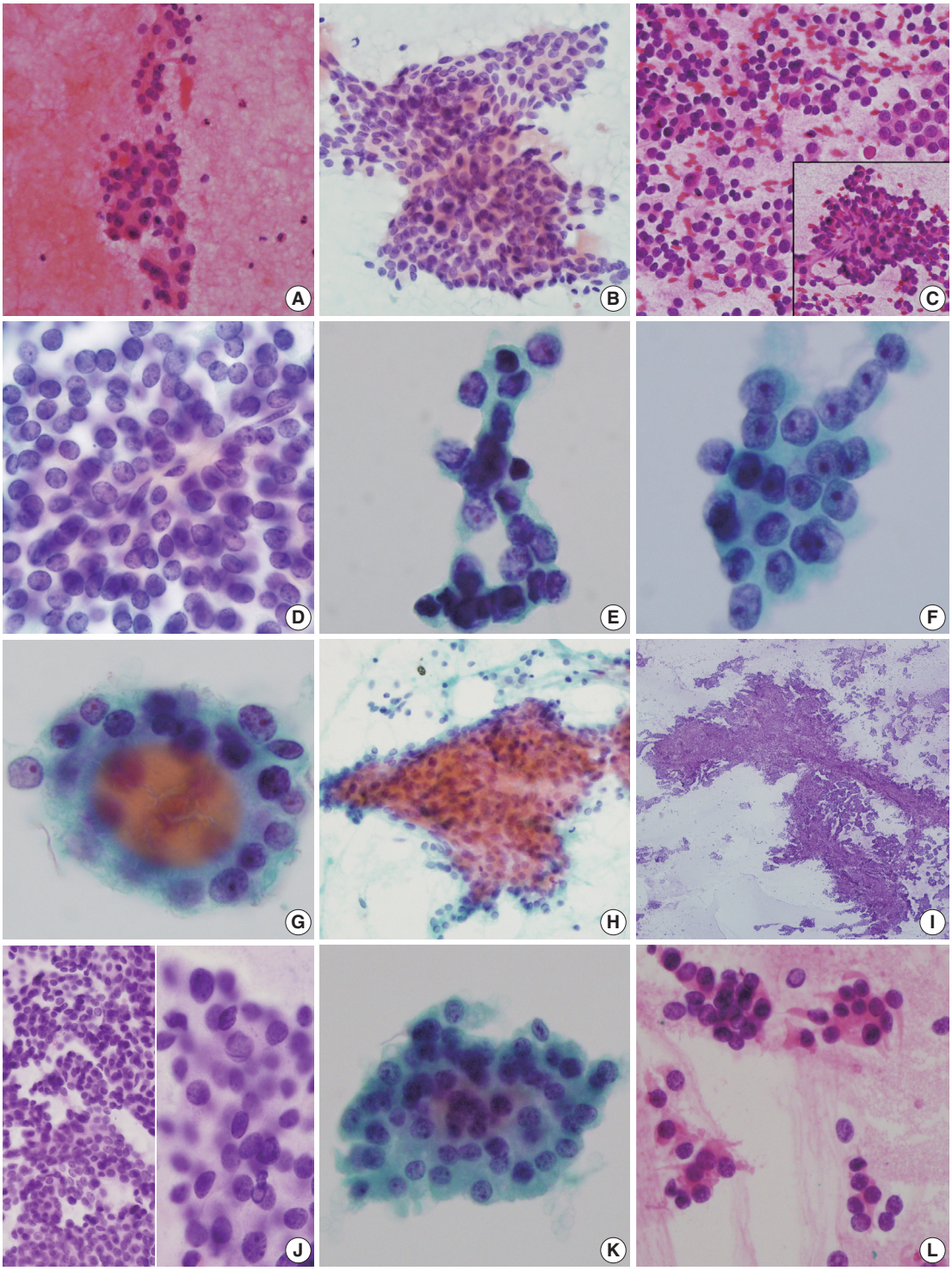

Fig. 1. Cytologic findings of poorly differentiated thyroid carcinoma. (A) Case 1. Fine needle aspiration (FNA) shows few clusters of follicular cells with atypia. (B–E) Case 2. (B) FNA shows few scattered sheets or singly scattered small cells with no nuclear inclusions or grooves. (C–E) Frozen imprint cytology of intraoperative excised mass shows round tumor cells containing scant cytoplasm and round heterochromatic nuclei (C, D). (E) High power view shows atypical follicular cells with small prominent nucleoli. (F) Case 3. FNA reveals cellular clusters of atypical follicular cells with irregular vesicular nuclei. (G) Case 4. FNA of case 4 shows few scattered clusters of follicular cells with mildly irregular nuclei. (H) Case 5. FNA of case 5 shows scant cellular smear with few microfollicles. (I, J) Frozen imprint smear of case 5 shows few papillary structures (I) with nuclear atypia and occasional nuclear inclusions (J). (K, L) Case 6. (K) FNA shows cluster of atypical follicular cells with prominent nucleoli. (L) Intraoperative frozen smears show scattered small cells with nuclear irregularities.

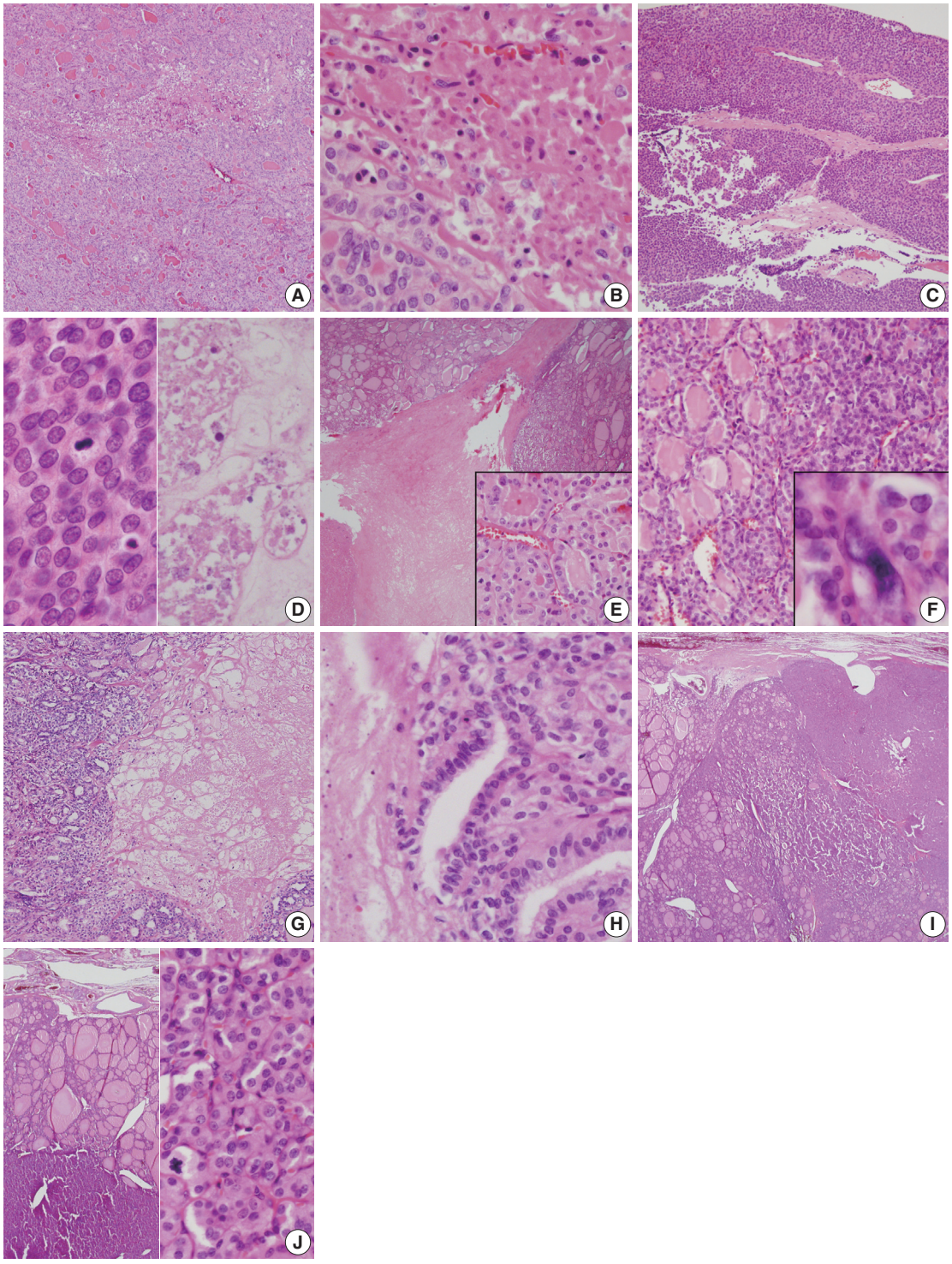

Fig. 2. Histology of resected poorly differentiated thyroid carcinomas. (A, B) Case 1. Mass with well-demarcated capsule filled with microfollicles with necrosis. (B) Necrosis. (C, D) Case 2. Histology shows large mass with solid growth pattern and multifocal necrosis in insular pattern (C). Frequent mitotic activity (D, left) and coagulation necrosis (D, right) are observed. (E) Case 3. Histology shows follicular carcinoma and intervening necrosis with focal poorly differentiated carcinoma (inset). (F) Case 4. Histology shows extensive necrosis in well-differentiated follicular carcinoma. Inset shows cellular atypia adjacent to necrosis. (G, H) Case 5. (G) Solid growth pattern in follicular carcinoma. (H) High power view shows necrosis with transition to poorly differentiated carcinoma. (I, J) Case 6. (I) Histology of total thyroidectomy shows background well-differentiated follicular carcinoma and foci of poorly differentiated carcinoma. (J) High power view (left) is shown. Note mitosis in tumor cells (right).

https://doi.org/10.4132/jptm.2019.12.03

occasional nuclear inclusions (Fig. 1I, J). FNA of case 6 showed scant cellularity and clusters of follicular cells with occasional oncocytic features and slight cellular atypia (Fig. 1K). This case was originally diagnosed as follicular neoplasm, Hurthle cell (oncocytic) type (diagnostic category IV). Frozen touch smears revealed scattered atypical small cells (Fig. 1L).

Histologic findings

Histologically, core needle biopsy of case 1 showed a microfollicular proliferative lesion with a fibrous capsule and no mitosis or necrosis. The lesion was categorized as category IV, follicular neoplasm/suspicious for follicular neoplasm. Total thyroidectomy revealed a 4.4 cm oval mass with a PDTC portion (30%) arising from follicular carcinoma (Fig. 2A). The PDTC area showed frequent mitosis (9 per 10 high-power field [HPF]) and focal necrosis (Fig. 2B). Case 2 showed a large mass with scattered adjacent satellite nodules and extensive vascular invasion in the right lobe (Fig. 2C). A diffuse solid growth pattern with frequent mitotic activity and necrosis were observed (Fig. 2D). Histology of case 3 showed PDTC (10%) arising from follicular carcinoma and measuring 6.5 cm (Fig. 2E). Total thyroidectomy in case 4 revealed a PDTC portion (20%) with a solid and trabecular pattern that arose from a 1.3-cm well differentiated follicular carcinoma confined within the thyroid (Fig. 2F). In case 5, total thyroidectomy revealed PDTC arising from a follicular carcinoma (Fig. 2G) with necrosis (Fig. 2H). In case 6, total thyroidectomy revealed a large bulging ovoid mass replacing the left lobe. The mass was a 2.2-cm poorly differentiated carcinoma with a trabecular pattern that arose from follicular carcinoma (Fig. 2I). Due to complete capsule formation with capsular invasion, follicular neoplasm including widely invasive follicular carcinoma was suspected. Up to 11 mitoses per 50 HPF was observed in the PDTC area (Fig. 2J). Size ranged from 1.8 to 7.0 cm (median, 5.2 cm). Three females and three men were included, and ages ranged from 35 to 73 years (median, 56 years). Resected tumors ranged from 1.8 to 7.0 cm (median, 5.2 cm).

Clinical, cytologic, and histologic summary of the six cases is provided in Table 1.

DISCUSSION

PDTC has morphology and biological behavior between those

Table 1. Clinicopathologic summary of six cases of poorly differentiated thyroid carcinoma

	Sex/age (yr)	Thyroid ultrasound	Initial diagnosis of FNA by the Bethesda System for Reporting Thyroid Cytopathology	Frozen cytology	Histology and gross morphology	TNM stage by AJCC (8th ed)	Treatment	Follow-up (mo)
1	M/55	4.4-cm oval hypoechoic mass at the right lobe	Category III. Atypia of undetermined significance/follicular lesion of undetermined significance	Not performed	PDTC (30%) arising in follicular carcinoma, 4.4 cm	T3N0M0	Total thyroidectomy with ablation ^{131}I Tx (100 mCi)	NER (7)
2	F/35	4.9-cm oval shaped ill-defined hypoechoic mass at right lobe	Category IV. Suspicious for follicular neoplasm; the possibility of FN or PTC of follicular variant	Performed	Pure PDTC 4.7 cm, confined within thyroid	T3N0M0	Total thyroidectomy with ablation ^{131}I (150 mCi)	NER (7)
3	M/65	7-cm replacing nearly entire right lobe	Category V. Suspicious for papillary carcinoma	Not performed	PDTC (10%) arising in follicular carcinoma, 6.5 cm, confined within thyroid	T3N0M0	Right lobectomy due to refusal of total thyroidectomy	Lost to follow-up
4	M/39	1.8-cm hypoechoic mass at right lobe	Category III. Follicular lesion of undetermined significance	Not performed	PDTC (20%) with solid and trabecular pattern arising in follicular carcinoma, 1.3 cm, confined within thyroid	T1N0M0	Total thyroidectomy with ablation ^{131}I (150 mCi)	NER (11)
5	F/73	5.5-cm predominantly solid heterogeneous mass at left lobe	Category II. Suggestive of benign follicular nodule	Performed	PDTC (25%) arising in follicular carcinoma, 5.5 cm confined within thyroid	T3 N0M0	Total thyroidectomy with ablation ^{131}I (100 mCi)	NER (45)
6	F/66	5.5 cm	Category IV. Suspicious for follicular neoplasm, Hurthle cell type	Performed	PDTC (45%) arising in follicular carcinoma, 5.5 cm confined within thyroid	T3 N0M0	Total thyroidectomy with ablation ^{131}I (100 mCi)	NER (22)

FNA, fine needle aspiration; AJCC, American Joint Committee on Cancer; PDTC, poorly differentiated thyroid carcinoma; NER, no evidence of recurrence; FN, follicular neoplasm; PTC, papillary thyroid carcinoma.

of WDTC and ATC. PDTC either develops by dedifferentiation of WDTC or de novo from benign thyroid follicular cells. All of the present six cases except for case 2 showed PDTC dedifferentiated from WDTC. The current histologic criteria of PDTC are as follows [5]: (1) presence of solid, trabecular, or insular growth pattern, (2) absence of conventional nuclear features of papillary carcinoma, and (3) presence of at least one of the following features: convoluted nuclei, mitotic activity > 3 per 10 HPF or 3 per 10 HPF, and tumor necrosis. These criteria achieved consensus in Turin in 2007 [4], and the recent WHO classification is also based on this consensus [7]. In the 2nd edition of the TBSRTC, cytologic criteria include a uniform population of malignant follicular cells with scant cytoplasm [7]. However, cytologic diagnostic criteria have not been standardized. The most recent edition of TBSRTC proposed the following criteria: (1) uniform population of malignant follicular cells with scant cytoplasm with/without oncocytic features, (2) high nuclear/cytoplasmic (N/C) ratio with variable nuclear atypia, (3) presence of necrosis, apoptosis, or mitosis, and (4) scant colloid and cytoarchitecture of an insular, solid, or trabecular pattern. However, these FNA findings have no great specificity in explanatory notes. Previous studies on the FNA findings of PDTC showed no universally accepted cytologic criteria, and the issue remains problematic [7]. The presence of tumor necrosis or mitotic figures on FNA provided helpful diagnostic clues in previous studies [11]. However, these high grade cytologic findings are shared with those of ATC. Combined WDTC with PDTC and ATC are also difficult to diagnose by cytology [12]. Even rare cases of follicular adenoma without capsular/vascular invasion may exhibit small foci of PDTC transformation or spindle cells mimicking PDTC and are not easily extracted by FNA [1,13]. Cytologic findings of PDTC tend to overlap those of WDTC or even medullary thyroid carcinoma (MTC). Bongiovanni et al. [7] suggested that PDTC exhibits four major characteristic cytologic features: insular/solid/trabecular pattern, high N/C ratio, severe crowding, and single cells [6]. In addition, bare nuclei, polymorphonuclear leukocytes, and endothelial wrapping have also been suggested as ancillary diagnostic features [14]. In previous reviews of diverse cytologic studies, the most commonly reported FNA findings of PDTC were granular or salt-and pepper-like chromatin pattern, small cells with high N/C ratio, nuclear overlapping, and mild nuclear pleomorphism [15]. Thus, primitive, small tumor cells with scant cytoplasm and high N/C ratio are a key diagnostic feature of PDTC. The most important differential diagnoses of scattered small cells in PDTCs are papillary carcinoma and a small cell variant of MTC [14-16]. The classic morphology of MTC presents as epithelioid cells with occasional plasmacytoid appearance and focal spindle cell morphology. Giant, clear, and oncocytic cells, and small cell variants may also be observed. The small cell variant of MTC mimic resembles PDTC, Ewing sarcoma, lymphoma, metastatic carcinoma, or primary small cell carcinoma [17]. The small cell variant of MTC also exhibits granular plasmacytoid cytoplasm and a salt-and-pepper-like nuclear chromatin pattern with occasional background amyloid; granular/coarse chromatin was reported in up to 95.5% of cases by Kane and Sharma [11] The oncocytic variant of PDTC should be distinguished from MTC, oncocytic (Hurthle cell) carcinoma, and metastatic carcinoma [15]. This rare variant of PDTC shows frequent small cell changes (as in case 2) and lymphoma, small cell carcinoma, and primary or metastatic neuroendocrine tumor should be included in differential diagnoses [17]. Necrosis or increased mitosis are rarely found in papillary carcinoma or well differentiated follicular carcinomas. These high grade cytologic features are more commonly found with undifferentiated thyroid carcinoma, but cytologic findings such as hypercellularity, insular pattern, small cell size, high N/C ratio, granular chromatin, severe nuclear overlapping, mild nuclear pleomorphism, abrupt nucleomegaly, apoptosis, mitosis, and necrosis are not observed in WDTC. Therefore, these diverse cytomorphologic features are crucial for cytologic diagnosis of PDTC.

Examination of smear backgrounds is also important for cytologic diagnosis of PDTC; hemorrhage without colloid and the occasional presence of necrotic debris may be important diagnostic clues. However, a background of necrotic debris is uncommon. In our six cases, only hemorrhagic background was found. Unfortunately, none of our FNA cytology cases fulfilled exact cytologic diagnostic criteria due to paucicellular, nonrepresentative samples (cases 1, 4, 5, and 6) or misinterpretation (cases 2 and 3). Case 3 was initially misinterpreted as papillary carcinoma; retrospective review showed small prominent micronucleoli and irregular nuclei that were overestimated as papillary carcinoma. TBSRTC suggests that the presence of isolated atypical follicular cells and focal necrosis and mitosis should be reported as suspicious for follicular neoplasm. A retrospective review of case 2 showed scattered discohesive small cells. However, the case should be considered highly suspicious for PDTC because dispersed scattered single cells or clusters of cells with a predominance of small cells is more commonly found in PDTC, MTC, and rarely solid variant of papillary carcinoma. The present six cases showed heterogeneous cytologic findings. Only one of six cases showed de novo PDTC without the WDTC component; small foci of PDTC can interfere with precise cytologic diagnosis.

 https://doi.org/10.4132/jptm.2019.12.03

WDTC components comprise most of the tumors and interfere with precise preoperative cytologic examination. As shown in Table 1, one case was originally diagnosed as category II (case 5), one was diagnosed as category V (case 3), two were diagnosed as category IV (cases 2 and 6), and the remaining two were diagnosed as category III (cases 1 and 4). This variable cytologic categorization is in line with a review by Saglietti et al. [6]. Initial cytologic diagnosis in cases 2 and 6 was category IV, i.e., follicular neoplasm/suspicious for follicular neoplasm, which is plausible because PDTC shares monotonous uniform tumor cells with well differentiated follicular adenoma/carcinoma. In case 5, cytologic misdiagnosis as category II was caused by inadequate sampling of scarce cellularity. According to TBSRTC, 1/3 of PDTCs are reported as follicular neoplasm/suspicious for follicular neoplasm (category IV), and only 1/3 cases are reported as PDTC, or poorly differentiated carcinoma, not otherwise specified [18].

TBSRTC is now applied in preoperative FNA diagnosis and has improved the quality of reporting by decreasing diagnostic discrepancies and facilitating consistency in management plans. However, as shown above and in previous cytologic studies, the lack of consensus and standardization in FNA cytology of PDTC leads to ambiguity in both cytologic diagnoses and clinician interpretation of these diagnoses. More accurate and improved reporting of PDTC is anticipated with a recently suggested modified Bethesda system informing cytologic adequacy [18,19]. Previous studies correlating clinical information, cytomorphology, and ancillary immunohistochemical stains such as Pax8, BRAF, or thyroglobulin report improved diagnostic accuracy in thyroid FNA cytology, but these studies are theoretical and inconsistent [20].

In TBSRTC, inadequate samples caused by paucicellularity, cystic fluid only, obscuring blood, drying artifact, or calcified material result in low sensitivity and high false-negative rates. Adequacy criteria may be important to establish a benign category and minimize false negative results. Paucicellularity is caused by a small component of PDTC in most cases, and standardization of cytologic diagnostic criteria is limited. However, nuclear atypia, pleomorphism, and irregularity are frequent cytologic findings of PDTC. The mitosis and necrosis that are frequently found on histology are uncommonly encountered on FNA because most cases have small foci of PDTC. Only one of the six present cases had scattered poorly differentiated small cells, a helpful cytologic finding. Preoperative core needle biopsy may be non-representative because of a relatively small proportion of PDTC, leading to misdiagnosis. Cytologic diagnostic accuracy for PDTC is challenging and should be improved by recognizing its diverse cytologic findings.

ORCID

Na Rae Kim: https://orcid.org/0000-0003-2793-6856
Jae Yeon Seok: https://orcid.org/0000-0002-9567-6796
Yoo Seung Chung: https://orcid.org/0000-0001-9912-051X
Joon Hyop Lee: https://orcid.org/0000-0003-0470-7719
Dong Hae Chung: https://orcid.org/0000-0002-4538-0989

Author Contributions

Conceptualization: NRK.
Data curation: NRK.
Investigation: NRK, JYS, DHC.
Resources: YSC, JHL.
Supervision: DHC.
Validation: JYS, DHC.
Writing—original draft: NRK.
Writing—review & editing: NRK, DHC.

Conflicts of Interest

The authors declare that they have no potential conflicts of interest.

Funding

No funding to declare.

REFERENCES

1. Sakamoto A, Kasai N, Sugano H. Poorly differentiated carcinoma of the thyroid: a clinicopathologic entity for a high-risk group of papillary and follicular carcinomas. Cancer 1983; 52: 1849-55.
2. Ibrahimpasic T, Ghossein R, Shah JP, Ganly I. Poorly differentiated carcinoma of the thyroid gland: current status and future prospects. Thyroid 2019; 29: 311-21.
3. Haugen BR, Alexander EK, Bible KC, et al. 2015 American Thyroid Association management guidelines for adult patients with thyroid nodules and differentiated thyroid cancer: the American Thyroid Association Guidelines Task Force on Thyroid Nodules and Differentiated Thyroid Cancer. Thyroid 2016; 26: 1-133.
4. Volante M, Collini P, Nikiforov YE, et al. Poorly differentiated thyroid carcinoma: the Turin proposal for the use of uniform diagnostic criteria and an algorithmic diagnostic approach. Am J Surg Pathol 2007; 31: 1256-64.
5. Tallini G, Asioli S, Aubert S, et al. Poorly differentiated thyroid carcinoma. In: Lloyd RV, Osamura RY, Kloppel G, Rosai J, eds. WHO

classification of tumours of endocrine organs. Lyon: IARC Press, 2017; 100-3.
6. Saglietti C, Onenerk AM, Faquin WC, Sykiotis GP, Ziadi S, Bongiovanni M. FNA diagnosis of poorly differentiated thyroid carcinoma: a review of the recent literature. Cytopathology 2017; 28: 467-74.
7. Bongiovanni M, Fadda G, Faquin WC. Poorly differentiated thyroid carcinoma. In: Ali SZ, Cibas ES, eds. The Bethesda System for Reporting Thyroid Cytopathology: definitions, criteria, and explanatory notes. 2nd ed. Cham: Springer International Publishing, 2018; 177-88.
8. Gharib H, Papini E, Paschke R, et al. American Association of Clinical Endocrinologists, Associazione Medici Endocrinologi, and European Thyroid Association medical guidelines for clinical practice for the diagnosis and management of thyroid nodules: Executive Summary of recommendations. J Endocrinol Invest 2010; 33: 287-91.
9. Jung CK, Min HS, Park HJ, et al. Pathology reporting of thyroid core needle biopsy: a proposal of the Korean Endocrine Pathology Thyroid Core Needle Biopsy Study Group. J Pathol Transl Med 2015; 49: 288-99.
10. Amin MB, Edge S, Greene F, et al. AJCC cancer staging manual. 8th ed. Chicago: Springer, 2017.
11. Kane SV, Sharma TP. Cytologic diagnostic approach to poorly differentiated thyroid carcinoma: a single-institution study. Cancer Cytopathol 2015; 123: 82-91.
12. Bichoo RA, Mishra A, Kumari N, et al. Poorly differentiated thyroid carcinoma and poorly differentiated area in differentiated thyroid carcinoma: is there any difference? Langenbecks Arch Surg 2019; 404: 45-53.
13. Burke A, Staats P. Follicular adenoma of the thyroid with spindle cell metaplasia mimicking insular thyroid carcinoma and lacking thyroglobulin expression. Am J Surg Pathol 2019; 24: 84-6.
14. Onenerk M, Canberk S, Gunes P, Erkan M, Kilicoglu GZ. Oncocytic variant of poorly differentiated thyroid carcinoma: "Is diagnosis possible by fine-needle aspiration?". Cytojournal 2016; 13: 23.
15. Laforga JB, Cortés VA. Oncocytic poorly differentiated (insular) thyroid carcinoma mimicking metastatic adenocarcinoma: a case report and review of the literature. Diagn Cytopathol 2019; 47: 584-8.
16. Verma A, Kane S, Vinarkar S, D'Cruz AK. Small cell medullary thyroid carcinoma: a diagnostic dilemma. Indian J Pathol Microbiol 2017; 60: 562-4.
17. Eloy C, Cameselle-Teijeiro JM, Rousseau E, Sobrinho-Simões M. Small cell tumors of the thyroid gland: a review. Int J Surg Pathol 2014; 22: 197-201.
18. Lee YB, Kim JY, Cho H, et al. Modified Bethesda system informing cytopathologic adequacy improves malignancy risk stratification in nodules considered benign or atypia(follicular lesion) of undetermined significance. Sci Rep 2018; 8: 13503.
19. Lee YB, Cho YY, Jang JY, et al. Current status and diagnostic values of the Bethesda system for reporting thyroid cytopathology in a papillary thyroid carcinoma-prevalent area. Head Neck 2017; 39: 269-74.
20. Cha YJ, Pyo JY, Hong S, et al. Thyroid fine-needle aspiration cytology practice in Korea. J Pathol Transl Med 2017; 51: 521-7.

 https://doi.org/10.4132/jptm.2019.12.03

JPTM
Journal of Pathology and Translational Medicine 2020; 54: 179-183
https://doi.org/10.4132/jptm.2019.10.15

CASE STUDY

Inconspicuous longitudinal tears of the intracranial vertebral artery in traumatic basal subarachnoid hemorrhage

Seongho Kim

Central Forensic Medical Center, National Forensic Service, Wonju, Korea

Blunt force trauma to the head or neck region can cause traumatic basal subarachnoid hemorrhage (TBSAH), which can result in rapid loss of consciousness and death; however, detecting such a vascular injury is difficult. Posterior neck dissection was performed to investigate the bleeding focus in TBSAH cases 2018 and 2019. In all four cases, autopsies revealed a longitudinal tear in the midsection of the vertebral artery's intracranial portion. The midportion of the intracranial vertebral artery appears to be most vulnerable to TBSAH. Interestingly, three of the cases showed only a vaguely visible longitudinal fissure in the artery without a grossly apparent tear; rupture was confirmed by microscopic examination. Longitudinal fissures of the intracranial vertebral artery, which are difficult to identify without detailed examination, may be overlooked in some cases of TBSAH. Thus, careful gross and microscopic examination of the vertebral artery is recommended in cases of TBSAH.

Key Words: Vertebral artery; Rupture; Basal subarachnoid hemorrhage; Trauma

Received: August 29, 2019 **Revised:** September 30, 2019 **Accepted:** October 15, 2019
Corresponding Author: Seongho Kim, MD, Central Forensic Medical Center, National Forensic Service, 10 Ipchun-ro, Wonju 26460, Korea
Tel: +82-42-866-4551, Fax: +82-42-866-4569, E-mail: rivebt99@gmail.com

Blunt force trauma to the head or neck region can cause traumatic basal subarachnoid hemorrhage (TBSAH). TBSAH can be fatal, as it can lead to instantaneous loss of consciousness and death. The most common site of vascular rupture is thought to be the vertebral artery, particularly the intracranial course [1,2]. However, because of the position of the vertebral artery in the cranial cavity, it is difficult to determine the bleeding focus on routine autopsy; also, the intracranial vertebral arteries are normally cut to remove the brain. In TBSAH cases, posterior neck dissection has been used to locate the bleeding focus in the dura-perforating and intracranial portions of the vertebral artery; using this method, tear sites in the vertebral artery can be identified more frequently [3,4]. In this report, the clinicopathologic features of four TBSAH cases are summarized.

CASE REPORT

Posterior neck dissection was performed during autopsy in four cases with a history of TBSAH by the National Forensic Service in South Korea from 2018 to 2019 to investigate bleeding focus. The deceased individuals were two men and two women aged 22–53 years. Another case of basal subarachnoid hemorrhage with a trauma history was excluded from this series of four cases because of underlying vasculopathy (aneurysmal rupture).

The posterior neck dissection method was previously described. Briefly, the posterior laminae of the upper cervical vertebrae are excised; then, an inverted wedge is cut from the posterior occipital bone above the foramen magnum. After the dura are opened and the spinal cord is exposed, the spinal cord is pulled to one side and the dura surrounding the penetrating portion of the vertebral artery is excised. Then, the intracranial vertebral artery is pulled up and the extracranial vertebral artery is severed just below the dura. The brain, spinal cord, and dissected intra- and extracranial vertebral arteries are removed together [3]. Finally, the dissected vessels are carefully examined to identify the source of hemorrhage.

The deceased individuals rapidly lost consciousness after being assaulted on the face, head, or neck. All of the deceased individuals were under the influence of alcohol. Two individuals died within 24 hours, whereas the other two individuals survived for two to

pISSN 2383-7837
eISSN 2383-7845

eight days on life support including mechanical ventilation. Autopsy revealed diffuse basal subarachnoid hemorrhage in all four cases, with vertebral artery injury. In all four cases of vertebral artery injury, a longitudinal tear was identified in the midportion of the vessels' intracranial portion. Interestingly, three of the four intracranial vertebral artery injury cases had a longitudinal fissure in the vertebral artery instead of a grossly evident tear; rupture was confirmed by the water injection method or microscopic examination. Neither postmortem computed tomography (CT) nor postmortem angiography was performed in any of the cases. The clinicopathologic findings are summarized in Table 1.

Case 1

A 58-year-old male argued with another male, was punched in the head and immediately lost consciousness. Cardiopulmonary resuscitation was performed in the hospital but he died approximately 1 hour after the assault. The postmortem examination showed muscular hemorrhage in the left infraauricular area and diffuse basal subarachnoid hemorrhage. The intracranial arteries in the basal portion of the brain were carefully examined. A vaguely visible longitudinal fissure was found in the midportion of the left intracranial vertebral artery. After injecting water into the proximal portion of the vertebral artery with a syringe, water leakage was noted along the longitudinal fissure. Fibrinous

Table 1. Clinicopathologic findings of 4 TBSAH cases

Case No.	Sex/ age (yr)	Main site of impact	Relevant autopsy findings	Cause of impact	Survival	Injured vessel	Portion of the injured vessel	Shape of injury	Drinking
1	M/53	Lt infra-auricular	Intramuscular hemorrhage in the left infra-auricular lesion	Fist	1 hr	Lt IVA	Mid 1/3	Longitudinal fissure 7 mm	+
2	F/30	Lt posterior neck	Intramuscular hemorrhage in the left posterior neck	Fist	23 hr	Lt IVA	Mid 1/3	Longitudinal fissure 5 mm	+
3	F/22	Lt infra-auricular	Contusions and intramuscular hemorrhage in the left infra-auricular lesion and mandible Multiple contusions of the face, chest, arm, and thigh Stent and coils in the ruptured vertebral artery	Fist	2 days	Lt IVA	Mid and distal	Longitudinal 14 mm	+
4	M/41	Face and head, multiple	Multiple contusion, laceration, and intramuscular hemorrhage involving head and neck Fractures of the mandible and maxilla	Fist knee	8 days	Lt IVA	Mid 1/3	Longitudinal fissure 5 mm	+

TBSAH, traumatic basal subarachnoid hemorrhage; M, male; Lt, left; IVA, intracranial vertebral artery; F, female.

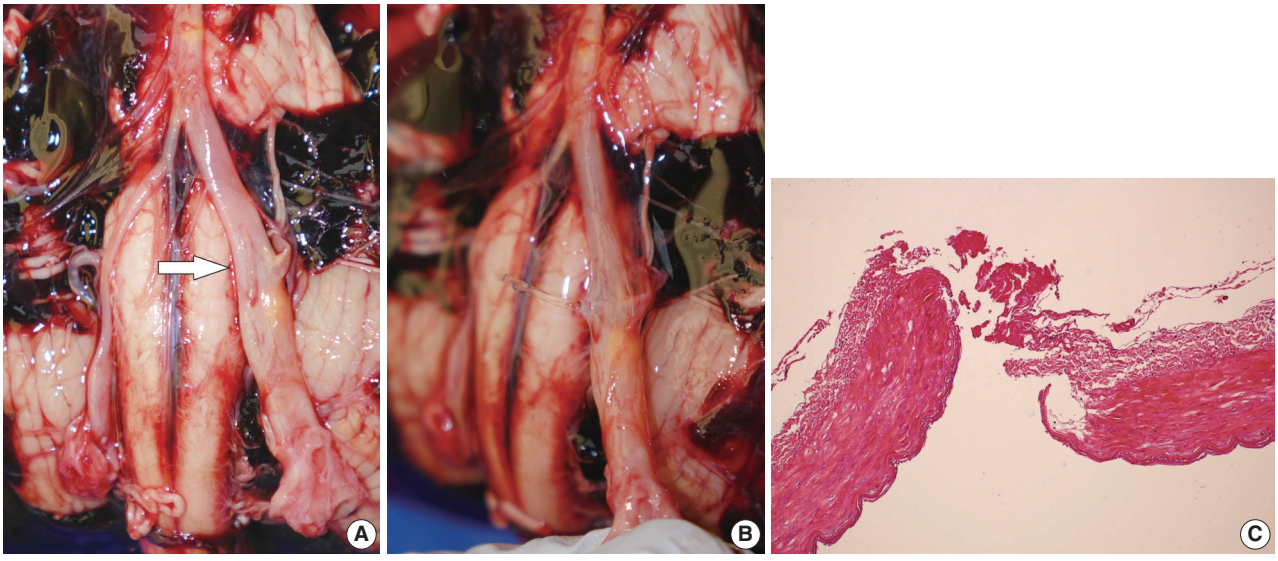

Fig. 1. (A) A vague longitudinal fissure in the left vertebral artery (white arrow). (B) Water leakage through the ruptured portion. (C) Histology of the left vertebral artery at the point of rupture showing fibrinous material at the rupture site.

https://doi.org/10.4132/jptm.2019.10.15

material was identified in the ruptured portion of the vessel on microscopic examination (Fig. 1).

Case 2

A 30-year old female was punched in the head. She immediately lost consciousness and was taken to the hospital. She died 23 hours after the assault. Postmortem examination revealed a deep muscular hemorrhage in the left posterior neck and diffuse basal subarachnoid hemorrhage. A vaguely visible longitudinal fissure was found in the midportion of the left intracranial vertebral artery. Water was injected into the proximal portion of the vertebral artery, but did not leak through the longitudinal fissure. However, water leakage was observed in the basilar artery. Microscopically, the longitudinal fissure of the vertebral artery was completely clogged with fibrin clots. In the area of the basilar artery where the water escaped, neither neutrophil infiltration nor fibrin materials were observed. Thus, the longitudinal fissure in the vertebral artery was identified as the true site of rupture (Fig. 2).

Case 3

A 22-year-old female was punched on the left side of the neck. She immediately lost consciousness and was taken to the hospital. CT and cerebral angiography were performed and revealed injury to the left vertebral artery. A stent and coils were inserted in the injured artery, but the patient died 2 days after the assault. Postmortem examination revealed muscular hemorrhage in the left infra-auricular area and diffuse basal subarachnoid hemorrhage. A longitudinal rupture was observed in the left vertebral artery and a stent and coils were visible in the affected artery.

Case 4

A 41-year-old man was punched on the left side of his jaw, and he collapsed. He was then struck in the face and head several times by the perpetrator's fist and knee. The victim was taken to the hospital but died eight days after the assault. Postmortem examination revealed multiple contusions of the face and head, along with fractures of the mandible and maxilla. A longitudinal fissure was found in the midportion of the left intracranial vertebral artery. Water was injected into the proximal portion of the vertebral artery, but did not leak through the longitudinal fissure. Microscopically, fibrinous material was identified in the ruptured portion of the vessel, and the lumen of the injured vessel was clogged with thrombus (Fig. 3).

Decedents are generally not considered to be human subjects for the purposes of research, and therefore are not generally under the purview of an institutional review board. For these autopsy case reports, consent was obtained for autopsy, and further informed consent was not required.

DISCUSSION

Previously, extracranial vertebral artery rupture was thought to cause fatal traumatic subarachnoid hemorrhage [5,6]. However, Leadbeatter suggested that extracranial vertebral artery injury could be a concomitant lesion and that the bleeding focus might be an unidentified vascular tear inside the cranial cavity [7]. Currently, many pathologists believe that the more common site of rupture in TBSAH is the intracranial vertebral artery [2,8].

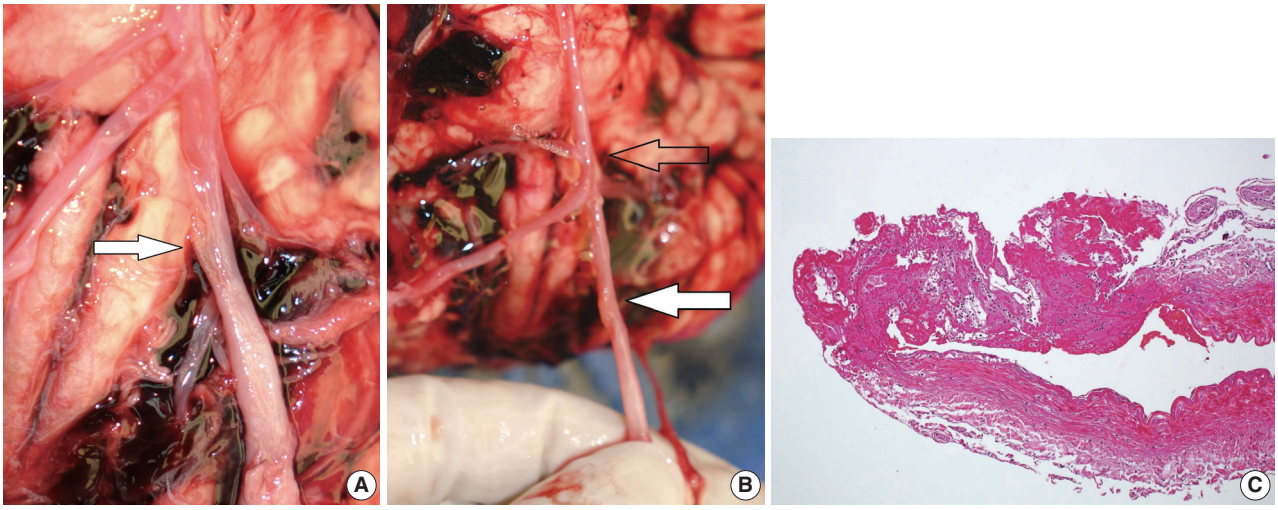

Fig. 2. (A) Longitudinal fissure in the left vertebral artery (white arrow). (B) Water leakage through the artificially ruptured portion of the proximal basilar artery (empty arrow). The true site of rupture is indicated (white arrow). (C) Histology of the true rupture site showing complete blockage by a fibrinous plug.

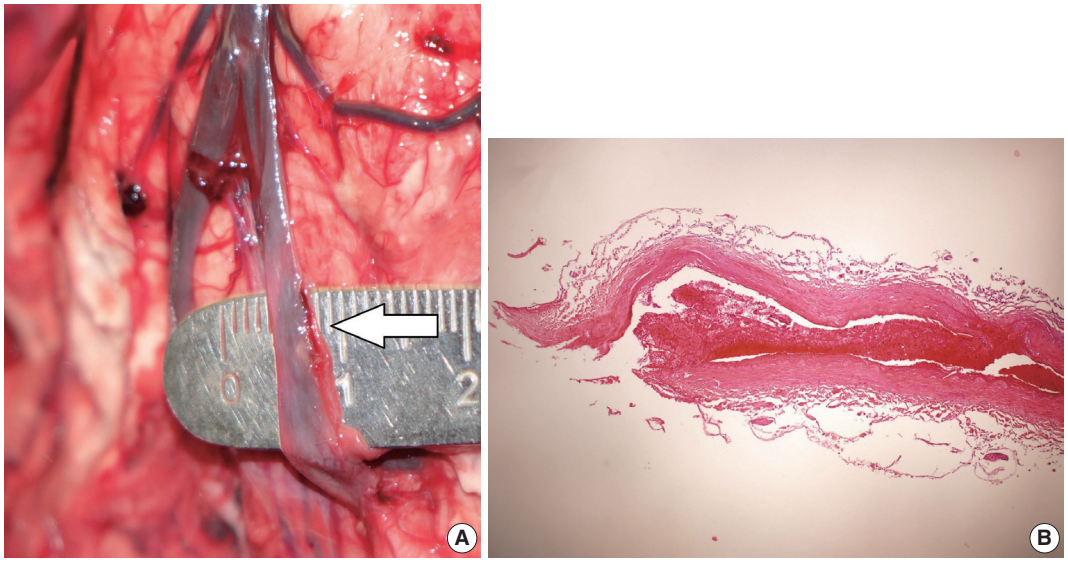

Fig. 3. (A) Longitudinal fissure in the left vertebral artery (white arrow). (B) Histology of the ruptured portion showing thrombus in the vascular lumen.

Because of the deep location of the vertebral artery in the cranial cavity, it is difficult to examine on autopsy. In case of vertebral artery injury, it can be challenging to locate the bleeding focus. When the injured vertebral artery portion is not visible on autopsy, a water injection method is commonly used, which identifies the rupture site via water leakages after injection into the origin of the vertebral artery [9].

Posterior neck dissection was used to investigate the bleeding focus in 11 TBSAH cases between 2013 and 2019, including previously published cases and the four cases described herein; intracranial vertebral artery laceration was identified in nine cases [3,4]. All of the deceased individuals were under the influence of alcohol, were struck in the head or neck via punching or kicking, and lost consciousness instantaneously during the assault. The individuals lived less than 24 hours in three cases and survived from 2 to 9 days in eight cases. In the past, most TBSAH patients died soon after loss of consciousness; however, advanced life support including mechanical ventilation now enables sustained survival in an unconscious state.

Longitudinal tears were identified in all nine injured intracranial vertebral arteries in this series. These findings agree with those of other studies reporting that longitudinal tears are the characteristic intracranial vertebral arterial injury in TBSAH [10,11]. Vascular tears in nine of the cases were observed in the midportion of the intracranial vertebral artery; in one of these cases, the tear was seen in the mid and distal portions of the intracranial course, and in another in the mid and proximal portions [4]. Although the mechanism remains unclear, based on these results, the midportion of the intracranial vertebral artery seems to be the portion most vulnerable to TBSAH. Therefore, when autopsy is performed in cases of TBSAH, it is necessary to pay close attention to the midportion of the intracranial vertebral artery. In TBSAH, the suggested mechanisms for the vertebral artery injury are direct trauma to the vessel, extensive stretching of the vessel during hyperextension or rotation of the neck, oscillation of the brain with shearing force, and increased intravascular pressure [8]. Considering that vertebral artery injury is observed mainly in the middle portion of the intracranial regions, stretching or shearing forces on the vessels are likely to play an important role.

Three of four verified intracranial vertebral artery ruptures consisted of vaguely visible longitudinal fissures in the vertebral artery without a grossly evident tear. On gross examination, the longitudinal fissures in the external surface of the vertebral arteries seemed rough and fluffy, as opposed to the typical smooth and glistening appearance. Because it was difficult to determine with gross examination alone whether a rupture had occurred, the rupture site was confirmed by injecting water into the blood vessel to identify areas of leakage or through microscopic examination. One of the cases showed water leakage at the longitudinal fissure. In one case, water leakage was observed in the basilar artery rather than at the site of the longitudinal fissure in the intracranial vertebral artery. Histological examination revealed that the longitudinal fissure in the vertebral artery was completely obstructed with a fibrin clot and that fibrin deposition and inflammatory cell infiltration were absent in the basilar artery. Therefore, the vertebral artery area was determined to be the true

https://doi.org/10.4132/jptm.2019.10.15

site of the rupture and water leakage in the basilar artery was attributed to an artificial rupture that occurred during autopsy. In another case, water leakage was not observed because of thrombotic occlusion of the vessel. A longitudinal fissure occurring after vertebral artery injury may be part of the hemostatic process caused by vasoconstriction, platelet plug formation, and fibrin deposition after vascular trauma [12]. Because this subtle injury may be difficult to identify on gross examination, longitudinal fissure may be an overlooked sign of vascular trauma in some cases of TBSAH. Therefore, sufficient attention and time should be invested in identifying minute vascular injuries during autopsy in TBSAH cases.

Generally, damage to the vertebral artery ipsilateral to the blunt impact is more frequent than damage to the vertebral artery contralateral [8]. One case in this series showed multiple contusions or muscular hemorrhages on both sides of the face, head, and neck. As a result, it was difficult to determine whether the intracranial artery injury occurred ipsilaterally or contralaterally to the site of impact. In the remaining three cases with the impact on the left side of the head or neck demonstrated injury to the left vertebral artery, showing a relationship between the site of impact and the site of vascular injury

This study has several limitations. First, the number of cases was small. Second, in two cases, the survival period was longer than that reported in previous publications, and interpretation of some of the gross and histological findings may have been affected by changes occurring in the vascular lesions during the survival period. Therefore, further study is needed to determine whether these distinctive vascular injuries are commonly observed in TBSAH cases.

In conclusion, the majority of TBSAH cases showed intracranial vertebral artery injuries; therefore, the intracranial vertebral artery should be kept intact as far as possible up to its proximal portion during autopsy. Posterior neck dissection can be performed to examine the entire intracranial vertebral artery without inflicting artificial injury. If posterior neck dissection is not performed, removing the cerebral hemisphere before cutting the vertebral artery enables examination of longer portions of the intracranial vertebral artery. After brain removal, detailed examination is needed to identify minute vascular injury. Although the mechanism remains unclear, the midportion of the intracranial vertebral artery seems to be the portion most vulnerable to TBSAH. Therefore, it is necessary to pay close attention to the midportion of the intracranial vertebral artery. If any lesions suspicious for vascular damage are found, rupture should be confirmed using the water injection method or microscopic examination.

ORCID

Seongho Kim: https://orcid.org/0000-0002-1412-7630

Conflicts of Interest

The authors declare that they have no potential conflicts of interest.

Funding

No funding to declare.

REFERENCES

1. Lee CK, Gray L, Maguire J. Traumatic vertebral artery injury: detailed clinicopathologic and morphometric analysis of 6 cases. Am J Forensic Med Pathol 2009; 30: 134-6.
2. Wong B, Ong BB, Milne N. The source of haemorrhage in traumatic basal subarachnoid haemorrhage. J Forensic Leg Med 2015; 29: 18-23.
3. Kim S, Kim M, Lee BW, Kim YH, Choi YS, Seo JS. Investigation of bleeding focus in the intracranial vertebral artery with the use of posterior neck dissection method in traumatic basal subarachnoid hemorrhage. J Forensic Leg Med 2015; 34: 151-4.
4. Kim S, Jun YJ, Na JI, Kim M. Rupture portions in the vertebral artery in traumatic basal subarachnoid hemorrhage. J Forensic Leg Med 2017; 52: 221-2.
5. Contostavlos DL. Massive subarachnoid hemorrhage due to laceration of the vertebral artery associated with fracture of the transverse process of the atlas. J Forensic Sci 1971; 16: 40-56.
6. Harland WA, Pitts JF, Watson AA. Subarachnoid haemorrhage due to upper cervical trauma. J Clin Pathol 1983; 36: 1335-41.
7. Leadbeatter S. Extracranial vertebral artery injury: evolution of a pathological illusion? Forensic Sci Int 1994; 67: 33-40.
8. Ong BB, Milne N. Vertebral artery trauma. In: Rutty GN, ed. Essentials of autopsy practice: reviews, updates, and advances. Cham: Springer, 2017; 23-41.
9. McCarthy JH, Sunter JP, Cooper PN. A method for demonstrating the source of bleeding in cases of traumatic subarachnoid haemorrhage. J Pathol 1999; 187: 30A.
10. Coast GC, Gee DJ. Traumatic subarachnoid haemorrhage: an alternative source. J Clin Pathol 1984; 37: 1245-8.
11. Hiraiwa K, Sato T, Sasaki T, Mizusawa I, Nata M, Kodama N. Medico-legal aspects of traumatic injury of the vertebrobasilar artery. Neurol Med Chir (Tokyo) 2005; 45: 549-55.
12. Kumar V, Abbas AK, Aster JC. Robbins basic pathology. Philadelphia, PA: Elsevier, 2018; 101-11.

JPTM
Journal of Pathology and Translational Medicine 2020; 54: 184-187
https://doi.org/10.4132/jptm.2019.11.07

CASE STUDY

Primary carcinoid tumor in the external auditory canal

Dong Hae Chung[1]*, Gyu Cheol Han[2]*, Na Rae Kim[1]

Departments of [1]Pathology and [2]Otolaryngology, Gil Medical Center, Gachon University College of Medicine, Incheon, Korea

A 39-year-old man visited the department of otolaryngology due to an ongoing hearing disturbance that had lasted for 1 year. Temporal bone computed tomography revealed soft tissue density nearly obliterating the left external auditory canal (EAC). The mass was composed of sheets of round tumor cells containing moderate amounts of fine granular cytoplasm and salt and pepper chromatin. Neither mitosis nor necrosis was found. The Ki-67 proliferation index was less than 2%. Cells were positive for CD56 and synaptophysin but negative for chromogranin, cytokeratin (CK) 20, and CK7. Based on these findings, the tumor was diagnosed as a carcinoid tumor, well differentiated neuroendocrine carcinoma, grade 1 (G1) according to current World Health Organization (WHO) classification of head and neck tumors; and a neuroendocrine tumor, G1 according to neuroendocrine neoplasm (NEN)-2018 WHO standard classification. He remained free of local recurrence and metastasis after 20 months of follow up. To date, only six cases of primary NENs in the EAC have been reported. Metastatic tumor should be included in the differential diagnoses. Because of its rarity, the prognosis and treatment have not yet been clarified.

Key Words: Carcinoid tumor; Neuroendocrine neoplasms; Carcinoma, neuroendocrine; External auditory canal

Received: August 5, 2019 **Revised:** October 21, 2019 **Accepted:** November 7, 2019

Corresponding Author: Na Rae Kim, MD, PhD, Department of Pathology, Gil Medical Center, Gachon University College of Medicine, 21 Namdong-daero 774 beon-gil, Namdong-gu, Incheon 21565, Korea
Tel: +82-32-460-3073, Fax: +82-32-460-2394, E-mail: naraech@empal.com

*Dong Hae Chung and Gyu Cheol Han contributed equally to this work.

Neuroendocrine neoplasms (NENs) exhibit epithelial and neuroendocrine features derived from the primitive common precursor cells of the neural crest. NENs may occur throughout the body, but the gastrointestinal tract is the most commonly encountered location. Head and neck locations, especially those within the ear, are rare. A literature search identified fewer than 30 cases of NEN in the middle ear [1], with cases of middle ear adenoma, neuroendocrine adenoma of the middle ear, or amphicrine adenoma. However, only six cases of NEN of the external auditory canal (EAC) have been reported [2-7].

Here, we report an extremely rare case of a carcinoid, well differentiated neuroendocrine tumor (NET) grade 1 (G1) occurring in the EAC [8]. In addition, we review the new uniform 2018-World Health Organization (WHO) classification of NENs proposed for consistent taxonomy [9].

CASE REPORT

A 39-year-old Korean man presented at the department of otolaryngology complaining of left hearing disturbance and tinnitus for one year. Physical examination revealed an EAC filled with a rubbery hard mass (Fig. 1A). Temporal bone computed tomography (CT) depicted soft tissue density in and almost obliterating the left EAC (Fig. 1B) with bone erosion and extension beyond the EAC. Initially, otitis externa and a benign tumorous condition were included in the differential diagnoses. An endaural incision was performed under local anesthesia, and widening of the inferior and posterior walls of the EAC was achieved by drilling. The mass nearly obliterated the EAC and was located near the tympanic membrane, which remained intact. Microdissection was performed using a micro scissors.

Grossly, the excised ovoid mass measured 0.9×0.8×0.5 cm and had a hard rubbery texture. Microscopically, the mass was composed of round tumor cells that formed loose cohesive cords, sheets, or trabecula of glandular architecture (Fig. 2A). Tumor cells contained abundant amounts of fine granular cytoplasm and small nucleoli with salt and pepper nuclear chromatin. Endolymphatic and vascular tumor emboli were observed, but neither

pISSN 2383-7837
eISSN 2383-7845

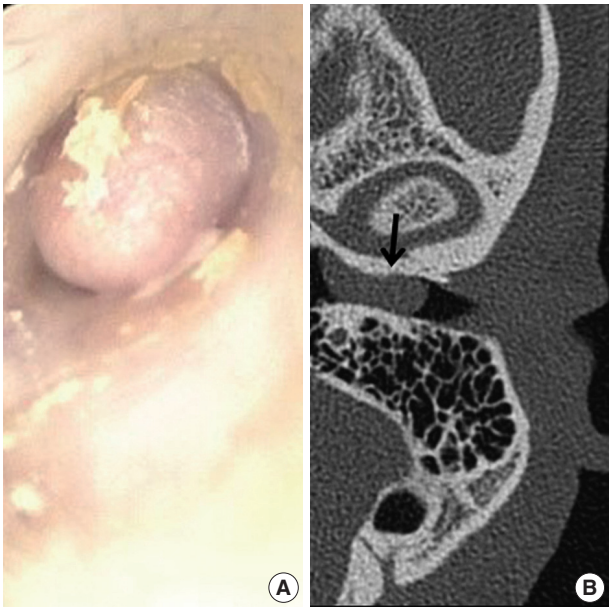

Fig. 1. Myringoscopy revealed a grayish-colored firm mass obliterating the left external auditory canal (A), and temporal bone computed tomography revealed soft tissue density (arrow) at the external auditory canal (B).

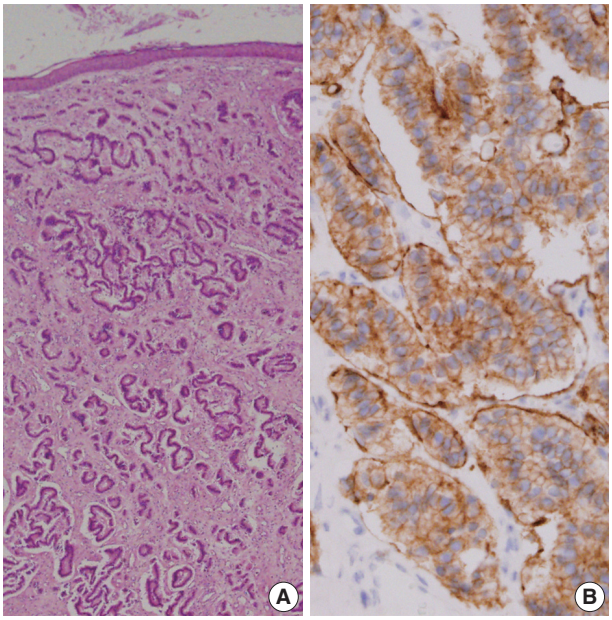

Fig. 2. Low-power view revealed small uniform tumor cells arranged in cords, trabecular, and nested patterns (A). Tumor cells were strongly positive for synaptophysin (B).

mitosis nor necrosis was evident. Immunohistochemically, tumor cells were positive for synaptophysin (prediluted, DAK-SYNAP, Dako, Glostrup, Denmark) (Fig. 2B, left) and CD56 (1:100, CD564, Novocastra, Newcastle upon Tyne, UK) (Fig. 2B, right) but negative for chromogranin (1:100, DAK-A3, Dako), CK20 (1:100, KS 20.8, Dako), and CK7 (1:100, OV-TL 12/30, Dako). The Ki-67 (1:100, MIB-1, Dako) proliferation index was less than 2%. Accordingly, the tumor was diagnosed as a carcinoid tumor with no necrosis or mitosis; neuroendocrine carcinoma (NEC) G1 according to the 4th edition of WHO classification of head and neck tumors and NET G1-2018 WHO according to the uniform standard classification framework.

To exclude metastatic tumor from another site, esophagogastroscopy, colonoscopy, and abdominopelvic CT; torso positron emission tomography (PET); and a bone scan were performed, but there was no evidence of a primary or metastatic tumor.

Hearing sensation was recovered after surgery, and the patient showed no systemic symptom, including those of carcinoid syndrome. Radiation and chemotherapy were withheld. Instead, we followed the patient with annual PET and head and neck CT imaging. During the 20 months of follow up, he showed no local recurrence or metastasis.

Ethics statement

Approval was obtained from our Institutional Review Board (No. GBIRB-2019-238) for publication of this case report with a waiver of informed consent.

DISCUSSION

Most malignant tumors arising from the EAC are primary tumors, among which squamous cell carcinoma and basal cell carcinoma are the most common; others include malignant melanoma, lymphoma, and ceruminous gland carcinoma. Few reports on metastasis to the EAC from extra-auditory malignancies are reported in the literature [10]. Primary middle ear adenoma extending to the EAC has been occasionally reported [1], but only six cases of NENs isolated to the EAC were reported to date [2-7]. NENs contain epithelial and neuroendocrine components and originate from primitive undifferentiated pluripotential stem cells and neural crest cells distributed throughout the body, especially in the gut and bronchopulmonary system. However, the origin of NENs of EAC remains uncertain, like those of skin, because there seem to be no neuroendocrine cells in normal skin except for Merkel cells [8]. Cells of neural crest origin and epidermal origin should be considered, but further study is required to elucidate the origins of EAC and skin NENs.

Clinically, unlike NENs of the bronchopulmonary tract or pancreas, the typical carcinoid syndrome symptoms of flushing or diarrhea are uncommon in cases of cutaneous or EAC NEN [11]. Previously reported EAC NENs have been associated with

unilateral conductive hearing loss, ear fullness, tinnitus, and dizziness. Because of its rarity, the NEN of the EAC in the present case was indistinguishable from its metastatic counterpart by morphology alone [8].

According to the 4th edition of WHO classification of head and neck tumors, NENs are categorized into well-differentiated (carcinoid, G1), moderately differentiated (atypical carcinoid, grade 2 [G2]), and poorly differentiated (small and large cell) NECs [8]. NETs arising in the head and neck are histologically classified as carcinoid tumors including well-differentiated NETs (NEC G1), atypical carcinoid tumors (moderately-differentiated NEC or NEC G2), poorly-differentiated or high-grade NECs (including small cell carcinomas and Merkel cell carcinomas [MCCs]), and mixed tumor-like adenocarcinoma [1,11,12]. Mitotic count and necrosis under light microscopy are important in grading: NENs lacking necrosis and low mitosis (< 2/10 high-power fields [HPFs]) belong to NECs G1; NENs showing necrosis and/or mitosis (2–10 mitoses/10 HPFs) are categorized as NECs G2; and NENs showing necrosis and high mitotic rate (> 10 mitoses/10 HPFs) are categorized as NECs grade 3 (G3). Those are collectively named NENs including well-differentiated and moderately differentiated NECs defined as NETs of G1 and G2, respectively, and the poorly differentiated NECs as small and large cell NECs in NEN-2018 WHO [9]. This new, common, and standardized classification of NENs of all organs is recommended to be used in a pathologic report as follows. Firstly, the parameters used for grading (mitotic count, Ki-67 labeling index [%], and necrosis) be stated clearly; secondly, the site-specific tumor nomenclature must be used according to current WHO classifications; and finally, the uniform classification framework is added in brackets, e.g., NEN-WHO 2018.

In review of the seven reported cases of EAC NENs, including the present case, we categorized four cases as NECs (MCCs) and three were well differentiated NENs. Even if NEN of the ear has non-high-grade histology and an indolent biological behavior, metastatic potential may exist, and the tumor may recur [7]. The recurrence rate of middle ear NEN has been reported to be up to 15% [13]. Recently, one case of low-grade NEN treated by wide local resection recurred as a pulmonary metastatic nodule 8 years later [7], which was the first report of recurrent metastatic NEN of the EAC. Due to the limited number of reported EAC NENs, further study is required to ascertain its exact bio-

Table 1. Summary of seven reported cases of EAC NENs, including the present case

Case No.	Study	Age (yr)/ Sex	Symptom	Pathologic finding	WHO classification of NEN according to 4th edition [8] (NEN-2018 WHO) [9]	Treatment	Prognosis (duration of follow-up)
1	Manipoud et al. (1994) [2]	NA	NA	NA	Merkel cell carcinoma (NEN-2018 WHO)	NA	NA
2	Litofsky et al. (1998) [3]	86/F	Otalgia and hearing loss	SYN+ Vimentin+ NF+ CK+ Chromogranin-focal+ S100– HMB45– GFAP– Serotonin– ER– PR–	Merkel cell carcinoma (NEN-2018 WHO)	Gross total resection, RT	No evidence of recurrence (8 mo)
3	Mahalingam et al. (2006) [4]	32/F	Progressive hearing loss	NSE+ SYN+ PanCKweak+ Chromogranin– CK20– S100– HMB45– Melan A–	NEC G1 (NET G1-2018 WHO)	Second-look tympanomastoidectomy	No evidence of recurrence (8 mo)
4	Palma et al. (2007) [5]	72/M	Painless swelling of retroauricular region and sudden onset of bleeding	CK perinuclear dot+ Chromogranin+ NSE+ SYN+	Merkel cell carcinoma (NEC-2018 WHO)	CTx	Died due to underlying multiple malignancies
5	Li et al. (2012) [6]	62/M	Painless mass at EAC	CK+ NSE+ Vimentin+	Merkel cell carcinoma (NEC-2018 WHO)	Sleeve mastoidectomy and tympanotomy, RT, CTx	No evidence of recurrence (2 yr)
6	McCrary et al. (2017) [7]	38/F	Otalgia, aural fullness, and decreased hearing	PanCK+ CD56+ SYN+ Chromogranin+ CK7– Mucin–	NEC G1 (NET G1-2018 WHO)	Gross total resection	Recurrence (8 yr)
7	Present case	39/M	Progressive hearing loss	SYN+ CD56+ Chromogranin– CK7– CK20–	NEC G1 (NET G1-2018 WHO)	Gross total resection	No evidence of recurrence (20 mo)

EAC, external auditory canal; NET, neuroendocrine tumor; WHO, World Health Organization; NEN, neuroendocrine neoplasm; NA, not available; NEC, neuroendocrine carcinoma; SYN, synaptophysin; NF, neurofilament; CK, cytokeratin; HMB45, human melanoma black 45; GFAP, glial fibrillary acidic protein; ER, estrogen receptor; PR, progesteron receptor; RT, radiotherapy; G1, grade 1; NSE, neuron specific enolase; CTx, chemotherapy.

https://doi.org/10.4132/jptm.2019.11.07

logic behavior. These seven cases are summarized in Table 1.

Based on considerations of late recurrence and metastases despite a bland histology and a low proliferation index, complete surgical resection including complete soft tissue removal, canaloplasty, and removal of underlying bone is recommended. Prophylactic neck dissection may be recommended in neuroendocrine carcinomas of the EAC [6]. However, small, low-grade NEN may be treated by conservative surgery [7]. Chemoradiotherapy may be considered for high-grade or incompletely excised NEN. Despite limited data, consideration of patient age and physical condition, tumor staging, and histological categorization should be taken into consideration when determining treatment modalities. Additional study of NENs of the EAC is required to further understand this rare clinical entity.

Primary NENs of the EAC pose a unique diagnostic and surgical challenge. Although rare, otolaryngologist and radiologist should bear in mind metastatic NENs in the differential diagnoses of EAC masses. Here, we highlight the histologic findings of NEN of the EAC, a rare entity, and emphasize that close work up and follow up are mandatory, especially for low-grade NEN treated by wide surgical resection with or without chemoradiotherapy.

ORCID

Dong Hae Chung: https://orcid.org/0000-0002-4538-0989
Gyu Cheol Han: https://orcid.org/0000-0002-0112-8183
Na Rae Kim: https://orcid.org/0000-0003-2793-6856

Author Contributions

Conceptualization: NRK.
Data curation: NRK.
Investigation: NRK, GCH, DHC.
Resources: GCH.
Supervision: DHC.
Validation: GCH, DHC.
Writing—original draft: GCH, DHC.
Writing—review & editing: NRK, DHC.

Conflicts of Interest

The authors declare that they have no potential conflicts of interest.

Funding

No funding to declare.

REFERENCES

1. Pelosi S, Koss S. Adenomatous tumors of the middle ear. Otolaryngol Clin North Am 2015; 48: 305-15.
2. Manipoud P, Mom T, Kemeny JL, Fouilloux G, Lafaye M. Cutaneous neuroendocrine carcinoma of the external ear canal. Ann Otolaryngol Chir Cervicofac 1994; 111: 111-4.
3. Litofsky NS, Smith TW, Megerian CA. Merkel cell carcinoma of the external auditory canal invading the intracranial compartment. Am J Otolaryngol 1998; 19: 330-4.
4. Mahalingam M, Kveaton JF, Bhawan J. Cutaneous neuroendocrine adenoma: an uncommon neoplasm. J Cutan Pathol 2006; 33: 315-7.
5. Palma S, Cavazzini L, Bovo R, et al. Merkel cell tumour of the external ear: report of a case. Auris Nasus Larynx 2007; 34: 229-32.
6. Li YK, Chi FL, Wang SY, Wang WQ, Yang JM, Huang YB. Cutaneous neuroendocrine carcinoma of the external auditory canal: a case report and review of the literature. Case Rep Otolaryngol 2012; 2012: 941065.
7. McCrary HC, Faucett EA, Reghunathan S, et al. The first reported case of recurrent carcinoid tumor in the external auditory canal. Otol Neurotol 2017; 38: 114-7.
8. Perez-Ordonez B, Bishop JA, Gnepp DR, Hunt JL, Thompson LD. Neuroendocrine tumours. In: El-Naggar AK, Chan JK, Grandis JR, Takata T, Slootweg PJ, eds. WHO classification of head and neck tumours. 4th ed. Lyon: IARC Press; 2017; 95-8.
9. Rindi G, Klimstra DS, Abedi-Ardekani B, et al. A common classification framework for neuroendocrine neoplasms: an International Agency for Research on Cancer (IARC) and World Health Organization (WHO) expert consensus proposal. Mod Pathol 2018; 31: 1770-86.
10. Sari S, Battal B, Akgun V, Salih Deveci M. Metastasis of breast carcinoma to the external auditory canal: report of an unusual case and literature review. J Belg Soc Radiol 2015; 99: 53-7.
11. Katabi N. Neuroendocrine neoplasms of the ear. Head Neck Pathol 2018; 12: 362-6.
12. Xu B, Chetty R, Perez-Ordoñez B. Neuroendocrine neoplasms of the head and neck: some suggestions for the new WHO classification of head and neck tumors. Head Neck Pathol 2014; 8: 24-32.
13. Bell D, El-Naggar AK, Gidley PW. Middle ear adenomatous neuroendocrine tumors: a 25-year experience at MD Anderson Cancer Center. Virchows Arch 2017; 471: 667-72.

JPTM
Journal of Pathology and Translational Medicine 2020; 54: 188-191
https://doi.org/10.4132/jptm.2019.09.07

BRIEF CASE REPORT

Tumor-to-tumor metastasis: metastatic invasive lobular carcinoma of the breast within adenocarcinoma of the lung

Myoung Jae Kang, Ae Ri An, Myoung Ja Chung, Kyoung Min Kim

Department of Pathology, Research Institute for Endocrine Sciences, Research Institute of Clinical Medicine of Jeonbuk National University-Biomedical Research Institute of Jeonbuk National University Hospital, Jeonbuk National University Medical School, Jeonju, Korea

Tumor-to-tumor metastasis (TTM) is an extremely rare phenomenon in patients with multiple synchronous or metachronous primary malignancies. Previous studies reported that renal cell carcinoma and meningioma are the most common recipients of TTM, whereas the most prevalent donors are lung and breast carcinomas [1]. Although the lung is one of the organs most vulnerable to metastases, a lung carcinoma is one of the most rare recipients of TTM. To the best of our knowledge, only two cases of lung carcinoma harboring metastatic breast carcinoma have been reported in English literature [2]. Herein, we report another TTM case in which an invasive lobular carcinoma of the breast metastasized to a lung adenocarcinoma.

CASE REPORT

A 52-year-old woman's medical check-up and ultrasonography revealed a 6.2-cm-sized mass in the right breast, which was diagnosed as invasive lobular carcinoma by needle biopsy. Before surgery, the patient underwent a full-body evaluation. Computed tomography revealed a mass in the right lung, which was diagnosed as pulmonary adenocarcinoma by needle biopsy (Fig. 1). Since the patient was suspected to have synchronous primary carcinomas in her lung and right breast with no sign of metastasis, she underwent right lower lobectomy for the lung adenocarcinoma and right mastectomy for the invasive lobular carcinoma of the right breast. The lung mass measured 2.3 cm in diameter. Microscopically, most of the lung mass exhibited typical growth patterns of lung adenocarcinoma. However, in one focus, the tumor cells showed a different arrangement and cytology; the tumor cells had minimal cytoplasm without nucleoli in a compact trabecular pattern. The typical adenocarcinoma cells were positive for thyroid transcription factor-1 (TTF-1) and E-cadherin and negative for estrogen and progesterone receptors. In contrast, tumor cells in the morphologically different focus expressed immunoreactivity for estrogen and progesterone receptors while they were negative for TTF-1 and E-cadherin (Fig. 2). Based on these findings, we concluded that the invasive lobular carcinoma of the patient's right breast had metastasized to the lung adenocarcinoma. This study was approved by the Institutional Review Board of Chonbuk National University Hospital with a waiver of informed consent (IRB No. 2019-05-027).

DISCUSSION

TTM is an extremely rare phenomenon. Moreover, only approximately 180 cases have been reported in English literature. The most referenced and used criteria to diagnose TTM were proposed by Campbell et al. [3] as follows: (1) more than one primary tumor must be present; (2) the recipient tumor must be a true benign or malignant neoplasm; (3) the metastatic neoplasm must be a true metastasis with established growth in the host's tumor, not the result of contiguous growth ('collision tumor') or embolization of tumor cells; and (4) tumors that have metastasized to the lymph nodes with existing lymphoreticular malignant tumors are excluded.

According to previous reports, renal cell carcinoma and meningioma are common recipient tumors of TTM (Table 1) [1]. They are both rich in vasculature and have high cytoplasmic

Received: July 18, 2019 **Revised:** August 30, 2019
Accepted: September 7, 2019

Corresponding Author: Kyoung Min Kim, MD, PhD
Department of Pathology, Jeonbuk National University Medical School, 567 Baekje-daero, Deokjin-gu, Jeonju 54896, Korea
Tel: +82-63-270-4691, Fax: +82-63-270-3135, E-mail: kmkim@jbnu.ac.kr

pISSN 2383-7837
eISSN 2383-7845

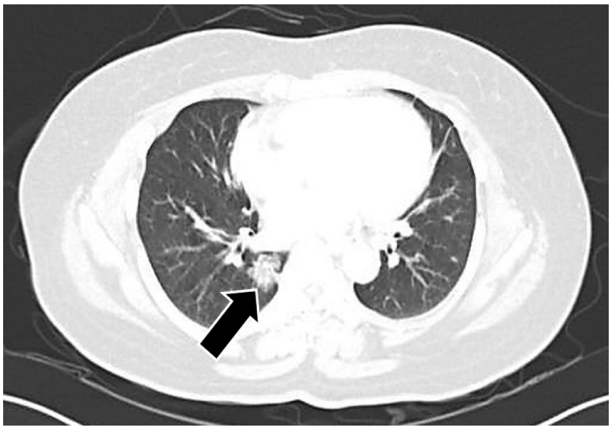

Fig. 1. High resolution view of computed tomography scan shows pulmonary mass (arrow). The mass is located at right lower lobe of the lung and shows ground glass opacity.

lipid and glycogen content [4]. These conditions might be able to serve as a favorable microenvironment for disseminated cancer cells to metastasize. The lung is one of the most frequent sites of metastasis for extrathoracic malignancies. However, lung carcinomas are extremely rare to serve as a recipient tumor in a TTM phenomenon [1,2,5-7]. A possible explanation for this paradox is that lung carcinomas, when compared with normal lungs, are often accompanied by fibrosis and are lacking in the rich network of thin-walled vasculature [6,8]. Additionally, most lung carcinomas grow rapidly; therefore, they are less likely to provide enough nutrition for the immigrant cancer cells than renal cell carcinoma or meningioma [8].

A lung mass detected in a patient with a history of prior cancer proves to be a big challenge to clinicians, radiologists, and pathologists. Even worse, in TTM cases like our patient, it is nearly impossible for a radiologist to detect the metastatic lesion located inside the primary tumor. Besides, the needle biopsy, if not containing both primary and metastatic tumors of the mass, could be of no use. In our study, we interpreted the needle biopsy of the lung mass as a primary lung adenocarcinoma. Even after evaluation of the resection specimen, it is not an easy task to detect the metastasis whose focus is small and embedded in the recipient tumor. Therefore, if pathologists identify a histologically different focus in a morphologically typical primary lung tumor of a patient with two different primary cancers, they should always take TTM occurrence into consideration despite the slim chance.

In conclusion, we report a rare case of an invasive lobular carcinoma of the breast metastasizing to a lung adenocarcinoma. To avoid an incorrect diagnosis of a tumor with dimorphic appearance, the TTM phenomenon should be considered as a possibility. Moreover, it is of great importance to identify metastases because metastatic and non-metastatic tumors require different treatments.

Table 1. Approximately estimated number of reported cases of tumor-to-tumor metastasis

Recipient tumor	Donor tumor	No. of reported cases
Renal cell carcinoma	Lung carcinoma	55
	Breast carcinoma	6
	Prostate carcinoma	4
	Gastric carcinoma	2
	Thyroid carcinoma	2
	Colon carcinoma	2
	Tonsil carcinoma	1
	Melanoma	1
	Rhabdomyosarcoma	1
	Uterine cervix carcinoma	1
Meningioma	Lung carcinoma	30
	Breast carcinoma	13
	Renal cell carcinoma	2
	Gastric carcinoma	1
	Melanoma	1
	Thyroid cancer	1
	Esophageal carcinoma	1
Thyroid neoplasm	Renal cell carcinoma	10
	Lung carcinoma	5
	Colon carcinoma	2
	Endometrial carcinoma	1
	Breast carcinoma	1
Lung cancer	Thyroid carcinoma	5
	Breast carcinoma	2
	Head and neck carcinoma	1
	Colon carcinoma	1
Ovary neoplasm	Uterine cervix carcinoma	1
	Breast carcinoma	1
	Appendix carcinoma	1
	Colon carcinoma	1
	Gastric carcinoma	1
Pituitary adenoma	Breast carcinoma	1
	Gastric carcinoma	1
	Prostate carcinoma	1
	Pancreatic endocrine neoplasm	1
Adrenocortical adenoma	Lung carcinoma	2
	Bladder carcinoma	1
	Breast carcinoma	1
Pheochromocytoma	Breast carcinoma	2
	Renal cell carcinoma	1
Oligodendroglioma	Colon carcinoma	1
	Breast carcinoma	1
	Melanoma	1
Prostate cancer	Melanoma	1
	Lung carcinoma	1
Thymic neoplasm	Pancreatic carcinoma	1
	Breast carcinoma	1

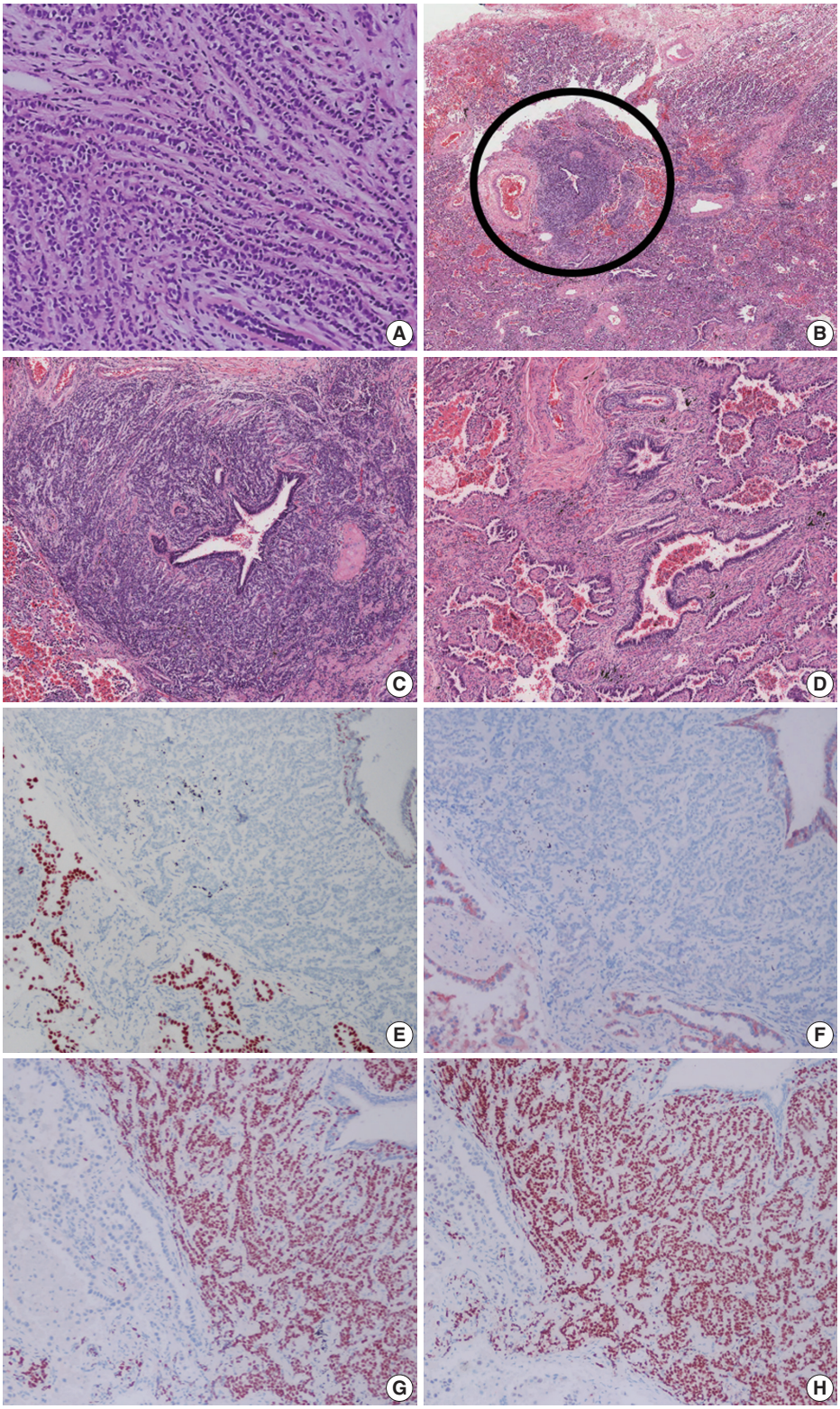

Fig. 2. Histologic features of the breast needle biopsy and resected lung mass. (A) The tumor cells of the breast mass are arranged in infiltrating single linear cords. (B) Scan view of the pulmonary mass shows dimorphic growth pattern (circular area vs. other region). (C) Higher magnification of the circular area of Fig. 2B. The tumor cells are arranged in compact trabecular pattern with minimal cytoplasm. (D) Other region of the lung mass showing typical acinar growth pattern. The tumor cells of the circular area of panel B are negative for thyroid transcription factor-1 (E) and E-cadherin (F) and positive for estrogen (G) and progesterone receptor (H).

https://doi.org/10.4132/jptm.2019.09.07

ORCID

Myoung Jae Kang: https://orcid.org/0000-0003-0424-6078
Ae Ri An: https://orcid.org/0000-0002-6047-1627
Myoung Ja Chung: https://orcid.org/0000-0003-4165-7167
Kyoung Min Kim: https://orcid.org/0000-0001-7074-7183

Author Contributions

Conceptualization: KMK, MJC.
Data curation: ARA, KMK.
Investigation: ARA, KMK.
Writing: MJK, KMK.

Conflicts of Interest

The authors declare that they have no potential conflicts of interest.

Funding

No funding to declare.

REFERENCES

1. Petraki C, Vaslamatzis M, Argyrakos T, et al. Tumor to tumor metastasis: report of two cases and review of the literature. Int J Surg Pathol 2003; 11: 127-35.
2. Piacentini F, Rossi G, Casali C, Cadioli A, Barbieri E, Guarneri V. Primary pulmonary cancer colliding with metastatic breast carcinoma: hitherto unreported cases of cancer-to-cancer metastasis focusing on clinical implications. Lung Cancer 2011; 74: 145-8.
3. Campbell LV Jr, Gilbert E, Chamberlain CR Jr, Watne AL. Metastases of cancer to cancer. Cancer 1968; 22: 635-43.
4. Ortega P Jr, Li IY, Shimkin M. Metastasis of neoplasms to other neoplasms. Ann West Med Surg 1951; 5: 601-9.
5. Kim KM, Kim YN, Chu HH, Jin HY, Kim MH, Chung MJ. Papillary carcinoma of thyroid metastatic to adenocarcinoma in situ of lung: report of an unusual case. Korean J Pathol 2012; 46: 282-6.
6. Lee T, Cha YJ, Ahn S, Han J, Shim YM. A rare case of tumor-to-tumor metastasis of thyroid papillary carcinoma within a pulmonary adenocarcinoma. J Pathol Transl Med 2015; 49: 78-80.
7. Roscoe KJ, Raja S, Tronic B, Dou Y. Single F-18 fluorodeoxyglucose positron emission tomography hypermetabolic focus containing metastatic papillary thyroid cancer within a primary scarring adenocarcinoma lung cancer. Clin Nucl Med 2006; 31: 359-60.
8. Xue L, Luan Z, Liu Y, et al. Pulmonary metastasis of a papillary thyroid carcinoma and primary lung adenocarcinoma: two coincident carcinomas at the same location. Diagn Pathol 2013; 8: 26.

JPTM
Journal of Pathology and Translational Medicine 2020; 54: 192-195
https://doi.org/10.4132/jptm.2019.11.14

BRIEF CASE REPORT

Pseudomesotheliomatous carcinoma of the lung in the parietal pleura

Ae Ri An, Kyoung Min Kim, Jong Hun Kim, Gong Yong Jin, Young Hoon Choe, Myoung Ja Chung

Department of Pathology, Jeonbuk National University Medical School, Jeonju, Korea

Pseudomesotheliomatous carcinoma of the lung (PCL) is a rare and unique subtype of lung adenocarcinoma located in the pleura, which clinically and/or radiologically mimics the growth of malignant mesotheliomas (MM). It is characterized by pleural thickening without lung mass; however, ultrastructural, immunohistochemical, and molecular characteristics suggest type II pneumocyte origin [1]. The original definition of this cancer by Harwood et al. described it as a unique form of lung cancer [1]. PCL is known to have a very poor prognosis due to diffuse pleural involvement, multiple extrapulmonary metastasis, and no effective treatment [2]. Advances in our understanding of the genomic alterations of cancers have profoundly altered the treatment options and prognosis for cancers. However, few studies are available on the molecular analysis of PCLs regarding genetic alteration. In this study, we report a case of PCL in the parietal pleura with results on the genetic alteration of cancer-related genes using a targeted next-generation sequencing (NGS) method.

CASE REPORT

A 69-year-old male patient presented with dyspnea and recurrent pleural effusion. He was a current smoker with a 30-pack year. He had no history of chronic pulmonary disease or asbestos exposure. The patient received thoracentesis and antibiotic treatment, but his condition did not improve. A computed tomography (CT) of the chest revealed left pleural effusion and pleural thickening with multiple nodules, suggestive of metastatic carcinoma. No parenchymal mass was observed in the lung (Fig. 1A). Positron emission tomography (PET)-CT showed fluorodeoxyglucose uptake in the areas of pleural thickening (Fig. 1B). Video-assisted thoracoscopic surgery (VATS) showed diffuse multiple nodules in the parietal pleura, and a biopsy was performed for histologic diagnosis. The histopathological examination presented glandular and cord-like structures of tumor cells within desmoplastic stroma (Fig. 2A). Under high-power field, a hobnail-like appearance of tumor cells with hyperchromatic nuclei and inconspicuous nucleoli was identified (Fig. 2B). Immunohistochemistry (IHC) was performed using an automatic immunostainer (BenchMark XT, Ventana Medical Systems, Tucson, AZ, USA) according to the manufacturer's instructions. Immunohistochemically, the tumor cells were positive for thyroid transcription factor-1 (ready to use [RTU], Ventana Medical Systems) (Fig. 2C), carcinoembryonic antigen (RTU, Ventana Medical Systems), Napsin A (RTU, Ventana Medical Systems), and epithelial membrane antigen (1:50, Dako, Glostrup, Denmark). Calretinin (RTU, Ventana Medical Systems) (Fig. 2D), cytokeratin 5/6 (RTU, Ventana Medical Systems), Wilms' tumor product-1 (1:100, Dako), and D2-40 (RTU, Ventana Medical Systems) were negative. With these immunohistochemical results and clinical presentation, the tumor was diagnosed as PCL. The patient refused chemotherapy and is only receiving treatment for pleural effusion.

Targeted NGS was performed using formalin-fixed paraffin-embedded (FFPE) tumor tissue. Total nucleic acid was isolated from FFPE tumor tissue using RecoverAll Total Nucleic Acid Isolation Kit for FFPE according to the manufacturer's specifications (Thermo Fisher Scientific, Waltham, MA, USA). The samples were sequenced using the Oncomine Comprehensive Assay Cancer Panel (Ion torrent S5 XL, Thermo Fisher Scientific), which covers 2737 amplicons (2530 DNA + 207 RNA) within 143 cancer-related genes. The number of mapped DNA reads was 8,755,214 (≥Q20) and the mean coverage per target ampli-

Received: September 27, 2019 **Revised:** November 11, 2019
Accepted: November 14, 2019

Corresponding Author: Myoung Ja Chung, MD, PhD
Department of Pathology, Jeonbuk National University Medical School, 567 Baekje-daero, Deokjin-gu, Jeonju 54896, Korea
Tel: +82-63-270-3072, Fax: +82-63-270-3135, E-mail: mjchung@jbnu.ac.kr

pISSN 2383-7837
eISSN 2383-7845

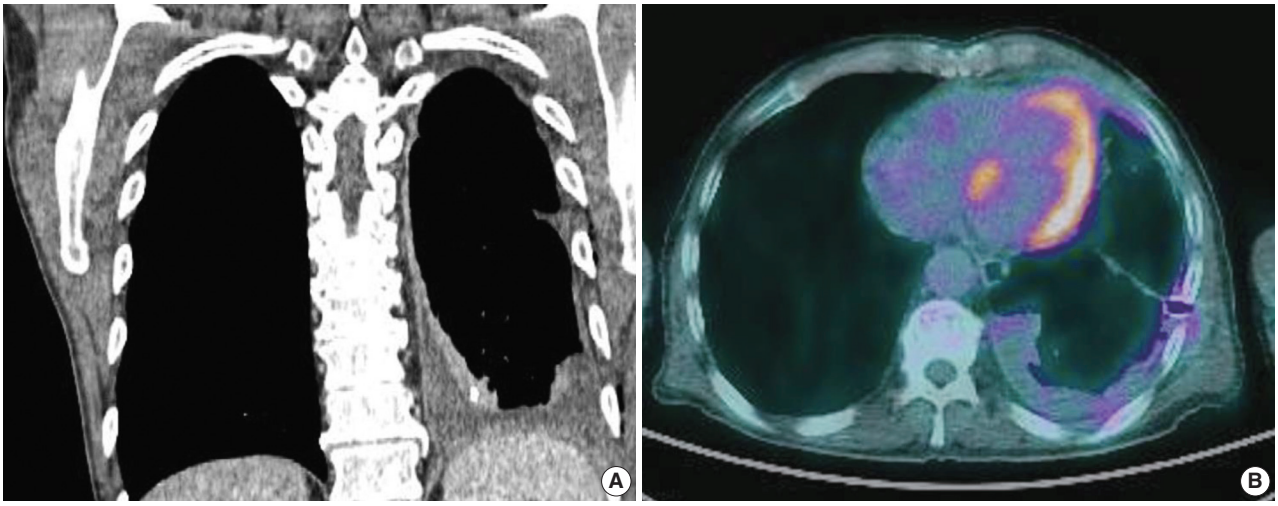

Fig. 1. (A) Computed tomography (CT) of the chest shows the extremely thickened pleura along the left lobe. (B) Positron emission tomography–CT shows fluorodeoxyglucose uptake in the left pleural thickening areas.

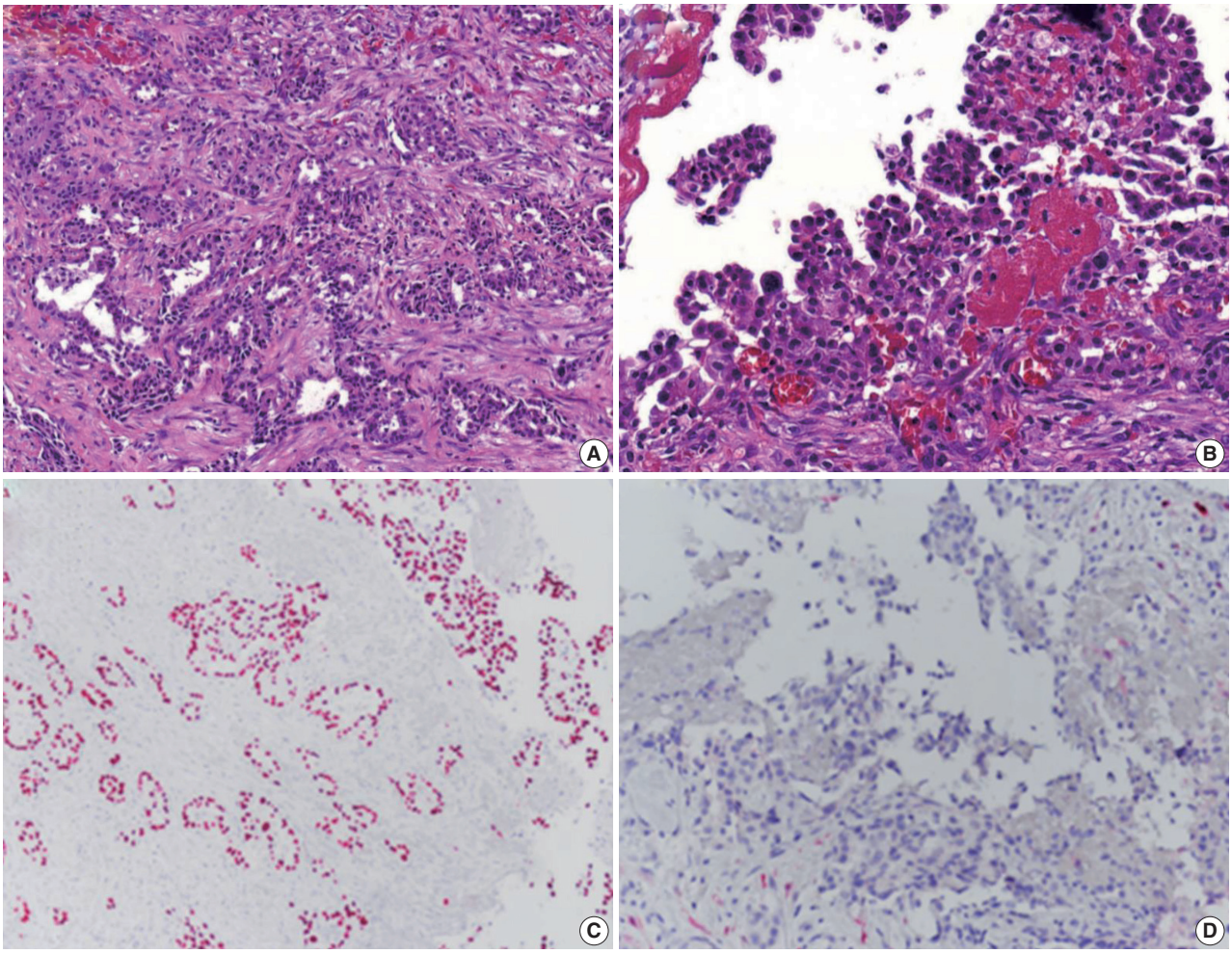

Fig. 2. Histopathological sections showing tumor cells with glandular and papillary, cord-like structures (A) and a hobnail-like appearance of tumor cells with irregular and hyperchromatic nuclei resembling malignant mesothelioma (B). Immunohistochemical evaluation demonstrates the tumor cells to be positive for thyroid transcription factor-1 (C) and negative for calretinin (D).

con was ×3,616. The percentage of amplicons that were covered by greater than 20% of the mean amplicon coverage was 95%. Reads were aligned to the hg19 reference genome and allele frequencies < 5% were excluded. We identified one pathogenic somatic mutations in splicing factor 3B subunit 1 (*SF3B1*) gene, NM_012433.3(SF3B1):c.2098A > G (p.Lys700Glu).

Ethics statement

This study was approved by the Institutional Review Board of Chonbuk National University Hospital with a waiver of informed consent (IRB No. 2019-04-040).

DISCUSSION

PCLs were first reported by Harwood et al. in 1976 [1]. The authors defined this tumor entity as a malignant epithelial neoplasm, which presents with radiological, macroscopic, and microscopic features similar to those of diffuse malignant pleural mesothelioma [1]. PCL is mostly found in men, and the age of onset is between the sixth and seventh decades of life. The majority of patients are cigarette smokers [3]. In association with asbestos exposure, some researchers reported on the presence of asbestos bodies in cancer tissue, and Koss et al. [3] reported the possibility of occupational exposure in 21% of the patients. However, the relationship between cancer development and asbestos exposure is unclear. The tumor growth pattern makes it difficult to differentiate PCL from MM based on radiologic findings alone, and histologic confirmation is needed. IHC provides an adequate sensitivity and specificity for distinguishing PCL from MM. The tumor cells are positive for thyroid transcription factor-1, Napsin A, epithelial membrane antigen, and carcinoembryonic antigen and negative for mesothelial markers such as calretinin and D2-40.

PCL is characterized mainly by visceral pleural thickening; however, our case showed a unique presentation of only parietal pleural thickening without visceral pleural thickening. These clinical features created a diagnostic difficulty, and in this case, it was important to recognize PCL for an accurate diagnosis.

PCL shows a distinctly different biological behavior from the usual type of adenocarcinoma of the lung. Because of its extensive invasion of the pleura and lack of effective treatment, patients have a poor prognosis [4]. Recently, identification of the genetic alteration of cancer-related genes through sequencing in cancer has been widely used for application of targeted cancer treatment. Because PCL does not yet have an established guideline on effective treatment and the prognosis is poor, it would be meaningful to know the genetic alterations of PLC in terms of therapeutic development. No studies about genetic alterations in PCL have been reported [5]. We investigated the mutational status of cancer-related genes using targeted NGS and identified genetic alteration in *SF3B1* gene, which is involved in transcription and mRNA processing. The mutation of *SF3B1* gene has been recurrently observed in hematologic malignancies, breast cancer, pancreas cancer, prostate cancer, and others. *SF3B1* mutations have been reported to be associated with poor outcome and drug resistance in chronic lymphocytic leukemia [6]. Although neither the mutation of known genes that have target drugs nor driver mutation were observed in this study, an accumulation of information on genetic alteration is expected to be useful for understanding the pathogenesis or developing an effective treatment in the future.

The histogenesis of PCL is not clear. Harwood et al. [1] reported a small subpleural adenocarcinoma associated with some PCL and suggested a possible origin of PCL, as this small subpleural tumor became widely disseminated via subpleural lymphatics. A second suggestion is that the fibrous thickening of the pleura may be an early event. Furthermore, the cancer developed in subpleural lung parenchyma and subsequently spread rapidly through the thickened pleura. In the present case, VATS showed diffuse pleural thickening with multiple nodules in the parietal pleura instead of the visceral pleura. Neither chest CT nor PET-CT revealed lung parenchymal lesions. In our case, with these presentation characteristics, the possibility of different histogenesis can be considered. The possibility of pulmonary heterotopia of the pleura can be considered based on reports that lung tissue is found in an ectopic location [7]. However, there is no report of ectopic lung tissue in the parietal pleura, and there is no evidence to support this hypothesis in our case.

We report a case of PCL presented with parietal pleural thickening without lung parenchymal lesions. The present report is the first case of PCL with gene mutation results approached through NGS.

ORCID

Ae Ri An: https://orcid.org/0000-0002-6047-1627
Kyoung Min Kim: https://orcid.org/0000-0001-7074-7183
Jong Heon Kim: https://orcid.org/0000-0001-9289-1178
Gong Yong Jin: https://orcid.org/0000-0002-1426-554X
Young Hoon Choe: https://orcid.org/0000-0002-7982-7822
Myoung Ja Chung: https://orcid.org/0000-0003-4165-7167

https://doi.org/10.4132/jptm.2019.11.14

Author Contributions

Conceptualization: MJC.
Data curation: ARA, KMK, YHC, JHK, GYJ.
Investigation: ARA, KMK.
Writing: ARA, MJC.

Conflicts of Interest

The authors declare that they have no potential conflicts of interest.

Funding

No funding to declare.

REFERENCES

1. Harwood TR, Gracey DR, Yokoo H. Pseudomesotheliomatous carcinoma of the lung: a variant of peripheral lung cancer. Am J Clin Pathol 1976; 65: 159-67.
2. Attanoos RL, Gibbs AR. 'Pseudomesotheliomatous' carcinomas of the pleura: a 10-year analysis of cases from the Environmental Lung Disease Research Group, Cardiff. Histopathology 2003; 43: 444-52.
3. Koss MN, Fleming M, Przygodzki RM, Sherrod A, Travis W, Hochholzer L. Adenocarcinoma simulating mesothelioma: a clinicopathologic and immunohistochemical study of 29 cases. Ann Diagn Pathol 1998; 2: 93-102.
4. Vuković J, Plavec G, Aćimović S, et al. Pseudomesotheliomatous carcinoma of the lung. Vojnosanit Pregl 2016; 73: 1168-72.
5. Sakata S, Sakamoto Y, Takaki A, Ishizuka S, Saeki S, Fujii K. Reversible restrictive lung disease in pseudomesotheliomatous carcinoma in a lung harboring a *HER2*-mutation. Intern Med 2018; 57: 2223-6.
6. Rossi D, Bruscaggin A, Spina V, et al. Mutations of the *SF3B1* splicing factor in chronic lymphocytic leukemia: association with progression and fludarabine-refractoriness. Blood 2011; 118: 6904-8.
7. Jeon GW, Han SW, Jung JM, Kang MS, Sin JB. The first Korean case of cutaneous lung tissue heterotopia. J Korean Med Sci 2010; 25: 1387-9.

JPTM
Journal of Pathology and Translational Medicine 2020; 54: 196
https://doi.org/10.4132/jptm.2020.02.17

CORRIGENDUM

Correction of acknowledgments: PD-L1 testing in non-small cell lung cancer: past, present, and future

Hyojin Kim[1], Jin-Haeng Chung[1,2]

[1]Department of Pathology, Seoul National University Bundang Hospital, Seongnam;
[2]Department of Pathology, Seoul National University College of Medicine, Seoul, Korea

To the Editor:

We found an error in our published article.

Kim H, Chung JH. PD-L1 testing in non-small cell lung cancer: past, present, and future. Journal of Pathology and Translational Medicine 2019; 53(4): 199-206. https://doi.org/10.4132/jptm.2019.04.24.

On page 204, the Acknowledgments should be corrected as follows: This work was supported by the National Research Foundation of Korea (NRF) Grant funded by the Korean Government (MSIT) (No. 2017R1A5A1015626) and the Korea Health Technology R&D Project through the Korea Health Industry Development Institute (KHIDI), funded by the Ministry of Health & Welfare, Republic of Korea (grant number: HI17C1290).

We apologize for the error.

pISSN 2383-7837
eISSN 2383-7845


JPTM
Journal of Pathology and
Translational Medicine